

Particle Astrophysics with High Energy Neutrinos

Thomas K. Gaisser^a, Francis Halzen^b and Todor Stanev^a

^a*Bartol Research Institute, University of Delaware, Newark, DE 19716, USA*

^b*Department of Physics, University of Wisconsin, Madison, WI 53706, USA*

Abstract

The topic of this review is the particle astrophysics of high energy neutrinos. High energy is defined as $E_\nu > 100$ MeV. Main topics include:

- atmospheric neutrinos and muons from π , K and charm decay. They probe uncharted territory in neutrino oscillations and constitute both the background and calibration of high energy neutrino telescopes,
- sources of high energy neutrino beams: the galactic plane, the sun, X-ray binaries, supernova remnants and interactions of extra-galactic cosmic rays with background photons,
- an extensive review of the mechanisms by which active galaxies may produce high energy particle beams,
- high energy neutrino signatures of cold dark matter and,
- a brief review of detection techniques (water and ice Cherenkov detectors, surface detectors, radio- and acoustic detectors, horizontal airshower arrays) and the instruments under construction.

1 Introduction

The scope of this paper is neutrino astronomy for $E_\nu > 100$ MeV. Our main interest is neutrinos from energetic astrophysical sources such as binary stars and accreting black holes in Active Galactic Nuclei (AGN). We will also discuss atmospheric neutrinos at some length because they are the only neutrinos with $E > 100$ MeV that have yet been detected. Atmospheric neutrinos are both background and calibration beam for high energy neutrino astronomy. They are of interest in their own right because they probe an uncharted range of neutrino oscillation parameter space. For stellar collapse neutrinos and solar neutrinos we refer the reader to the recent review of Totsuka [1] and, for solar neutrinos to the reviews of Bahcall *et al.* [2,3] and Turck-Chieze *et al.* [4].

In his classic review of cosmic ray showers in 1960 [5], Greisen ends with a discussion of the prospects for gamma ray and neutrino astronomy at very high energy. He notes that “Since photons and neutrinos propagate in straight lines, success in their detection will open up broad new areas of astronomy.” He discussed the relation between photons and neutrinos from decay of pions produced in the interstellar medium or near a source. He described a detector very much like the present water Cherenkov detectors (complete with veto shield against entering muons), and he estimated the rate of interactions of atmospheric neutrinos in 3 kilotons of sensitive volume to be 500 events per year.

The idea of detecting neutrinos by looking for neutrino-induced upward or horizontal muons was suggested by Markov & Zheleznykh [6] at about the same time. The process is

$$\nu_\mu + N \rightarrow \mu + \text{anything}, \quad (1)$$

where N is a nucleon in the material surrounding the detector. The muon range increases with energy. This extends the effective target volume and makes it possible to see neutrino-induced muons with detectors of moderate size. Two groups (Kolar Gold Fields [7,8] and Case-Wittwatersrand [9,10]) reported the first observations of atmospheric neutrinos with the detection of horizontal muons in detectors so deep that the muons could not have been produced in the atmosphere.

Atmospheric neutrinos are of current interest, despite their long history and apparently mundane origin, because of the anomalous flavor ratio observed for neutrino interactions in the large proton decay detectors, Kamiokande [11] and IMB [12]. The essential point is that, because of their large volume, these detectors can measure interactions of neutrinos inside the detector. They need not depend on the large external target mass provided by the long range of energetic muons produced in charged current interactions of muon-type neutrinos. They can therefore study both ν_e and ν_μ interactions. In all, more than a thousand atmospheric neutrino events have now been measured by the various underground experiments[11,12,13,14,15,16] The anomaly is that the observed ratio of events produced by electron neutrinos to those from muon neutrinos is significantly larger than expected.

Several new detectors designed specifically for high energy neutrino astronomy are about to come into operation. The Baikal experiment [17] has already reported some muon measurements [18]. The DUMAND [19] and AMANDA [20,21] are being partially deployed at present, and other detectors, such as NESTOR [22] are in advanced prototype stages. A major stimulus for this activity is the prospect that Active Galactic Nuclei (AGN) may be

prolific particle accelerators and beam dumps, and therefore intense sources of high energy neutrinos.

We have divided our review into three major sections: (a) atmospheric neutrinos, (b) possible sources of high energy neutrinos of extraterrestrial origin and (c) neutrino detection. We include some comments about high energy gamma ray astronomy relevant to possible neutrino sources at the beginning of part (b). We begin with a brief treatment of neutrino production in cosmic ray cascades, which is relevant both for atmospheric and astrophysical neutrinos.

2 Neutrino production

Unlike the typical monoenergetic beam produced by a machine, cosmic accelerators produce power law spectra of ions at high energy,

$$\phi_p \propto E^{-(\gamma+1)}. \quad (2)$$

The observed high energy cosmic ray spectrum at Earth is characterized by $\gamma \sim 1.7$. In general, a cosmic accelerator in which the dominant mechanism is first order diffusive shock acceleration (first order Fermi mechanism), will produce a spectrum with $\gamma \sim 1 + \epsilon$, where ϵ is a small number. The observed spectrum is thought to be steeper than the accelerated spectrum because of the energy dependence of the cosmic ray diffusion in the galaxy. The simplest way to understand this is to think of the observer as inside a volume of “containment” from which the characteristic escape time decreases with energy

$$\tau(E) \propto E^{-\delta}. \quad (3)$$

If $Q(E)$ is the rate of production of cosmic rays per unit volume, then the observed cosmic ray density will be

$$\rho_{\text{CR}}(E) \sim Q(E) \times \tau(E) \propto E^{-(2+\epsilon+\delta)}. \quad (4)$$

For $1 \leq E \leq 100$ GeV, a value of $\delta \sim 0.6$ can be inferred from observed ratios of secondary cosmic ray nuclei (e.g. Li, Be, B) to their progenitors (e.g. carbon and oxygen) [23].

Production of secondary particles (S) is related to the spectrum of accelerated primaries (P) by

$$\frac{dP_S}{dE_S} = \frac{\Delta}{\lambda_P} \int_{E_S}^{\infty} \frac{dn_{PS}(E_S, E_P)}{dE_S} \phi_P(E_P) dE_P, \quad (5)$$

where Δ/λ_P is the probability of interaction in traversing a small amount (Δ) of target. If the distribution of secondaries depends only on the ratio of energies, $x = E_S/E_P$, then the integral in Eq. (5) becomes

$$\phi_P(E_S) \int_0^1 x^{\gamma-1} F_{PS}(x) dx \equiv \phi_P(E_S) Z_{PS}, \quad (6)$$

where

$$F_{PS} = \frac{1}{\sigma} \int d^2 p_T E_S \frac{d\sigma_{PS}}{d^3 p} \approx E_S \frac{dn_{PS}}{dE_S}. \quad (7)$$

For $\gamma > 1$, $F(0)$ does not contribute to the integral, and the scaling approximation made here is an adequate approximation for rough estimates. This treatment generalizes readily to decay chains, such as $p \rightarrow \pi^\pm \rightarrow \mu^\pm$, etc., and it can be applied to cascades in galactic and stellar environments as well as in the Earth's atmosphere. In case of a thick target in which the primary beam is fully attenuated, the production spectrum of secondaries is given by Eq. (5) with the replacement

$$\frac{\Delta}{\lambda_P} \rightarrow \frac{\Lambda_P}{\lambda_P}, \quad (8)$$

where Λ_P is the attenuation length of the primary.

In general, the flux of neutrinos from decay of pions is given by [24]

$$\frac{dN_\nu}{dE_\nu} = \frac{N_0(E_\nu)}{1 - Z_{NN}} \times \left\{ \frac{A_{\pi\nu}}{1 + B_{\pi\nu} \cos\vartheta E_\nu/\epsilon_\pi} + (\dots) \right\}, \quad (9)$$

where $A_{\pi\nu} = Z_{N\pi}(1 - r_\pi)^\gamma/(\gamma + 1)$, $r_\pi = (m_\mu/m_\pi)^2$ and $B_{\pi\nu}$ is a constant that depends on nucleon and pion attenuation lengths. The first term inside the curly brackets represents neutrinos from decay of pions. The energy ϵ_π is a characteristic energy that reflects the competition between decay and interaction in the medium. For cascade development in the Earth's atmosphere $\epsilon_\pi \sim 115$ GeV; it is larger for more tenuous media, such as the atmosphere of the Sun.

The (\dots) represents the contributions of other mesons, with $\epsilon_{K^\pm} \sim 850$ GeV and $\epsilon_{D^\pm} \sim 4 \times 10^7$ GeV in the Earth's atmosphere. Each term also contains the appropriate branching ratio, e.g. 0.635 for $K^\pm \rightarrow \mu + \nu_\mu$. For $E_\nu \ll \epsilon_i$, all parent mesons decay, and the neutrino spectrum is parallel to the primary nucleon flux. For $E_\nu \gg \epsilon_i$ the neutrino spectrum steepens by one power of E_ν . In the atmosphere, muons with $E_\mu \gg \mu c^2 \times 15 \text{ km}/c\tau_\mu \sim 2$ GeV reach the surface and stop before they decay.

In the energy range important for contained events ($0.1 < E_\nu < 2$ GeV) decay in flight of atmospheric muons is the dominant source of ν_e , and an important source of ν_μ . At much higher energy, the dominant source of atmospheric ν_e is

$$K_L^0 \rightarrow \pi e \nu_e, \quad (10)$$

The relative contributions of the various decay modes to lepton spectra in the Earth's atmosphere are discussed in detail by Lipari [25]. If we consider neutrino production in astrophysical settings, with typical matter densities of 10^{10} atoms/cm³, pions and kaons will always decay and the neutrino spectrum will follow the nucleon spectrum also at very high energy.

In addition, muon decay will continue to be an important source of neutrinos at high energy as well as low. Thus we can define three types of neutrino spectra that can be produced by cosmic rays:

1. Atmospheric neutrinos, which follow the incident cosmic ray spectrum with $\gamma \sim 2.7$ up to ~ 100 GeV and steepen toward $\gamma \sim 3.7$ at higher energy. The position of the bend increases with increasing zenith angle, which generates a characteristic angular dependence of the atmospheric neutrino spectrum described by the angular factor in Eq. (9). Electron neutrinos, that come mostly from muon decays have a spectrum with one power of E steeper.

2. Neutrinos produced by galactic cosmic rays in interactions with interstellar gas. These extraterrestrial neutrinos should follow the cosmic ray spectrum up to the highest energies, since all interaction products, including muons, decay.
3. Neutrinos produced by cosmic rays *at their acceleration sites* and following the hard ($\gamma \sim 2.0\text{--}2.2$) cosmic ray source spectra, which are not yet affected by the energy-dependent escape from the Galaxy.

These three types of neutrino fluxes are illustrated schematically in Fig. 1.

Atmospheric neutrinos have been detected and studied extensively. Diffuse galactic neutrinos should exist with intensities comparable to the diffuse galactic gamma ray background [26]. They should be detected by a future generation of detectors of sufficient size to see neutrinos at a rate of several per 10^5 m^2 per year [27]. These two fluxes can be used for calibration of high energy neutrino telescopes, which have as their principal goal the search for high energy neutrinos from energetic astrophysical systems.

The existence of neutrinos associated with cosmic ray sources is more problematic. It requires substantial acceleration in compact sources with sufficient local gas to act as a beam dump. The *possibility* (not certainty) of such point sources is suggested by the fact that the standard model of cosmic ray acceleration by supernova blast waves in the diffuse interstellar medium cannot accelerate particles to the highest observed energies. An alternative for the higher energy cosmic radiation is acceleration in compact sources. The argument goes as follows.

First order Fermi acceleration at supernova blast shocks offers a very attractive model for a galactic acceleration mechanism, providing about the right power and spectral shape. Shock acceleration takes time, however, because the energy gain occurs gradually as a particle diffuses back and forth across the shock front. The finite lifetime of the shock thus limits the maximum energy per particle that can be achieved at a particular supernova. The acceleration rate is

$$\frac{dE}{dt} \simeq K \frac{u^2}{c} Z e B, \text{ so } E_{\text{max}} < \frac{u}{c} Z e B L, \quad (11)$$

where u is the shock velocity, Ze the charge of the particle being accelerated and B the ambient magnetic field. The numerical constant $K \sim 0.1$ depends on the details of diffusion in the vicinity of the shock. The crucial length scale in Eq. (11) is given by $L \sim uT$, where $T \sim 1000$ yrs for the free expansion phase of a supernova. Using this kind of argument, Lagage & Cesarsky [28] show that, in its simplest version (shock velocity parallel to magnetic field direction, $B = B_{\text{ISM}} \sim 3\mu\text{Gauss}$) E_{max} can only reach energies $\lesssim 10^{14} \text{ eV} \times Z$ for an accelerated nucleus. That leaves a large gap of some three orders of magnitude that cannot be explained by the “standard model” of cosmic ray origin. To reach a higher energy one has to increase significantly B and/or L .

One possibility is to use the much higher magnetic fields associated with some energetic astrophysical systems. There is no shortage of such objects in the Galaxy, the most obvious being neutron stars and black holes, as well as young supernova remnants. Some examples of possible acceleration sites will be discussed in Section 6 below. Any such compact region with active particle acceleration would be a likely site for production of high energy neutrinos and photons through interactions of the accelerated particles with the ambient gas and radiation fields.

We emphasize that this is not the only possibility. Some argue [29,30] that explaining the higher energy cosmic rays by a new source is unnatural because it requires fine tuning to produce a smooth spectrum where cosmic rays from the second source join onto those from the first.

There are several ways to extend the basic supernova mechanism to higher energies. One possibility [31] takes advantage of the fact that some supernovas explode into the stellar wind of a progenitor star rather than the interstellar medium. If the progenitor wind carries a high enough magnetic field, then higher top energies can be achieved (see Eq. 11). Other possibilities involve a configuration in which the magnetic field is quasi-perpendicular to the shock normal [32] or the interaction of high energy cosmic rays with expanding shocks of several supernovas in an active region [30]. Mechanisms such as these would not be correlated with point sources of high energy gamma rays and neutrinos.

Perhaps the most exciting possibility at present is the suggestion [33,34] that particle acceleration plays a central role inside AGN and that interactions of these high energy particles with dense photon fields and gas in the central regions of AGN [35,36,37,38] will lead to production of neutrinos of very high energies. This possibility is the subject of §6.

Figure 1 illustrates the window of opportunity for high energy neutrino astronomy. The steepening at high energy of the spectrum of atmospheric neutrinos, which dominate the total neutrino flux at low energy, allows the possibility of reasonable signal/background ratios, shown schematically by the shaded area on Fig. 1. The small angle between the parent neutrino and the secondary lepton in charged current interactions at high energy allows for accurate source location and enhanced signal/background ratio in the case of point sources. The exact position of the crossover from atmospheric to astrophysical neutrinos, depends on luminosity, distribution and distances of potential sources and on energy response and, in the case of point sources, angular resolution of the detectors. These will be discussed for a number of sources in Sections 6–8 below.

3 Atmospheric neutrinos

The atmospheric cascade that produces the cosmic ray neutrino beam is depicted in Eq. (12):

$$\begin{aligned}
 p &\longrightarrow \pi^+ (+ K^+ \dots) \longrightarrow \mu^+ + \nu_\mu \\
 &\quad \quad \quad \searrow e^+ + \bar{\nu}_\mu + \nu_e, \\
 n &\longrightarrow \pi^- (+ K^- \dots) \longrightarrow \mu^- + \bar{\nu}_\mu \\
 &\quad \quad \quad \searrow e^- + \nu_\mu + \bar{\nu}_e.
 \end{aligned}
 \tag{12}$$

Protons also produce negative mesons and neutrons produce positive mesons, but the same charge processes are slightly favored by the steep spectra and the excess of same-charge mesons in the forward fragmentation region.

Although analytic expressions like Eq. (9) are qualitatively correct, more detailed calculations are needed for a precise evaluation of the atmospheric neutrino flux. Several complications must be accounted for:

- The primary cosmic ray spectrum is not a simple power law, especially $\lesssim 10$ GeV and $\gtrsim 100$ TeV. Moreover, it depends on location and direction (because of the geomagnetic cutoff) and on the epoch of the solar cycle.
- Muon energy loss, decay and polarization must be accounted for.
- The inclusive cross sections do not have exactly scale-invariant forms. Furthermore, nuclei, as well as nucleons, are involved in the collisions.

3.1 Contained Events

Contained events are those neutrino interactions that originate within the detector's fiducial volume and whose interaction products are all contained within that volume. Most such events have lepton energies in the GeV range or less. In this case, most muons decay, and all the complications listed above come into play.

Qualitative expectations for the neutrino ratios follow from simple kinematics of the $\pi \rightarrow \mu \rightarrow e$ decay chain. Because of the asymmetry of the $\pi \rightarrow \mu + \nu_\mu$ decay mode, each of the two neutrinos from muon decay has about the same energy as the neutrino from pion decay. Thus in a given energy range

$$\frac{\nu_e}{\nu_\mu} \approx \frac{1}{2}, \quad \frac{\bar{\nu}_\mu}{\nu_\mu} \approx 1, \quad \text{and} \quad \frac{\bar{\nu}_e}{\nu_e} \approx \frac{\mu^-}{\mu^+} < 1. \quad (13)$$

The excess of ν_e to $\bar{\nu}_e$ is a consequence of the excess of protons to neutrons in the incident cosmic ray beam.

Several detailed calculations [39,40,41,42] of the \sim GeV neutrino fluxes agree with each other in finding a value for the neutrino flavor ratio within 5% of each other. Attention is focussed on the flavor ratio because most of the sources of uncertainty in the calculation of neutrino fluxes cancel in calculating the ratio. (These uncertainties include normalization of primary spectrum, treatment of geomagnetic effects and parameterization of pion production in collisions of cosmic ray protons and helium with nuclei of the atmosphere.) Specifically, the neutrino flux calculations give

$$R_{e/\mu} = \frac{\nu_e + \frac{1}{3}\bar{\nu}_e}{\nu_\mu + \frac{1}{3}\bar{\nu}_\mu} = 0.49 \pm 0.01 \quad (14)$$

for $0.1 < E_\nu < 1$ GeV [43]. The fact that this expectation is apparently significantly violated [11,12] is largely responsible for the great interest in atmospheric neutrinos.

The water Cherenkov detectors [11,12] in fact see as many [11] or more [12] electrons than muons. Part of the difference between expectation and observation is a consequence of the fact that the acceptance of the detectors spans a larger energy range for electrons than for muons. Even after accounting for flavor-dependence of the acceptance, however, a significant discrepancy remains.

Detailed simulations of the detector response, including acceptance effects, lead to the result that the ratio of ratios for charged leptons from interactions of ν and $\bar{\nu}$ is

$$\frac{(\mu/e)_{data}}{(\mu/e)_{sim}} = 0.60 \pm 0.06 \pm 0.05 \quad (15)$$

for Kamiokande with 6.2 kT-yrs of data (389 contained, single-ring events) [44]. The corresponding IMB result is

$$\frac{(\mu/e)_{data}}{(\mu/e)_{sim}} = 0.54 \pm 0.03 \pm 0.05 \quad (16)$$

for 7.7 kT-yrs of data (507 contained, single-ring events [12]). The water detectors thus show at least a 4σ discrepancy between observation and expectation for the ν_μ/ν_e ratio.

Measurements with tracking calorimeters give mixed results, and the statistical uncertainties are significantly larger than for the water detectors. NUSEX (0.74 kT-yrs, [15]) and Frejus (1.56 kT-yrs, [14]) are both consistent with expectation. In contrast, Soudan 2 (1.0 kT-yrs, [16]) finds a ratio of ratios similar to Kamiokande. The number of events is relatively low in all three experiments, and the systematic effects are also different.

In view of the complexity of the analysis involved, it is of interest to ask to what extent the data from the two water detectors are consistent with each other. Beier *et al.* [45] compared the IMB and Kamiokande data at stage when Kamiokande had 4.92 kT years of data [11] and IMB had 3.4 kT years [46]. They found the data to be fully consistent between the two experiments.

Table 1 shows a comparison based on the more complete data sets, 7.7 kT years for IMB [12] and 6.2 kT years for Kamiokande [44]. The comparison is made by converting Kamiokande data to IMB. Three factors are involved:

- 1) The larger exposure of IMB ($7.7/6.2 = 1.24$).
- 2) Higher muon threshold at IMB—the muon threshold is 300 MeV/c for IMB as compared to 200 MeV/c for Kamiokande. Using the momentum spectra of Ref. [47], we estimate that this reduces the Kamiokande muon rate by 0.79.
- 3) The lower geomagnetic cutoffs at IMB. Using the cutoff effects from Ref. [39], this increases the muon rate by a factor 1.23 and the electron rate by 1.34. The larger correction factor for electrons is a consequence of the fact that the electron threshold (100 MeV/c for both experiments) is lower than the muon threshold, and the geomagnetic filter affects low energies more than high.

These three correction factors are applied successively to the Kamiokande column to obtain the converted Kamiokande numbers that may be compared directly with the IMB column.

Table 1: Comparison of contained event rates.

	Kamiokande	exposure	μ -threshold	geomagnetic	IMB
muons	191	$\rightarrow 237$	$\rightarrow 187$	$\rightarrow 230$	182
electrons	198	$\rightarrow 246$	$\rightarrow 246$	$\rightarrow 330$	325
total	389	$\rightarrow 483$	$\rightarrow 433$	$\rightarrow 560$	507

After the conversion, the Kamiokande muon/electron ratio (230/330) appears somewhat higher than for IMB (182/325). Another consideration that must be borne in mind is that the second half of the IMB data was taken during a period of maximum solar modulation.

The event rate at IMB is expected to be somewhat lower during maximum solar modulation, whereas Kamiokande, with its higher geomagnetic cutoff is much less sensitive to modulation [39]. This effect should be the same for ν_μ and ν_e , however. Recently, Beier & Frank [48] have pointed out that the momentum spectra of the electrons in the two experiments are also somewhat different. Beam tests of the response of water Cherenkov detectors to electrons and muons will soon be carried out at KEK. This should help to resolve questions about the efficiency for discrimination between neutrino flavors as a systematic error in this type of detector.

Another possible source of systematic error that has been pointed to is the cross section for charged current interactions of neutrinos in nuclei. The Fermi gas model has been used for calculation of the spectra of the produced charged leptons by both Kamiokande [49] and IMB [50]. Recent calculations by Engel *et al.* [51] include several effects that go beyond the Fermi gas model. They find no significant shift in the spectra of electrons relative to muons which would distort the inferred ν_e/ν_μ ratio. In addition, there is some direct confirmation of the Fermi gas model for $E_\nu > 400$ MeV in data discussed in Ref. [52]. Another experiment [53], which appears to show an anomalous result for the muon spectrum in $\nu_\mu + \text{carbon} \rightarrow \mu + \dots$, is in any case below the energy range of interest here ($p_\mu > 200$ MeV/c for Kamiokande and $p_\mu > 300$ MeV/c for IMB).

Assuming that the problem with the contained events reflects an intrinsic property of particle physics (rather than a lack of understanding of detector response or neutrino cross sections), one needs to know whether there are too few ν_μ or too many ν_e . For example, [54] with the calculation of Refs. [39,41], an interpretation in terms of neutrino oscillations can be explained by ν_μ disappearance (e.g. $\nu_\mu \leftrightarrow \nu_\tau$ oscillations), but not by $\nu_\mu \leftrightarrow \nu_e$, which would increase the predicted flux of ν_e . On the other hand, comparison of the data to the calculations of Refs. [40,42] (which are some 30% lower than those of Refs. [39,41]) prefers $\nu_\mu \leftrightarrow \nu_e$ in order to boost up the predicted ν_e flux as well as lower the ν_μ flux. Fogli *et al.* [55] have recently reviewed the limits of various neutrino oscillation scenarios that could explain the atmospheric neutrino anomaly.

A more exotic explanation is the suggestion that there is an excess of electrons due to proton decay in the mode $p \rightarrow e \nu \bar{\nu}$ [56]. This interpretation requires a calculated atmospheric flux with a low normalization (so the muon rate is correctly predicted). The atmospheric flux should also have a shape such that the deficit of electrons from atmospheric ν_e 's occurs preferentially at low energy. The deficit can then be filled in by the characteristic energy spectrum of a three-body proton decay. The calculation of Ref. [42] has just these features.

A subset of the authors of Refs. [39,40,41,42] is investigating the source(s) of the difference among the normalization and shapes of the calculations. It appears that the main cause of the characteristic shape and low normalization of the calculation of Ref. [42] is the parameterization of pion production in collisions of protons with light nuclei [57].

The production of π^\pm with $E_\pi < 2$ GeV is significantly lower in the parameterization of Ref. [42] than in Refs. [39,41].

This uncertainty could be reduced by comparison to measurement of muon fluxes at high altitude. Existing high altitude data [58,59,60] have large uncertainties, but they somewhat favor the higher flux calculations. A new set of experiments [61] should be able to fix the normalization to perhaps 10%. If the contained neutrino anomaly is due to $\nu_\mu \leftrightarrow \nu_\tau$ oscillations, then the derived parameters suggest the effect should also show up as an

apparent deficit in the neutrino-induced upward muon sample. We return to this question in the next section.

3.2 Upward Muons

Neutrino-induced muons are of interest for two reasons: first, they extend the study of the atmospheric neutrino spectrum to higher energy, and second, they are the expected signal of high energy astrophysical neutrinos. In this section we first discuss the relation between a spectrum of neutrinos from any source and the muon flux that it produces. We then review the current status of muons produced by atmospheric neutrinos including the extent to which these measurements restrict the neutrino oscillation interpretations of the contained event anomaly. In later sections of the paper we use the formulas of this section to discuss possible signals of high energy astrophysical neutrinos.

3.2.1 Neutrino-induced muons

The detection of neutrino interactions inside the detector volume becomes more difficult for higher energy neutrinos because of the steeply falling neutrino spectrum. It is possible to enhance the effective volume of the detector by looking for muons generated in charged-current interactions of ν_μ ($\bar{\nu}_\mu$) in the rock below the detector. The effective detector volume is then the product of the detector area and the muon range in rock R_μ . TeV muons have a typical range of one kilometer in rock, which leads to a significant increase in effective detector volume. The technique works only for muons entering the detector from below or near the horizontal (upward going muons), because the the background of downward atmospheric muons dominates any neutrino-induced signal from above.

The average muon energy loss rate is

$$\left\langle \frac{dE}{dX} \right\rangle = -\alpha(E) - \beta(E) \times E, \quad (17)$$

where X is the thickness of material in g/cm^2 . The first term represents ionization losses, which are approximately continuous, with $\alpha \sim 2 \text{ MeV g}^{-1}\text{cm}^2$. The second term includes the catastrophic processes of bremsstrahlung, pair production and nuclear interactions, for which fluctuations play an essential role. Here $\beta \sim 4 \times 10^{-6} \text{ g}^{-1}\text{cm}^2$.

The energy-dependent energy loss rates for each process are tabulated in Ref. [62]. The critical energy above which the radiative processes dominate is

$$E_{\text{cr}} = \alpha/\beta \approx 500 \text{ GeV}. \quad (18)$$

To treat muon propagation properly when $E_\mu > E_{\text{cr}}$ requires a Monte Carlo calculation of the probability P_{surv} that a muon of energy E_μ survives with energy $> E_\mu^{\text{min}}$ after propagating a distance X [63]. The probability that a neutrino of energy E_ν on a trajectory through a detector produces a muon above threshold at the detector is [64,63]

$$P_\nu(E_\nu, E_\mu^{\text{min}}) = N_A \int_0^{E_\nu} dE_\mu \frac{d\sigma_\nu}{dE_\mu}(E_\mu, E_\nu) R_{\text{eff}}(E_\mu, E_\mu^{\text{min}}), \quad (19)$$

where

$$R_{\text{eff}} = \int_0^\infty dX P_{\text{surv}}(E_\mu, E_\mu^{\text{min}}, X). \quad (20)$$

The flux of ν_μ -induced muons at the detector is given by a convolution of the neutrino spectrum ϕ_ν with the muon production probability (19) as

$$\phi_\mu(E_\mu^{\text{min}}, \theta) = \int_{E_\mu^{\text{min}}} P_\nu(E_\nu, E_\mu^{\text{min}}) \exp[-\sigma_{\text{tot}}(E_\nu) N_A X(\theta)] \phi_\nu(E_\nu, \theta). \quad (21)$$

The exponential factor here accounts for absorption of neutrinos along the chord of the Earth, $X(\theta)$. Absorption becomes important for $\sigma(E_\nu) \gtrsim 10^{-33} \text{ cm}^2$ or $E_\nu \gtrsim 10^7 \text{ GeV}$.

The event rate is now simply calculated by multiplying Eq. (21) with the effective area of the detector. One can now tabulate $P_{\nu \rightarrow \mu}$ for a given muon energy threshold and fold it with fluxes of neutrinos of different origin to calculate the expected event rate. Figure 2 shows P_ν for two values of muon threshold energy, 1 GeV and 1 TeV. The solid lines are for ν and the dashed lines for $\bar{\nu}$.

There is some uncertainty in the calculation of the neutrino cross sections for $E_\nu \gg 10 \text{ TeV}$ because of the required extrapolations of the structure functions to small $x \ll 10^{-4}$. We have used the charged current cross section of Ref. [65]. For back-of-the-envelope calculations $P_\nu(E_\nu, 0)$ can be approximated by two power laws (shown by the straight lines for the 1 GeV case in Fig. 2):

$$\begin{aligned} P_{\nu \rightarrow \mu} &\simeq 1.3 \times 10^{-6} E^{2.2} \quad \text{for } E = 10^{-3} \text{--} 1 \text{ TeV} \\ &\simeq 1.3 \times 10^{-6} E^{0.8} \quad \text{for } E = 1 \text{--} 10^3 \text{ TeV} \end{aligned} \quad (22)$$

where E is in TeV. The two energy regimes directly reflect the energy dependence of the neutrino cross section and the effective muon range in Eq. (19). $\sigma_\nu \sim E$ at low energy followed by a slower energy dependence above 1 TeV reflecting the effect of the W propagator. The muon range makes a transition from increasing linearly to constant behavior in a similar energy range.

3.2.2 Atmospheric neutrinos above 1 GeV

The atmospheric neutrino spectrum is quite steep at high energy, approaching $E^{-(\gamma+2)} \approx E^{-3.7}$ for $E \gg 1 \text{ TeV}$ (see Eq. 9). For this reason, despite the increase of P_ν with energy, the contribution to the upward muon flux from atmospheric neutrinos with $E > 10 \text{ TeV}$ is small. We illustrate this in Fig. 3, which shows the distribution of energies of atmospheric neutrinos that gives rise to upward muons. In this example, “throughgoing” is defined as $E_\mu > 4 \text{ GeV}$ and “stopping” as $1 < E_\mu < 4$, and the fluxes are averaged over all angles below the horizontal. The response curve for contained interactions is shown for comparison.

The upward going neutrino rate has been measured with significant statistical accuracy by three experiments—IMB [66,67], Baksan [68] and Kamiokande [69]. Since the experimental arrangements, biases and effective areas as a function of the zenith angle are quite different, it is impossible to compare these results exactly. One can, however, scale the quoted experimental E_μ^{min} to a common value of 3 GeV, which is the effective threshold at

Kamiokande.¹ The data are converted using Eq. 21 for each angular bin. A comparison between angular distribution of upward muons, measured by the three experiments is shown in Fig. 4. The quoted muon energy thresholds, measured rates averaged over the upward hemisphere and the rates converted to a common threshold are given in Table 2. The units are $10^{-13}\text{cm}^{-2}\text{s}^{-1}\text{sr}^{-1}$. The numbers in the last column of Table 2 are to be compared with a calculation of the upward muon flux due to atmospheric neutrinos. Calculated values range from 1.95 to 2.36, depending on the neutrino cross section and muon flux used for the calculation [70]. Given the experimental errors and uncertainties in the input to the calculations, the observed rates are consistent with expectation.

Table 2: Measured upward muon rates (*data*) *shifted* to a common threshold.

Experiment	$E_{\mu}^{\text{min}}(\text{GeV})$	<i>data</i>	<i>shifted</i>
Baksan [68]	1.0	2.77 ± 0.17	2.08
IMB [66,67]	2.0	2.26 ± 0.11	1.92
Kamioka [69]	3.0	2.04 ± 0.13	2.04

The question then arises whether the agreement between calculation and measurement of upward muons is good enough to rule out some possible explanations of the contained event anomaly in terms of neutrino oscillations. We first note that the “allowed region” [11] of parameter space for explanation of the contained event anomaly in terms of $\nu_{\mu} \leftrightarrow \nu_{\tau}$ oscillations should lead to a significant depletion of the neutrino-induced muon flux.

For example, for $\delta m^2 = 8 \times 10^{-3} \text{ eV}^2$, and $L = 10^4 \text{ km}$ (a typical propagation distance for an upward neutrino that interacts below the detector) the first node of

$$1 - P_{\nu_{\mu} \rightarrow \nu_{\mu}} = P_{\nu_{\mu} \rightarrow \nu_{\tau}} = \sin^2 2\theta \sin^2 \left(1.27 \delta m^2 \frac{L_{\text{km}}}{E_{\text{GeV}}} \right) \quad (23)$$

is at $E = 65 \text{ GeV}$. This energy is in the middle of the energy range important for generation of neutrino-induced upward muons (see Fig. 3). Thus, for large mixing angles the upward muon flux would be significantly suppressed, approaching the level of $1 - \frac{1}{2} \sin^2 2\theta$ for $L \delta m^2 / E \gg \pi/2$.

Zenith angle dependence of the neutrino signal probes oscillation lengths L varying from ~ 10 (downwards) to 10^4 km (upward). For small values of E and large values of L the value of the second \sin^2 in Eq. (23) will average to $1/2$ and the zenith angle dependence will not be observable. This is the case for the contained events. Explicit variation with zenith angle may be observable for higher energy neutrinos if the contained event anomaly is due to neutrino oscillations.²

¹Kamiokande does not use a sharp threshold of $E_{\mu}^{\text{min}} = 3 \text{ GeV}$. Rather, the definition of a throughgoing muon is any muon with a projected trajectory $> 7 \text{ m}$ inside the detector which actually exits from the detector.

²There is a hint of such behavior in the recent Kamiokande preprint [71], received after this manuscript was prepared.

The major sources of uncertainty in Eq. (21) are the neutrino flux and, to a lesser extent, the charged current cross section in the relevant energy range from ~ 1 to $\sim 10^4$ GeV. Various calculated values of the neutrino flux are listed in Table 3 at three characteristic energies. In the most important region for upward, throughgoing muons the calculations differ by as much as 17%. Different standard parametrization of the charged current cross sections also differ by as much as 13%.

Table 3: $\frac{dN}{d \ln E_\nu} (\nu_\mu + \bar{\nu}_\mu, \text{ cm}^{-2} \text{ s}^{-1} \text{ sr}^{-1})$

	10 GeV	100 GeV	1000 GeV
Volkova [72]	6.0×10^{-4}	6.1×10^{-6}	4.5×10^{-8}
Mitsui [73]	6.3	6.2	4.1
Butkevich [74]	7.3	6.9	4.2
Bartol [75]	6.9	7.2	4.7

Both IMB [66] and Kamiokande [69] used low values of the cross section [76] and the neutrino flux [72] as central values for comparison with their data. In Ref. [70] it was shown that, with this input the Kamiokande data on throughgoing muons rule out a region of parameter space for $\nu_\mu \leftrightarrow \nu_\tau$ oscillations for $\sin^2 2\theta > 0.4$ and $\delta m^2 \gtrsim 5 \times 10^{-3}$. This is very similar to the excluded region obtained by the IMB group starting from the same assumptions.

When a better representation of the cross section [77] and a higher neutrino flux [74] are used, however, the region excluded by upward, throughgoing muons is much smaller. In particular, much of the region “allowed” by the Kamiokande contained events [11] is also allowed by the Kamiokande measurement of upward muons. In the further numerical examples below the neutrino cross section and flux used for calculations correspond to these higher inputs [77,74].

Although consistent conclusions seem to emerge from interpretation of the Kamiokande and IMB data on upward muons, the same cannot be said for Baksan. The Baksan group still exclude most of the Kamiokande “allowed” region even when they use the highest neutrino flux calculation [74]. The Baksan limit on $\nu_\mu \leftrightarrow \nu_\tau$ oscillations is based on upward events near the vertical, specifically zenith angles in the interval $-1 < \cos \theta < -0.6$.

They observe 161 upward muons in this angular range during a live time of 7.15 years. With the low neutrino flux [72] they expect 142, as compared to 163 with the high neutrino flux [74]. In the comparable angular region the Kamiokande measurement is $(1.42 \pm 0.18) \times 10^{-13}$ upward muons per $(\text{cm}^2 \text{ s sr})$. The calculated result with high flux is 1.76 and with low flux 1.55. The prediction of Kamiokande with the high neutrino flux but assuming $\nu_\mu \leftrightarrow \nu_\tau$ oscillations is 1.34 (instead of 1.76), which is completely consistent with the experimental value of 1.42 ± 0.18 . This is for $\sin^2 2\theta = 0.5$ and $10^{-2} < \delta m^2 < 10^{-1} \text{ eV}^2$. The preliminary result from MACRO [78] is similar to the Kamiokande result: they measure $74 \pm 9 \pm 8$ events as compared to a calculated number for the same exposure of 101 ± 15 .

In summary, therefore, we conclude that the present data on upward muons *do not* rule

out a $\nu_\mu \leftrightarrow \nu_\tau$ oscillation at a level sufficient to explain the contained event anomaly. A tenfold increase in statistics would help resolve the situation, particularly if the full zenith angle range can be measured accurately. For example, with $\delta m^2 \sim 0.1 \text{ eV}^2$ the flux would be significantly suppressed near the horizontal as well as for $\cos\theta < -0.2$, but for $\delta m^2 \sim 0.01 \text{ eV}^2$ the near horizontal flux would not be suppressed.

The IMB group points out that the fraction of upward muons that stop in the detector is relatively insensitive to uncertainties in the calculation because the flux normalization cancels. They find [66] that the measured fraction of stopping muons rules out a portion of the $(\delta m^2, \sin^2\theta)$ plane for $3 \times 10^{-4} < \delta m^2 < 10^{-2} \text{ eV}^2$ and large mixing angle. The constraint on the δm^2 parameter from the fraction of stopping muons comes from the absence of a distortion of the muon energy spectrum. The relevant neutrino energies are illustrated in Fig. 3. For example, if $\delta m^2 \sim 10^{-3} \text{ eV}^2$ the transition probability (23) is relatively large for $E_\nu \sim 10 \text{ GeV}$ (and $L \sim 10^4 \text{ km}$) but negligible for $E_\nu \sim 100 \text{ GeV}$. In this case one would have a significant distortion of the energy spectrum of upward muons and hence an anomaly in the stopping fraction provided the mixing angle is sufficiently large. On the other hand, if $\delta m^2 \gtrsim 10^{-2}$ then both the high and low energy portions will be affected similarly and no distortion of the stopping/throughgoing ratio would occur.

It should be mentioned that the IMB constraint from the stopping fraction is based on use of a single neutrino flux calculation [72]. It therefore reflects a particular assumption about the slope of the primary cosmic ray spectrum and other factors that could affect the shape of the neutrino spectrum. One example of such a factor is the uncertainty in the production of kaons, because kaons contribute about 50% of the throughgoing signal but only about 25% of the stopping muons. Nevertheless, as Table 3 illustrates, the uncertainty in shape is less than the uncertainty in normalization.

3.3 Neutrinos and Muons from Charm production

So far in discussing atmospheric neutrinos we have considered only those which come from decay of pions, kaons and muons. The (semi)-leptonic decay of charmed particles, produced in the interactions of cosmic rays in the atmosphere, is also a source of atmospheric muons and neutrinos—the “prompt” leptons. These prompt leptons are also described by Eq. (9), but with a much larger value of $\epsilon_{\text{charm}} \sim 10^4 \text{ TeV}$, which is a consequence of the short lifetime of charmed particles. Charmed particles almost always decay before they interact in the atmosphere.

Thus, whereas the spectrum of conventional muons and neutrinos becomes one power of energy steeper than the primary spectrum for $E \gtrsim 1 \text{ TeV}$, the prompt leptons continue with the same power as the primary spectrum to much higher energy. Prompt leptons eventually dominate the atmospheric spectra at energies above 10–100 TeV as a result of their flatter energy spectrum. For this reason, an estimate of prompt neutrinos is important for estimating the background for astrophysical neutrinos. Prompt neutrinos and muons have a characteristic isotropic angular distribution, in contrast to the characteristic $\sec\theta$ dependence of the decay products of pions and kaons above $\sim 1 \text{ TeV}$ (see Eq. 9).

Searching for an isotropic component of the atmospheric muon spectrum with deep underground detectors is a traditional technique to look for a prompt component and hence to estimate the charm cross section. Underground detectors exploit the depth-intensity rela-

tions for muons in order to obtain different muon thresholds. There is some weak evidence [79,80] for a prompt muon component at a level corresponding to one prompt muon for every 1000 pions produced at the same energy. Because of the small probability for pion decay at high energy, this would actually correspond to a rather large charm cross section. The raw measurements are, however, difficult to interpret [81]. This is not surprising as there are many problems in detecting prompt muons with underground experiments [82].

It is also difficult to predict accurately the flux of prompt leptons because the experimental status of charm production at laboratory energies is rather confusing. Especially large uncertainties are associated with the production of mesons and baryons in the Feynman $x_f \rightarrow 1$ region. As is the case for strange particles, the (forward) $x_f \rightarrow 1$ behavior is expected to vary strongly with the nature of the produced particle. Neutrino and muon fluxes are rather sensitive to the behavior of the cross section at large x_f because of the steep parent cosmic ray spectrum. Theory cannot come to the rescue. Perturbative calculations are unreliable at low energies because of their sensitivity to the assumed quark mass and renormalization scale. Because charm is predominantly produced by the fusion of gluons at high energies, the cross section critically depends on the low- x behavior of the gluon structure function which is poorly or totally unknown depending on the energy [83]. A calculation of the high-energy charm cross section is actually beyond the scope of perturbative QCD because it requires the resummation of large logarithms of $1/x$ [84].

Prompt neutrino (or muon) fluxes corresponding to five parametrizations of the high energy behavior of the charm production cross section [82] are shown in Fig. 5 (solid lines). For comparison, we also show the conventional muon flux from the decay of pions and kaons. The left dashed line is for vertical muons and the right for horizontal. The prompt curves represent both neutrino and muon fluxes which are very nearly identical for two-body decays of massive particles into light leptons. The prompt muon flux from charm decay is independent of zenith angle up to 10^8 GeV.

In contrast, the conventional muon and neutrino fluxes have a strong dependence on zenith angle, with a ratio of vertical to horizontal fluxes approaching an order of magnitude at high energy.

Prompt production dominates above an energy whose value depends on zenith angle and, of course, on the assumption for the high-energy charm cross section. This cross-over energy is lower for neutrinos than for muons because the conventional muon flux exceeds the conventional neutrino flux. The five models for the hadroproduction of charm are discussed in detail in reference [82]. As an extreme guess on the high side they assume a charm production cross section which is 10% of the total inelastic cross section, σ_{in} [85]. It behaves like $\log^2(s)$ at high energies. The model is inspired by the fact that a high energy gluon fragments 10% of the time into charm particles, and its applicability is limited to energies above a few TeV since at lower energies it violates charm cross-section measurements from accelerator experiments [86]. As a lower limit they evaluated the charm cross section from leading order perturbation theory [87] using relatively hard parton distributions. Some interesting results have been obtained by an X-ray chamber array measuring the vertical muon spectrum up to 50 TeV [88]. These data rule out the highest parametrization shown in Fig. 5, which is not totally surprising as it also overestimates the accelerator data at low energy. We therefore consider the curve labelled *B* in Fig. 5 to be the upper limit for the atmospheric background of neutrinos above 100 TeV.

3.4 Neutrinos and Muons in Horizontal Air Showers

Cosmic rays with energy of order 100 TeV and higher initiate air showers which penetrate deeply enough to be studied with particle detectors at ground level. The detected flux is a steeply falling function of zenith angle because the depth of atmosphere traversed by a cascade reaching the ground rises rapidly from 1030 to 36000 g cm⁻² as the zenith angle varies from zero to 90 degrees. Thus near the horizon (90°), close to a thousand radiation lengths of matter separate the interaction from the detector, and the configuration of the experiment is analogous to that of any accelerator-based beam dump experiment. Most secondaries such as pions and kaons are absorbed in the dump and only penetrating particles, such as muons and neutrinos produced in the initial interaction, reach the detector. High energy muons will traverse the atmosphere and occasionally lose energy by catastrophic photon bremsstrahlung. If the photon shower is produced close to the detector it will be recorded and is referred to as a horizontal air shower. Because horizontal air showers are a signature for penetrating particles in general, they can also be used to search for cosmic neutrinos, so we discuss them in some detail. For comparable muon and neutrino spectra, muons will dominate the horizontal air shower flux as a result of their larger interaction cross section. Therefore energetic atmospheric muons constitute the main background for horizontal air showers from cosmic neutrinos.

High energy muons produced in cosmic ray interactions in the first layers of the atmosphere, will radiate hard bremsstrahlung photons that initiate electromagnetic cascades. If the bremsstrahlung interaction occurs close to the particle detector the cascade will be registered. Neutrinos can similarly interact deep in the atmosphere and deposit a fraction y of their energy in particles which produce an electromagnetic shower close to the detector. The horizontal shower rate ϕ_{sh} is determined by convolution of i) the flux of parent muons or neutrinos ϕ_{par} and ii) the y -differential interaction cross section of the parent particles integrated over the atmospheric depth t at a given zenith angle,

$$\phi_{sh}(N_e) = \int_0^{t_{max}} dt \int_0^1 \frac{dy}{y} \phi_{par} \left(E_{par} = \frac{E(N_e, t)}{y} \right) \frac{d\sigma}{dy} \frac{dE}{dN_e}, \quad (24)$$

using the following notation for the differential and integral shower size spectra

$$\phi_{sh}(N_e) = \frac{d^4 N_{sh}}{dN_e dt dA d\Omega}, \quad (25)$$

$$\Phi_{sh}(N_e) = \int_{N_e}^{\infty} dN_e^* \phi_{sh}(N_e^*). \quad (26)$$

The notation for the parent spectrum ϕ_{par} is the same. For a given shower size and depth of first interaction the energy of the shower is fixed, on average, by the depth development of the cascade. This is the meaning of $E(N_e, t)$ in Eq. (24). This development is somewhat different for purely electromagnetic, hadronic or mixed showers. As a rule of thumb the shower size at maximum is roughly the half the energy in GeV units.

Calculation of the rates of horizontal cascades with fixed shower size N_e are discussed in detail in Refs. [89,82]. Both analytic and Monte Carlo calculations can be made [96]. Starting from the horizontal rate as given in Eq. 24, the number of observed showers above

a given size and angle is given by

$$N_{shower}(N_e > N_0, \theta > \theta_0) = T \int_{N_{e0}}^{\infty} dN_e A(N_e) \int_0^{\Omega_0} d\Omega \phi_{sh}(N_e, \theta) \quad (27)$$

where $A(N_e)$ is the effective area of the array and T is the observation time. The method described above has been used to calculate the horizontal air shower rates, shown in Fig. 18, associated with the muon fluxes of conventional and charm origin from Fig. 5.

Horizontal shower sizes in the range $N_e = 10^3$ – 10^5 have been extensively studied by the University of Tokyo [90], and their observed rate of showers with zenith angle $\theta > 70^\circ$ is consistent with production by conventional atmospheric muons [91]. The EASTOP group have also reported very recently a measurement of horizontal air showers with $\theta > 75^\circ$ that is consistent with a muonic origin [92].

For shower sizes above 10^5 the AKENO group has published an upper bound on muon-poor, air showers with zenith angle greater than 60° [93]. The bound is obtained by selection of muon poor showers in order to isolate purely electromagnetic showers initiated by bremsstrahlung photons from muons [94]. The high energy muon fluxes from charm decay are therefore bounded by this data which provide us with indirect, but relevant information on the charm production cross section. This is illustrated in Fig. 6. It is clear that the largest charm cross sections are ruled out by both the data of the University of Tokyo or by the AKENO bound.

It is interesting to point out that the differential muon spectrum from prompt decays at energy E_μ reflects pp interactions of average lab energy roughly a factor 10 (8) times the muon energy, for a 2.7 (3) spectral index [95,96]. The measurements for largest E_μ [88] thus correspond to an average proton lab energy around 500 TeV. Measurements of horizontal shower of sizes above 10^5 correspond to a primary photon energy of around 100 TeV, which has been on average produced by a primary p -air collision of lab energy of order 1.7 PeV just beyond the reach of TEVATRON. The AKENO bound extends the average energy reach for prompt production even further, to close to 100 PeV of laboratory energy, although the information should be taken with care. Firstly, there is some inconsistency between the rate of horizontal showers measured by the university of Tokyo and the bound [93]. Secondly, the measurement relies on selecting muon poor showers at zenith angles above 60° , and contamination from ordinary cosmic ray showers can be a problem. The already difficult selection of muon poor showers is further complicated by the presence of the original muon that gave rise to the bremsstrahlung photon. For a more detailed discussion of the relevance of this data to the charm cross section we refer the reader to reference [96].

4 Gamma ray astronomy

Many authors have discussed candidate point sources of \gtrsim TeV neutrinos, especially in connection with reported observations of air showers from point sources. Possible sources include accreting X-ray binaries [97,98,99], compact binary systems with interacting winds [100], a neutron star engulfed by a giant companion [98,101] and young supernova remnants [102,103,104,105].

There are two approaches to computing the signal expected from such sources. The first starts from observations (or limits) on photon signals from candidate sources. If the photons

are products of decay of neutral pions, then one expects a comparable flux of ν_μ . Photons can also be produced by electrons through synchrotron radiation, bremsstrahlung and inverse Compton scattering. To be as certain as possible that one is dealing with π^0 γ -rays it is therefore desirable to look in an energy range above that accessible to electrons, which are typically limited to energies in the TeV range by ambient magnetic fields. We use limits of observations on photons in the 100 TeV range, i.e. from air shower experiments. Typical limits for steady emission from point sources are in the range [106,107,108,109,110,111]

$$\frac{dN_\gamma}{d \ln E_\gamma} = E_\gamma \phi_\gamma \lesssim 10^{-13} \text{ cm}^{-2} \text{ s}^{-1} \quad (28)$$

for $E_\gamma \sim 100$ TeV. Limits on certain Northern hemisphere sources obtained using the muon rejection technique are somewhat lower, approaching $10^{-14} \text{ cm}^{-2} \text{ s}^{-1}$ [112].

To find the implied limit on the corresponding neutrino flux requires knowing the relation between photons and neutrinos at production and the fraction of the produced photons that is absorbed in the source. The latter is highly uncertain. For a spectrum of photons from π^0 -decay of the form

$$\phi_\gamma = \text{Const} \times E_\gamma^{-\alpha} \quad (29)$$

the corresponding spectrum of neutrinos from decay of π^\pm is

$$\phi_\nu = \text{Const} \times (1 - r_\pi)^{\alpha-1} \times \frac{1}{1 - A_\gamma}, \quad (30)$$

where A_γ is the fraction of photons absorbed at the source (which may in general be energy-dependent). For $\alpha \gtrsim 2$ the kinematic factor is approximately $\frac{1}{2}$. When ν_μ from decay of muons are added, the summed flux of $\nu_\mu + \bar{\nu}_\mu$ is approximately equal to the photon flux at production [24].

We can convolve the neutrino flux (30) corresponding to the limit (28) with the charged current neutrino cross section and muon range (see Eq. 21) to obtain a limit on the upward muon rate. For spectral index γ in the range 1.1 to 1.3, we find

$$\text{Flux}(\uparrow \mu) \lesssim \frac{2 \text{ events } (E_\mu > 1 \text{ TeV})}{10^5 \text{ m}^2 \text{ yr}} \times \frac{1}{(1 - A_\gamma)}. \quad (31)$$

The total number of upward muon events with $E_\mu > 1$ GeV is only a factor of two larger for such a flat spectrum.

A source producing at this limit and having $A_\gamma \gtrsim 0.98$, i.e. a factor 50 enhancement of the neutrino relative to the photon flux, would be detectable in DUMAND in the sense of giving ~ 20 events per year in $2 \times 10^4 \text{ m}^2$ with $E_\mu > 1$ TeV. (The exact number depends on “details” such as the location of the source relative to the detector, which determines the fraction of the time it is sufficiently below the horizon to produce a signal.)

The photon absorption factor A_γ could be much larger (e.g. in the case of the neutron star swallowed by a giant star), but this would be at the expense of requiring still greater power at the source.³ This leads to the other approach to estimating likely neutrino fluxes from

³It is shown in Ref. [113] that the power of a hidden source cannot be increased indefinitely without making the object so hot and bright as to violate observations.

various sources. It is straightforward to calculate the power in accelerated protons required to give a detectable signal of neutrino-induced muons independent of any model of photon reabsorption. The result depends on the distance to the source, the assumed spectral index and the fraction of the accelerated proton beam that interacts. Estimates [113,114] show that a power of about 10^{39} to 10^{40} erg/s of accelerated protons is required for a source at the distance of the Galactic radius to produce a detectable signal in DUMAND, assuming a fully absorbed proton beam. This could be a young supernova remnant or a young pulsar. A system accelerating particles with a power of 10^{38} erg/s (e.g. an X-ray binary accreting at the Eddington limit for a solar mass star with a large efficiency for converting accretion energy into high energy particles) would have to be relatively nearby (~ 1 kpc) to be detectable.

Recently the Whipple collaboration reported the observation of TeV (10^{12} eV) photons from the giant elliptical galaxy Markarian 421 [115], an observation which might be directly relevant to our quest for sources of high energy neutrinos. With a signal in excess of 6 standard deviations, this is the first convincing observation of TeV gamma rays from outside our Galaxy. That a distant source like Markarian 421 can be observed at all implies that its luminosity exceeds that of galactic cosmic accelerators such as the Crab, the only source observed by the same instrument with comparable statistical significance, by close to 10 orders of magnitude. The Whipple observation implies a Mkn 421 photon luminosity in excess of 10^{43} ergs per second. It is interesting that these sources have roughly the same flux of energy per logarithmic energy interval in the TeV region as in the GeV region.

Why Markarian 421? Whipple obviously zoomed in on the Compton Observatory catalogue of active galaxies (AGN) known to emit GeV photons. Markarian, at a distance of barely over 100 Mpc, is the closest blazar on the list. Stecker et al. [116] recently pointed out that TeV gamma rays are efficiently absorbed on infra-red starlight, anticipating that TeV astronomers will have a hard time observing 3C279 at a redshift of 0.54. Production of e^+e^- pairs by TeV gamma rays interacting with IR background photons is the origin of the absorption. The absorption is, however, minimal for Mkn 421 with $z = 0.03$, a distance close enough to see through the IR fog.

This observation was not totally unanticipated. Many theorists [117] argue that blazars such as Mkn 421 may be powerful cosmic accelerators producing beams of very high energy photons and neutrinos. Acceleration of particles is by shocks in the jets which are a characteristic feature of these radio-loud active galaxies. Many arguments have been given for the acceleration of protons as well as electrons. Inevitably beams of gamma rays and neutrinos from the decay of pions appear along the jets. The pions are photoproduced by accelerated protons on the dense target of optical and UV photons in the galaxy. The latter are the product of synchrotron radiation by electrons accelerated along with the protons. There are of course no neutrinos without proton acceleration. The arguments that protons are indeed accelerated in AGN are rather compelling. They provide a “natural” mechanism for i) the energy transfer from the central engine over distances as large as 1 parsec, ii) the heating of the dusty disc over distances of several hundred parsecs and iii) the near-infrared cut-off of the synchrotron emission in the jet. Protons, unlike electrons, efficiently transfer energy in the presence of the magnetic field in the jet. A detailed case for proton acceleration in active galaxies is made in reference [118].

Other possible models for the emission of gamma radiation up to 1 TeV from Mkn 421 involves inverse Compton scattering by accelerated electrons, rather than π^0 γ -rays

[119,120,121]. Such models therefore do not predict a corresponding flux of high energy neutrinos.

5 Guaranteed Sources of High Energy Neutrinos: the Galactic Plane and the Sun

By their very existence, high-energy cosmic rays do guarantee the existence of a definite source of high energy cosmic neutrinos [122]. Cosmic rays interact with the interstellar gas in our galaxy and are therefore inevitably accompanied by a flux of diffuse photons and neutrinos which are the decay products of the pions produced in these interactions. A rough estimate of the diffuse fluxes of gamma rays and neutrinos from the galactic disk can be obtained by convoluting the observed cosmic ray flux with interstellar gas with a nominal density of 1 particle per cm^3 . The target material is concentrated in the disk of the galaxy and so will be the secondary photon flux. Its observation would reveal “point sources” associated with molecular clouds and the spiral arm of the galaxy.

An estimate of the expected fluxes at TeV and PeV energy can be easily performed under the assumption of a constant cosmic ray density in the Galaxy. Imagine a concentration of matter of density ρ and linear dimension R . For example, the flux at Earth of photons generated by pions produced in cosmic ray interactions with this matter is given by

$$\Phi_{\gamma(\nu)} = \Phi_{CR} f_A \left[\frac{\sigma_{\text{inel}}}{m_N} \right] [\rho R] \frac{2Z_{N\pi^0}}{\gamma + 1}, \quad (32)$$

where $\Phi_{CR} \approx 1.8 E^{-2.7} \text{ cm}^{-2}\text{sr}^{-1}\text{s}^{-1}\text{GeV}^{-1}$ is the cosmic ray intensity, σ_{inel} is the total inelastic pp cross section, m_N is the nucleon mass and ρR is the column density of the source. The quantity $Z_{N\pi} = 1/\sigma \int dx x^\gamma d\sigma/dx$ is the spectrum-weighted moment for production of pions by nucleons with differential energy spectrum $E^{-(\gamma+1)}$, and $f_A (\simeq 1.22)$ is a correction factor to account for the fact that some primaries and targets are nuclei [123]. As noted in the previous section, the differential spectrum of $\nu + \mu + \bar{\nu}_\mu$ is very nearly equal to the that of photons after accounting for muon decay.

In a detailed calculation, as recently performed by Berezhinsky et al. [124], one must explicitly account for the energy dependence of the inelastic cross-section, of the particle physics parameters and of the spectral index γ . Nevertheless, Eq. (32), which neglects these energy dependences, can be used to make adequate first order estimates of the γ -ray and neutrino fluxes. Equation (32) states that the photon to cosmic ray ratio is directly proportional to the linear matter density ρR . The ratio is of order 6×10^{-5} for a column density of 0.1 grams/ cm^2 . Maps of the galactic linear column density can therefore be directly translated into photon or neutrino fluxes with the assumption that the cosmic ray density in the Galaxy is constant at its local value. The predicted flux is of order 10^{-5} of the cosmic ray flux in the PeV energy range, with the different estimates varying within “a factor”. Observation of a photon flux at this level has turned out to be challenging. The best experimental limits [125] are still an order of magnitude higher than expectation [124].

It is clear that a roughly equal diffuse neutrino flux is produced by the decay of charged pion secondaries in the same collisions. For example, from Eq. (32), and assuming a threshold of $E_\mu > 1 \text{ TeV}$, we can estimate the number of neutrino events from within 10 degrees of the

disc as 5 events per year for a 10^5 m^2 detector at the South Pole which views 1.1 steradian of the outer Galaxy with an average density of 0.013 grams/cm^2 . This would be increased to 15 events per year if the spectral index in the outer galaxy were indeed as small as 1.4, as suggested by an analysis [26] of the GeV γ -ray results of the COS-B satellite. Another interesting example is the direction of Orion, a molecular cloud with a column density of 0.04 g/cm^2 and an angular width of 0.07 sr [126]. For this case we estimate 0.3 neutrino-induced muons per year in a 10^5 m^2 detector in this angular bin. There are several gas concentrations of similar or smaller density in the galaxy. These numbers account for the fact that neutrinos are produced by the decay of muons as well as pions. Although these rates are significantly below the atmospheric background, the source is guaranteed and the event rate might be significantly higher if there are regions of the galaxy where the spectrum is flatter than the local spectrum.

The above estimates assume a cosmic ray intensity that is constant throughout the disk of the Galaxy and equal to that measured at Earth. A recent COMPTEL [126] observation of 3 to 7 MeV fluxes from the region of Orion may suggest, however, that the cosmic ray energy density could be significantly higher in that region. The observed γ -ray line intensities (from excited ^{12}C and ^{16}O nuclei) would correspond to cosmic ray energy density of more than 50 eV cm^{-3} , a factor of 100 higher than in the vicinity of the Earth. Although the lines are generated by cosmic ray nuclei of kinetic energy around 10 MeV, which are subject to strong solar modulation inside the solar system, it is quite possible that the cosmic ray density in a wider energy range is significantly higher in this active star-formation region. The limits derived from the COS-B data [127] allow a cosmic ray intensity and respectively neutrino fluxes higher by factor of 5 in the region of Orion.

The other guaranteed extraterrestrial source of high energy neutrinos is the Sun. The production process is exactly the same as for atmospheric neutrinos—cosmic ray interactions in the solar atmosphere. Neutrino production is enhanced because the atmosphere of the Sun is much more tenuous—the scaleheight of the chromosphere is $\sim 115 \text{ km}$, compared with 6.3 km for the upper atmosphere. As a result ϵ_π is higher by a factor of ~ 20 , as is the energy where the slope of the neutrino spectrum increases. The difference is even larger for cosmic rays that enter the Sun at large angles and never reach atmospheric densities higher than 10^{-7} g/cm^3 . A detailed calculation of the neutrino production by cosmic rays in the solar atmosphere [128] shows a neutrino spectrum higher than the angle averaged atmospheric flux by a factor of ~ 2 at 10 GeV and a factor of ~ 3 at 1000 GeV.

The decisive factor for the observability of this neutrino source is the small solid angle ($6.8 \times 10^{-5} \text{ sr}$) of the Sun. Although the rate of the neutrino induced upward going muons is higher than the atmospheric emission from the same solid angle by a factor of ~ 5 , the rate of muons of energy above 10 GeV in a 10^5 m^2 detector is only 5 per year. Taking into account the diffusion of the cosmic rays in the solar wind, which decreases significantly the value of the flux for energies below one TeV, cuts this event rate further by a factor of 3. Folded with a realistic angular resolution of 1 degree, observation of such an event rate also requires a 1 km^2 detector.

6 Possible Galactic Neutrino Sources

In §2 we noted that the galactic cosmic radiation above ~ 100 TeV might be accelerated in compact sources, and that, if so, these would be likely point sources of photons and neutrinos. In §4 it was shown that present limits on ~ 100 TeV gamma rays from potential point sources make it unlikely that there will be prolific galactic point sources of neutrinos. Before discussing several possible types of point sources in more detail, we give an example to set the scale for what may be the maximum reasonable expectation for neutrinos from galactic point sources. We consider a two-component model of the cosmic radiation as described in §2 in which the low energy component steepens around 100 TeV and a high energy component dominates at much higher energies. For this illustration we assume that the high energy component is produced in compact sources scattered in the disk of the Galaxy.

We start by estimating the power that would be needed to supply such a high energy component. In a two-component picture [129] the cosmic ray energy density in energy range between 100 and 1000 TeV is about 10^{-15} erg/cm³, of which about half would be from the high energy component. The local energy density in this component is thus estimated as

$$\rho_E = 5 \times 10^{-16} \text{ erg cm}^{-3}. \quad (33)$$

Assuming this is typical of the energy density elsewhere in the Galaxy, the luminosity of the galaxy in such particles is then

$$\epsilon \times \mathcal{L}_p = \frac{V_{\text{gal}} \rho_E}{\tau} = 1.5 \times 10^{38} \text{ erg s}^{-1}, \quad (34)$$

where V_{gal} is the volume of the galaxy and τ the confinement or lifetime of PeV cosmic rays in the galaxy. The values of these parameters are very uncertain and also depend on the model of propagation and escape of cosmic rays from the Galaxy. The numerical result in Eq. (34) is obtained for $V_{\text{gal}} = 5 \times 10^{66} \text{ cm}^3$ (the volume of the galactic disk) and $\tau = 5 \times 10^5$ year as an estimate of the time cosmic rays spend in the disk. The parameter $\epsilon < 1$ in Eq. (34) is the fraction of the accelerator power required just for the decade above 100 TeV. If we assume that these accelerators produce a hard spectrum with equal energy per logarithmic interval, then the estimate of the total power needed to maintain the steady observed PeV cosmic ray flux is $\mathcal{L}_p \sim 10^{39}$ erg/sec. This source will resupply the galaxy and compensate for the loss of cosmic rays resulting from their limited confinement time [130].

Let us next assume that a comparable amount of energy is absorbed by collisions of protons with gas near the high energy accelerators. Then the total power in neutrinos is related to the neutrino flux at Earth from all compact sources by

$$\mathcal{L}_p D_{p \rightarrow \nu_\mu} D_\nu = \sum_i (4\pi d_i^2) \int dE E \frac{dN_{i,\nu}}{dE} \quad (35)$$

Here $D_{p \rightarrow \nu_\mu}$ ($\simeq 0.3$) is the fraction of energy in an accelerated proton spectrum $\propto E^{-2}$ that goes into $\nu_\mu(\bar{\nu}_\mu)$, D_ν ($\simeq 1$) describes the fraction of neutrinos that escape from the sources and d_i is the distance to the i th source. If there are n such sources distributed throughout the galactic plane, then an estimate of the distance to the nearest source is $d \sim R_g/\sqrt{n}$

where $R_g \sim 10$ kpc is a nominal radius of the disk in which the sources are concentrated. If each source has a particle luminosity of \mathcal{L}_p/n , then number of sources cancels in the relation between the total cosmic ray luminosity \mathcal{L}_p and the neutrino luminosity of a “nearest neighbor” source [131]. One has

$$\int dE E \frac{dN_{i,\nu}}{dE} = \frac{\mathcal{L}_p D_{p \rightarrow \pi} D_\nu / n}{4\pi R_g^2 / n}, \quad (36)$$

from which we estimate the neutrino flux from a nearby source as

$$E \frac{dN_\nu}{dE} = 2 \times 10^{-11} \frac{100 \text{ TeV}}{E} \text{ cm}^{-2} \text{ s}^{-1}, \quad (37)$$

assuming an E^{-2} spectrum. Such a flux of high energy $\nu_\mu + \bar{\nu}_\mu$ would give some 300 events per year in 10^5 m^2 .

This is a very high flux and should be considered an extreme upper limit for a neutrino-induced signal from a galactic point source. To avoid the existing limits on photons from point sources (28), one would need a factor $A_\gamma \gtrsim 100$ absorption of high energy photons in the source. Absorption arguments depend strongly on the exact mechanism. If photon absorption is due to interactions and cascading on the ambient matter at source, the accelerated protons will also be absorbed, which weakens the original motivation for this estimate. It is, however, not only possible, but likely [132] that the high energy γ -rays would be absorbed in $\gamma\gamma \rightarrow e^+e^-$ collisions on the strong radiation field at the source. In this case the protons will not be absorbed since the photoproduction threshold is $(m_\pi/m_e)^2$ higher and the protons lose very little energy in $p\gamma \rightarrow e^+e^-$ collisions.

The preceding argument is based on an assumed random distribution of point sources in the disk of the galaxy. Because of the cancellation of the number n of sources in Eq. (36), a similar estimate can be made of the neutrino flux from a single source at the galactic center. We note that the upper bound on the > 100 TeV gamma flux from the galactic center is [109] $\sim 2 \times 10^{-13} \text{ cm}^{-2} \text{ s}^{-1}$. There could, however, be significant absorption of a high energy photon source from the galactic center. Thus, as pointed out by Berezhinsky [133], *not* seeing high energy neutrino emission from the center of the galaxy would be an interesting result.

We now look in somewhat more detail at two possible classes of galactic point sources of neutrinos.

6.1 X-ray Binary Systems.

The interest in X-ray binaries was initiated by the reports [134] of detection of UHE ($> 10^{14}$ eV) γ -rays from Cygnus X-3. Such γ -rays would most likely be produced in inelastic hadronic interactions, in which case they would be accompanied by high energy neutrinos. Current upper limits on steady emission from Cygnus X-3 are about an order of magnitude lower than the level implied by the original report, which referred to showers with energies above 2×10^{15} eV. Nevertheless, it is still interesting to consider X-ray binary systems as potential accelerators of UHE cosmic rays and to ask at what level one might expect accompanying neutrino fluxes.

X-ray binaries consist of a compact object (neutron star or a black hole) and a non-compact companion star. Such systems are dynamically complicated, involving mass transfer

from the companion onto the compact object through an accretion disk. Neutron stars are known to have very strong (10^{12} G) surface magnetic fields and sometimes millisecond periods. Both the accretion and the magnetic dipole radiation are possible energy sources. The existence of high magnetic fields and plasma flows creates the environment necessary for the formation of strong shocks, and corresponding particle acceleration. The companion star itself, the accretion flow, or the heavy stellar winds might be targets for inelastic nucleon interactions and neutrino production.

Calculations of the neutrino flux expected from Cygnus X-3 were done independently by different authors [135], and the results agree to better than a factor of two for similar assumptions about the input parameters and the configuration of the accelerated beam and beam dump. The total upward going muon flux for a distance of 10 kpc is $2\text{--}3 \times 10^{-15} \text{ cm}^{-2}\text{s}^{-1}$, i.e. 50–100 upward going muons per 10^5 m^2 per year for a fully efficient detector. Fluxes at this level are well above the atmospheric background for $E_\mu \gtrsim 100 \text{ GeV}$ [64]. Such a large flux corresponds to a proton luminosity at the source of $2 \times 10^{39} \text{ erg/s}$, comparable to the generic estimate in the introduction to this section. The estimated flux is a factor ~ 10 lower here, however, because the models typically assume a 10% duty cycle for the beam to intercept the target mass (e.g. the companion star).

Models motivated by the original Cygnus X-3 observations in which the high energy gamma rays emerge from source obviously cannot be correct for Cygnus X-3 in view of the current limits from air shower observations. Emission of neutrinos in other models in which the photons are absorbed can, however, be obtained by scaling from these calculations by an assumed proton luminosity and the distance of any potential source.

The crucial question then is the luminosity that might be expected from such systems. For accretion powered sources the luminosity is limited by the Eddington luminosity

$$L_{Edd} = 4\pi GMm_p/\sigma_T \text{ erg/s} , \quad (38)$$

which is the maximum X-ray luminosity that will not prevent accretion. Since the proton inelastic cross-section is lower than the Thomson cross section σ_T , technically the proton luminosity can exceed L_{Edd} . On the other hand L_{Edd} can only be achieved at the surface of the neutron star and a realistic luminosity limit depends on the ratio of the neutron star radius to the shock radius R_{ns}/R_s . Thus a reasonably optimistic limit for the proton luminosity will be

$$L_p^{max} = L_{Edd} \times (R_{ns}/R_s) \times (\sigma^{inel}/\sigma_T) , \quad (39)$$

i.e. of the order of or lower than $L_{Edd} = 1.4 \times 10^{38} \times M/M_\odot \text{ erg/s}$, corresponding to a rate of upward TeV muons < 50 events per year in a 10^5 m^2 detector for a source at 10 kpc.

Another potential source of energy in an X-ray binary is pulsar rotation. Harding & Gaisser [100] have studied proton acceleration at X-ray binaries powered by the pulsar through a pulsar wind shock. An absolute upper bound on the energy is the power released by magnetic dipole radiation,

$$L_d = 4 \times 10^{43} B_{12} P_{ms}^{-4} \text{ erg/s} , \quad (40)$$

where B_{12} is the pulsar surface magnetic field strength in 10^{12} G and P_{ms} is the pulsar period in milliseconds. Discussing different X-ray systems, however, they end up with a maximum

proton acceleration luminosity of 6×10^{38} erg/s for Cygnus X-3 with a pulsar period of 12.8 ms [136]. This is still factor of 2 smaller than the luminosities used in the Cygnus X-3 estimates above and illustrates that an X-ray binary has to put almost all of its energy in high energy protons to be detectable in neutrinos. For a more modest X-ray binary at the galactic center that accelerates $1/10 L_{Edd}$ in high-energy protons the actual upward muon rate will be ~ 3 events per 10^5 m^2 per year.

6.2 Young Supernova Remnants

Young supernova remnants are another candidate for production of observable neutrino fluxes [137,138]. If protons are accelerated inside a young supernova remnant, they will interact with the material of the expanding shell and produce γ -rays and neutrinos until the particle adiabatic losses exceeds the collision loss. In the approximation of a uniform density shell of mass M expanding with velocity $v = 10^9$ cm/s this occurs at

$$\tau_a = \left(\frac{3Mc\sigma_{pp}}{4\pi m_H v^3} \right)^{1/2} = 1.3 \times 10^7 \left(\frac{M}{M_\odot} \right)^{1/2} \text{ s}. \quad (41)$$

The active time during which the production is significant is of order 1 year. Two modifications of this idea [139] were motivated by the explosion of SN1987A and the proliferation of detailed supernova models that followed. If one accounts correctly for the velocity distribution of the supernova shell, the γ and ν emission time increases by a factor of three. Also, if the accelerated particles are contained within the shell as it expands the pathlength for collisions will increase and the duration of the signal will be extended for a period estimated in Ref. [139] as ~ 10 years, with a gradual decrease in intensity. If the accelerated protons are not confined in the shell, the duration of the signal would be 1–2 years [140].

All these considerations concern the target for inelastic interactions. The other ingredient is the abundance of accelerated protons at this stage of remnant evolution. The pulsar wind model [139] utilizes the pulsar spin down energy to create a shock inside the contact discontinuity of the shell. The proton luminosity is bounded by the magnetic dipole luminosity of the pulsar given in Eq. (40). The efficiency for producing a signal in such a model depends on the efficiency for accelerating protons and on the degree of mixing between the accelerated particles and the expanding shell. The latter depends on mixing the pulsar wind region with the shell through Rayleigh-Taylor instabilities.

Although it is clear now that SN1987A does not contain a strong pulsar, it is still of interest to discuss the signal that could be expected from a young galactic supernova (~ 10 kpc) with a rapidly spinning, strongly magnetized pulsar. The answer is extremely sensitive to the magnetic field and pulsar period assumed. Both parameters enter into the pulsar power and into the maximum energy. For example, for $P = 10$ ms and $B_{\text{surface}} = 10^{12}$ Gauss and a 25% efficiency for particle acceleration and interaction, the model of Ref. [139] gives 10^{39} erg/sec and $E_p^{\text{max}} \approx 10^5$ TeV. The corresponding neutrino luminosity would be sufficient to produce a signal of ~ 100 upward muons in 10^5 m^2 for several years. For a longer pulsar period and/or a smaller surface magnetic field, both the maximum energy and the available power rapidly decrease.

Berezinsky & Ptuskin [141] argued that acceleration at the supernova blast wave could also produce an observable signal, even though in this case the accelerated particles are not

deep inside the expanding shell. When a supernova expands into the surrounding medium it drives a blast wave ahead. There is also a reverse shock in the supernova ejecta. Particle acceleration occurs at both shocks, with the accelerated particles injected into the respective downstream regions, which are contained between the two shocks. The kinetic energy of the expanding shell is huge (of order 10^{51} erg/s) but the rate at which it is dissipated is limited by the rate at which matter is swept up by the expanding shell. Thus the luminosity from accelerated particles in this region is quite sensitive (quadratically [141]) to the mass loss rate of the progenitor star, which was relatively low for SN1987A. For what is considered a “typical” mass loss rate of $10^{-5} M_{\odot}$ [141], the estimated neutrino flux for a supernova at 10 kpc corresponds to several hundred upward muons with $E_{\mu} > 100 \text{ GeV}$ in the first 100 days [141]. The rate falls off slightly faster than $1/t$.

The big disadvantage of young supernova remnants as potential neutrino sources is, of course, that supernova explosions are rare events. The one that we were lucky to observe, SN1987A, was not only quite distant, in the LMC, but also shows no signs of pulsar activity at a level above $\sim 10^{37}$ erg/s.

7 Possible Extragalactic Sources

Active galactic nuclei are the most luminous objects in the Universe and have long been recognized as possible sources of high energy signals [142]. These first estimates were mostly based on the total AGN power and number density. More recent calculations [143,144] developed the idea in two important ways. They first identified the potential importance of hadrons (especially neutrons) for transporting energy in active galactic nuclei. Secondly, shock acceleration models were at least crudely incorporated into the AGN models, and the photoproduction process was shown to be the most important one for proton energy loss. This led to estimates of the maximum proton energy achievable in acceleration at AGN shocks and to the prediction of high energy neutrino fluxes.

Active galactic nuclei have luminosities ranging from 10^{42} to 10^{48} erg/s, which corresponds to black hole masses from 10^4 to $10^{10} M_{\odot}$ [145] on the natural assumption that they are powered by Eddington limited accretion onto a black hole. AGN’s have generally flat emission spectra with a luminosity up to $\sim 3 \times 10^{46}$ erg/s per decade of energy. In the IR band a steady dust emission is observed, most probably coming from a large region far away from the core. The main thermal feature is the UV bump, which is variable on a timescale of days and weeks [146].

Its energy source is either X-ray heating [147] or viscous heating of the accretion disk [146], either of which would be closely related to the central engine. X-rays have a hard, nonthermal spectrum, variable on even shorter timescales [148], which often cuts off at several MeV. AGN’s have been extensively studied at radio frequencies, where the most general identification is as *radio-loud* or *radio-quiet*, depending on the fraction of energy in the radio portion of the spectrum [149]. Roughly 10% of all observed AGN’s are classified as radio-loud [150]. Blandford [151] suggests that radio-loud AGN’s have rapidly spinning black holes and therefore also strong jets. The UV bump is not always easy to see in radioloud AGN’s.

Two possible sources within AGN’s of intense, high energy neutrino fluxes have been identified. The first is associated with the central engine and the second with production in

jets associated with blazars, which are radio-load AGN's in which the observer is illuminated by the beam of a jet. We first discuss central emission.

7.1 Generic AGN

To introduce most of the parameters important for the production of neutrinos, we briefly describe the spherical accretion model used in most of the calculations of the neutrino production in central regions of AGN's [144,36,152,38]. Some of the limitations of this model will be mention in §7.4 below. The model is based on work performed by Kazanas, Protheroe and Ellison [33,34]. They assume that close to the black hole the accretion flow becomes spherical and a shock is formed where the ram pressure of the accretion flow is balanced by radiation pressure near the black hole. The shock radius is parameterized by $R = x_1 \times R_S$, where R_S is the gravitational (Schwarzschild) radius of the black hole, and x_1 is estimated to be in the range 10 to 100 [38]. The continuous emission is dominated by the ultraviolet and X-ray radiation, which are assumed to emanate from inside the radius enclosed by the shock. Since the region inside the shock is optically thick, the radiation density at the shock can be estimated from the surface brightness of the AGN. This leads to the relation

$$U_{rad} \simeq L \times (\pi R^2 c)^{-1} \quad (42)$$

between luminosity and radiation density in the central region. Since $R = x_1 \times R_S \propto L_{\text{Eddington}}$, it follows from Eq. (42) that $U_{rad} \propto L^{-1}$. Numerically,

$$U_{rad} \sim 2 \times 10^6 \text{erg/s} \times \frac{1}{L_{45}} \times \left(\frac{30}{x_1}\right)^2, \quad (43)$$

where L_{45} is the luminosity divided by 10^{45} erg/s. The radiation energy density also defines the magnetic field value B at the shock under the assumption of equipartition of the radiation and magnetic energy. For the numerical example above $B \sim 7000 \text{ Gauss} \times (L_{45})^{-\frac{1}{2}} \times \frac{30}{x_1}$.

Acceleration of protons is assumed to occur by the first order diffusive Fermi mechanism at the shock, resulting in an E^{-2} differential spectrum that extends up to E_{max} . Energy loss processes occur during acceleration, including $p\gamma \rightarrow N\pi$ and $p\gamma \rightarrow p + e^+ + e^-$ in the dense radiation fields as well as pp collisions in the gas. All three processes contribute an energetic electromagnetic component, either through $\pi^0 \rightarrow \gamma\gamma$ or by production of electrons. Both photo-meson production and pp collisions also give rise to neutrinos via the $\pi^\pm \rightarrow \mu^\pm \rightarrow e^\pm$ decay chain. In the astrophysical environment all unstable particles (except quasi-stable neutrons) decay practically without energy loss. An important detail is that photoproduction of charged pions by protons is dominated by the $n\pi^+$ channel [153].

Although high energy neutrinos escape directly from the core, the electromagnetic component does not. The core is optically thick to photons with energies greater than ~ 5 MeV. All γ -rays generated in the dense photon field immediately lose energy in $\gamma\gamma \rightarrow e^+e^-$ collisions. Inverse Compton/pair-production cascades downscatter all electrons and photons to X-ray and lower energies. The essential ingredient of these models is that the observed X-ray spectrum is produced as the end product of the electromagnetic cascades initiated by high energy photons and electrons produced by the accelerated protons. Thus, estimates of

expected neutrino fluxes from individual AGN's are normalized through the model to their observed X-ray luminosities.

The proton density at the shock, $n_p(R)$, can be estimated from the accretion rate needed to support the black hole luminosity, and from the radius and accretion velocity at the shock. It is

$$n_p \simeq 1.3 \times 10^8 x_1^{1/2} R^{-1.5} L^{1/2} Q^{-1} \text{cm}^3, \quad (44)$$

where Q is the efficiency for converting accretion power into accelerated particles at the shock. Such proton densities are not only a good injection source for proton acceleration, but also a possible target for pp interactions.

The proton energy loss, however, is dominated at high energy by the photoproduction process $p\gamma \rightarrow n\pi^+(p\pi^0)$ simply because the target photon density n_{ph} is much higher than n_p . For thermal radiation with temperature $T^\circ\text{K}$ the density ratio would be

$$\frac{n_p}{n_{ph}} \simeq 2.5 \times 10^{-13} x_1^{3/2} T Q^{-1}. \quad (45)$$

The high cross-section pair production process ($p\gamma \rightarrow pe^+e^-$) is relatively unimportant because of the low proton energy loss per collision. The thermal radiation corresponds to photon energies in the range 1 to 40 eV.

The relative importance of the different energy-loss mechanisms depends in detail on the energy-dependence of the various cross sections and on the intensity and spectral shape of the target radiation field. The detailed calculations [36,38,144,152] use numerical and/or Monte Carlo techniques to follow the production, propagation and cascading of the secondary particles inside the central region and to determine the fluxes of neutrinos, nucleons and X-rays that emerge. Without going into such detail, it is still possible to describe in a semi-quantitative way the basic results, especially the shape and upper limit of the neutrino spectra. To do this, we make use of the approximate form of the radiation field given by Stecker *et al.* [36].

The minimum energy of a target photon for photoproduction by a proton of energy E_p is

$$\epsilon \approx \frac{\Delta^2 - m_p^2}{2E_p} \quad (46)$$

where $\Delta = 1.232$ GeV is the mass of the (3,3) resonance. The collision length of a nucleon against photoproduction is

$$\ell^{-1} = \int \sigma(\epsilon) n(\epsilon) d\epsilon, \quad (47)$$

where $n(\epsilon)$ is the number density of photons (differential in energy). Using a resonance approximation for the cross section gives

$$\ell^{-1} \approx \frac{\pi\Gamma\Delta}{\Delta^2 - m_p^2} \epsilon n(\epsilon) \times \sigma_{\text{peak}}, \quad (48)$$

where $\Gamma \approx 115$ MeV is the width of the Δ resonance and $\sigma_{\text{peak}} \approx 5 \times 10^{-28} \text{cm}^2$. Since $R \propto L$ and $n(\epsilon) \propto U_{\text{rad}} \propto L^{-1}$, the ratio R/ℓ is independent of luminosity in the model. From the spectrum of Ref. [36] one finds that $R/\ell < 1$ above the UV bump, i.e. for $\epsilon > 40$ eV.

From Eq. 46 this corresponds to $E_{\text{crit}} \approx 8 \times 10^6$ GeV. Thus nucleons with energy less than $\sim 10^{16}$ eV can escape from the central region ($r < R$) if they propagate rectilinearly.

Nucleons that escape no longer contribute to the production of secondary photons and neutrinos. This has little effect on the predicted down-scattering into the X-ray region since most of the energy has already been dumped by nucleons with higher energy (provided the accelerated spectrum extends to $E_{\text{max}} \gg 10^{16}$ eV). The assumption made about propagation of protons does, however, have a crucial effect on the predicted neutrino spectrum. If, as assumed by Stecker *et al.* [36], protons travel in straight lines inside the central region, then the neutrino spectrum will follow the proton spectrum only down to an energy roughly

$$\langle \frac{E_\nu}{E_p} \rangle \times 10^{16} \text{ eV} \sim 5 \times 10^5 \text{ GeV}. \quad (49)$$

At lower energy the neutrino spectrum dN_ν/dE_ν will be constant, reflecting the flat momentum distribution of neutrinos produced in a $p\gamma$ collision. If, as seems more likely, protons remain confined in the central region by the same turbulent magnetic fields necessary for the diffusive shock acceleration to work, then the neutrino spectrum will follow the proton spectrum down to much lower energy. Both Refs. [38] and [152] assume that protons will be confined to the central region.

Figure 7 illustrates the difference the assumption of proton confinement makes. It shows the model neutrino spectra ($\nu_\mu + \bar{\nu}_\mu$) for the extragalactic source 3C273. The thin lines show several of the models of Protheroe and Szabo [38], who performed their calculation for x_1 values from 10 to 100 and two different photon target spectra. The thick line represents the model of Stecker *et al.* [36]. For both sources the neutrino spectrum continues to follow the E^{-2} proton spectrum down to low energy in the calculation where the protons remain confined in the central region. Because of the large neutrino flux in the important region around 1 TeV, the models of Szabo and Protheroe generate significantly more upward going muons than predicted by Stecker *et al.* [36].

The slight dip in the spectra of Ref. [38] around 10^4 – 10^5 GeV is caused by proton energy loss to e^+e^- pair production, which dominates proton energy losses for proton energies between ~ 30 and ~ 3000 TeV. This feature is much more prominent in the calculation of Ref. [152] than in Ref. [38]. As a consequence of the larger relative contribution of pair production, the predicted neutrino-induced signal of Ref. [152] is somewhat smaller than that of Ref. ([38]), as shown with a dash line on Fig. 7. Sikora and Begelman [152] give only the spectral shape for a generic source. We have normalized their neutrino spectrum to the 3C273 luminosity. The exact position of the maximum neutrino energy is thus uncertain, because it depends on the parameters of the particular source.

Neutrons are not confined by magnetic scattering in the inner region. Thus neutrons with $E < E_{\text{crit}}$ escape from the central region inside R provided they do not decay first. For the relevant range of parameters, neutrons with energy above a TeV will usually escape. These energetic neutrons decay at distances ranging from ~ 0.01 to ~ 100 parsec, and their decay products can have a profound effect on energy transport in AGN's, for example driving winds [154] and producing radio emission [155] far from the core.

As far as neutrinos are concerned, the escape of neutrons from the core has an interesting consequence for the shape of the spectrum of electron antineutrinos. The dominant channels for photoproduction of charged mesons by nucleons are $p\gamma \rightarrow n\pi^+$ and $n\gamma \rightarrow p\pi^-$. The

kinematics of the $\pi^+ \rightarrow \mu^+ \rightarrow e$ decay chain is such that the flux of ν_μ from pion decay is approximately equal to the flux of $\bar{\nu}_\mu$ from muon decay, and vice versa for decay of π^- . Thus from protons one has roughly equal fluxes of ν_μ , $\bar{\nu}_\mu$ and ν_e from the π^+ . The neutron chain leads to $\bar{\nu}_e$ instead of ν_e . Thus for $E > E_{\text{crit}}$, when both neutrons and protons interact inside the core region, the flux of $\bar{\nu}_e$ is nearly equal to the flux of ν_e (only slightly suppressed by the small energy loss of the nucleon in $p\gamma \rightarrow n\pi^+$). At lower energies, the neutrons escape before interacting. One then gets $\bar{\nu}_e$ from $n \rightarrow p e^- \bar{\nu}_e$, with, however, a strong kinematic suppression because of the very small energy transfer to the leptons in β -decay of the neutron. For $\bar{\nu}_e$ from neutron β -decay, the spectrum of $\bar{\nu}_e$ is a factor $\sim 5 \times 10^{-4}$ lower than the parent neutron spectrum, as compared to a factor of about 5×10^{-2} when $E > E_{\text{crit}}$ and the process $n + \gamma \rightarrow \pi^- \rightarrow \mu^- \rightarrow \bar{\nu}_e$ can occur.

As it turns out, the photoproduction in the UV bump also limits the maximum proton acceleration energy E_p^{max} , and hence the maximum neutrino energy. This differs from the situation in a more diffuse environment, such as acceleration by a supernova blast wave expanding into the interstellar medium. In that case the upper limit is determined by the characteristic lifetime of the shock. (See the discussion of Eq. 11 above.) E_p^{max} is roughly proportional to $L^{\frac{1}{2}}$, reaching a value of 10^{17} eV for $L = 10^{45}$ erg/s, with at least a factor of two uncertainty [38].

This maximum energy can be estimated by comparing the acceleration rate (11) to the energy loss rate, $K_{\text{inel}} E_p c / \ell$. The acceleration rate in this case is

$$\frac{dE}{dt} \sim 0.1 \frac{u^2}{c} eB \approx 2 \times 10^5 \text{ GeV s}^{-1} \times \frac{30}{x_1} \times (L_{45})^{-\frac{1}{2}}, \quad (50)$$

where we have used the equipartition estimate of the magnetic field from Eq. (43). Since (see Eq. 47) $\ell^{-1} \propto n(\epsilon) \propto L^{-1}$, we estimate

$$E_p^{\text{max}} \propto L^{\frac{1}{2}}. \quad (51)$$

Using once again the radiation spectrum of Stecker *et al.*, one finds that the energy loss rate becomes comparable to the acceleration rate at the peak of the UV bump, where $E_p \approx 3 \times 10^8$ GeV. For E_p^{max} above $\sim 10^{19}$ eV, which in this model can be achieved only in AGN with total luminosity $\simeq 10^{48}$ erg/s, proton synchrotron radiation becomes the most important energy loss channel.

The results of the calculation of Szabo & Protheroe [38] can be summarized by the following approximate formula [156], which gives the neutrino flux at Earth from an AGN of given X-ray flux and E_p^{max} in $[\text{cm}^2 \cdot \text{s} \cdot \text{TeV}]^{-1}$

$$F_\nu E_\nu \simeq 0.25 F_X \exp(-20 E_\nu / E_p^{\text{max}}) \times E_\nu^{-2}, \quad (52)$$

where F_X is the 2–10 KeV X-ray flux ($\text{erg cm}^{-2} \text{s}^{-1}$) and E_ν is the neutrino energy in TeV.

The generic AGN model, described above, is a first order approximation of the physical processes that may take place in active galactic nuclei. The assumption of spherical accretion could be an adequate representation of the accretion flow inside a thick accretion disk.

An attempt to use a different geometry in the center of AGN's was made in the model due to Nellen, Mannheim & Biermann [157]. In this model it is assumed that protons are

accelerated somewhere near the central region, perhaps in the bases of the jets, and that both X-rays and neutrinos are generated in collisions of the accelerated protons in the inner regions of the disk. This model is less specific than those of Refs. [38,36,152], and the main production process is assumed to be quite different. Nevertheless, the predicted neutrino fluxes are rather similar to those of Refs. [38] and [152]. This is because the intensity is normalized to the X-ray luminosity and the protons are assumed to be confined to the central region until they lose all their energy through collisions.

Individual radioquiet AGN will be difficult to detect, although the atmospheric background in a 1° radius around the source is extremely small, $\sim 1.6 \times 10^{-6} \text{ m}^{-2}\text{yr}^{-1}$ muons above 1 TeV. Even with optimistic luminosities, the number of such events from individual sources is less than $2\text{--}3 \text{ yr}^{-1}$ in a 10^5 m^2 detector. For example, the estimated rates from the models of Ref. [38] are ~ 1 per $10^5 \text{ m}^2\text{yrs}$ for 3C273 and ~ 3 in the same units for NGC4151.

7.2 Diffuse AGN neutrino flux

In their pioneering paper Stecker *et al* [36] integrated the neutrino fluxes from single generic AGN's to obtain a diffuse flux of neutrinos from all cosmological AGN. The integration has to account for the AGN density and luminosity distribution, as well as for the neutrino adiabatic energy loss due to the expansion of the Universe. This procedure is identical to the integration used to calculate the value of the diffuse X-ray background. In fact, it uses the AGN luminosity function derived from X-ray observations [158,159] and assumes that the neutrinos and the X-rays have a common source.

The AGN luminosity function as a function of the redshift can be expressed as

$$\rho(L_X, z) = R_0^3 \frac{g(z)}{f(z)} \rho_0 \left(\frac{L_X}{f(z)} \right), \quad (53)$$

where ρ_0 comes from measurements of the AGN luminosity, R_0 is the present scale size of the Universe and $g(z)$ and $f(z)$ describe the number density and luminosity evolution of AGN in the co-moving volume. Any AGN induced background, including X-ray and neutrino, will then have energy spectrum [38]

$$\frac{dI}{dE} = \frac{1}{4\pi} \frac{c}{H_0} \frac{1}{ER_0^3} \int dL_X \int_0^{Z_{max}} dz \times \rho(L_X, z) (1+z)^{-\alpha} \frac{dL}{dE} \{E(1+z), L_X\}, \quad (54)$$

where L is the appropriate differential luminosity and $\alpha=5/2$ for the Einstein-de Sitter cosmological model.

Figure 8 shows the current estimates of the isotropic ν background ($\nu_\mu + \bar{\nu}_\mu$). The estimates of Szabo & Protheroe are made with different values of x_1 and photon target spectra, and they are integrated using two independent sets of luminosity functions [158,159]. The resulting ν flux extends to very high energy, where it dominates the atmospheric neutrino background by several orders of magnitude. Because of the isotropic nature of the background flux, its major feature is the extremely flat energy spectrum. The thick line shows the corrected prediction of Stecker *et al.* [36]. While the ν spectra are now in very reasonable agreement at the higher energy end, the biggest difference occurs at energies below 3×10^5 GeV, where Stecker *et al* spectrum becomes flat while the spectrum of Protheroe & Szabo

follows the primary proton spectrum, for the reason described in the previous subsection. The difference reaches 2.5–3 orders of magnitude at $E_\nu = 10^4$ GeV, which makes a crucial difference in the estimate of the ν_μ -induced upward muon signal.

Figure 9 shows the muon fluxes generated by the isotropic neutrino background as in the bracketing high and low models of Szabo & Protheroe [38] and by Stecker *et al.* [36]. These have been calculated [160] as described in § 3.2.1 for comparison with the Frejus measurement [161], which gives a 90% C.L. upper limit of 2.3 events with $E_\mu < 2$ TeV for the range of zenith angles $-0.3 < \cos \theta < 0.3$ [161]. The corresponding upper limit [162] is shown in Fig. 9. The muon flux generated by atmospheric neutrinos averaged over the same angular interval is shown for comparison. The AGN background dominates at muon energies above 1 TeV.

Although the diffuse neutrino flux from AGN’s is isotropic, the produced muons will be suppressed in the vertical direction (from below) by an amount that depends on the relative importance of high energy neutrinos in the spectrum. The interaction length of neutrinos in the Earth is less than an Earth radius when $\sigma_\nu \sim 10^{-33}$ cm², i.e. for $E_\mu \sim 10^7$ GeV [65]. Accounting for absorption in the Earth, the predicted TeV muon rate in a downward looking detector with acceptance of 10⁵m²sr will be 160 to 800 *per year* for Ref. [38] and ~ 40 for Ref. [36] over an atmospheric background of ~ 140 events. The higher range of predictions of Ref. [38], however, are already ruled out by the Frejus limit.

So far we have discussed signals generated by muon neutrinos and antineutrinos. Electron neutrinos of sufficiently high energy can generate air showers which could be observable above the background or ordinary showers near the horizontal because of the great penetrating power of neutrinos. Limits on horizontal showers have been given by the Akeno air shower experiment, as discussed in §3.4 above. The Fly’s Eye detector has searched for upward-going showers, which would be generated by electron neutrinos from below that interact near enough to the surface so the resulting electromagnetic cascade emerges from the ground before it is absorbed. For $E_\nu \gg 10^7$ GeV, these events would be mostly near the horizontal since the Earth would absorb the more vertical high energy neutrinos. The Fly’s Eye limits [164] apply for $E > 10^8$ GeV and are discussed further below in connection with cosmological neutrinos.

Electromagnetic cascades generated by charged current interactions of electron neutrinos can also be detected when they occur inside the volume of a Cherenkov detector. The rates are then simply the convolution of flux, cross section and fiducial volume. Figure 10 [163] shows the rates predicted for the $\nu_e + \bar{\nu}_e$ spectra of Refs. [36,38]. The dotted line shows the background of atmospheric electron neutrinos. Since the atmospheric neutrino spectrum is steeper for ν_e than for ν_μ , the flux of AGN ν_e crosses the atmospheric background at lower energy than for ν_μ . In the examples given in Fig. 10, there are ~ 10 interactions per 1000 kt years of electron neutrinos with $E_\nu > 1$ TeV in a typical model from Ref. [38] as compared to 0.5 in Ref. [36] and 0.2 atmospheric above the same energy threshold. The rates plotted in Fig. 10 are integrated over all directions. For $E_\nu \sim 10^7$ GeV, absorption of upward neutrinos by the Earth begins to be significant, suppressing the quoted rates of ν_e from AGN slightly.

The spike at 6×10^6 GeV in Fig. 10 represents the interaction of $\bar{\nu}_e$ at the “Glashow

resonance” [165]. The resonance cross section for $\bar{\nu}_e + e^- \rightarrow W^- \rightarrow \bar{\nu}_e + e^-$ is [166]

$$\sigma(\bar{\nu}_e e^-) = \frac{G_F^2 s}{3\pi} \times \left[\frac{M_W^4}{(s - M_W^2)^2 + \Gamma_W^2 M_W^2} \right] \quad (55)$$

where $\Gamma_W \approx 2.1$ GeV is the width of the W and resonance occurs for $E_\nu = E_0 = s/(2m_e) \approx 6.4 \times 10^6$ GeV. The peak cross section value is

$$\sigma(E_0) = \frac{1}{B_{W \rightarrow \bar{\nu}_e e^-}} \frac{G_F^2 M_W^4}{3\pi \Gamma_W^2} \approx 9 \times 5.2 \times 10^{-32} \text{cm}^2 \approx 4.7 \times 10^{-31} \text{cm}^2 \quad (56)$$

for a total of nine (3 leptonic and 6 hadronic) W^- decay channels. Integrating Eq. 55 gives the rate per electron as

$$\text{Rate} = \frac{\pi \sigma(E_0) \Gamma_W M_W}{2m_e} \phi_{\bar{\nu}_e} \left(\frac{M_W^2}{2m_e} \right) \approx \phi_{\bar{\nu}_e}(E_0) \times (2.4 \times 10^{-25} \text{GeV cm}^2). \quad (57)$$

Detection of other exotic phenomena, such as multi- W production [168], is also possible.

7.3 AGN Jets

The recent observations of GeV γ -rays from a large number of extragalactic objects by the EGRET instrument[170] on GRO has stimulated intense interest in models of particle acceleration in jets with relativistic bulk flow. This is because most, if not all, of the EGRET sources are radio-loud AGN, which are thought to be AGN’s viewed from a position illuminated by the cone of a relativistic jet. Jets carry a sizeable fraction of the AGN luminosity. Moreover, the apparent luminosity to an observer looking at a small angle to the jet axis is increased by a factor of up to 10^4 for a jet Lorentz factor of 10. This is a consequence [171] of the fact that $I(\nu)/\nu^3$ is a relativistic invariant, so that $I(\nu) = \Gamma^3 I^*(\nu\Gamma^{-1})$, where I^* is the photon intensity ($\text{erg s}^{-1}\text{cm}^{-2}\text{sr}^{-1}\text{Hz}^{-1}$) seen by an observer moving with the gas in the jet and Γ is the Lorentz factor of the jet averaged over the cone of the jet relative to the line of sight.

The interest intensified still further with the discovery of $\sim\text{TeV}$ photons from the nearby AGN Markarian 421 [115]. What is the origin of such high energy photons?

Proposed explanations can be divided into two classes. The traditional approach to the production of very high energy photons is based on inverse Compton (IC) scattering of accelerated electrons on a seed photon field. The photon field could be either external, i.e. generated outside the electron acceleration region, or due to the synchrotron radiation of the electrons (*synchrotron-self-Compton*). Examples in this category are Refs. [119,120,121].

An alternative approach is that of Mannheim *et al.* [37,172,173,176]. Following the arguments of Ref. [143], it is assumed that protons also are accelerated in the jets. These protons lose their energy by collisions on the synchrotron photons. In the process they dump energy into photons, electrons and neutrinos *via* production of π^0 and π^\pm . (The jets are sufficiently diffuse so that high energy neutrons escape and production of π^- is therefore greatly suppressed.) The photons and electrons are reprocessed, and cascade to form an E^{-2} power law differential photon spectrum down to the energy below which the

accelerating region becomes transparent. These photons which originate from interactions of accelerated protons dominate the high energy signal in this picture. At low frequency ($\nu \lesssim 10^{15}$ Hz) synchrotron radiation from the electrons dominates.

Both pictures have some difficulties to overcome. For example, the models that do not involve nucleons generally require a higher bulk Lorentz factor of the jet. The radiation target density has to be high enough for IC scattering and, at the same time, low enough for the generated γ -rays not to be absorbed by $\gamma\gamma$ collisions. This is difficult to arrange for, especially when IC scattering in the Klein-Nishina regime is the relevant process. In addition, the energy densities in soft photons (IR to X-rays) and γ -rays are comparable, which requires that the two types of radiation are generated in different locations [121]. To prevent the electrons from losing too much energy to synchrotron radiation, the energy of the magnetic field in the jet has to be of order 5% of the radiation density [120], far from the 0th order assumption of equipartition.

There is a corresponding set of problems that the models of hadronic origin have to overcome. Because of the smaller rate of energy loss by protons, the jet Lorentz factor is no longer a big limitation. The seed photon density, however, has to be high enough for photoproduction to occur, and, as a consequence, γ -ray absorption in the source is a problem. Similarly, there are several other free parameters of the model, such as the ratio of power in protons and in electrons. These are fixed from multi-frequency observations. In Fig. 11 we compare results of quasi-simultaneous observations of 3C273 in the optical, X-ray and γ -ray bands [177] with the predictions of a synchrotron-self-Compton model [119] (solid line) and a hadronic model [176]. The hadronic model gives correctly the spectral shape at X-ray and γ -ray energy. The turn-up in the >10 GeV region can not be detected at Earth, because of the absorption on the IR/optical background on propagation from the distant source ($z = 0.158$ for 3C273).

The detection of neutrinos from blazars would confirm the hadronic model, since there is no source of neutrinos in the electromagnetic models. In this connection, the uncertainty in optical depth for photons in the source is particularly problematic because it introduces extra model-dependence in the relation between the observed photon flux and the predicted neutrino flux. This problem, of course, disappears once the neutrinos are detected. In the remainder of this section we review the estimates of the predicted neutrino signals in the hadronic model of production of high energy photons in jets of AGN.

A calculation of the neutrino production in AGN jets was first published by Biermann and Mannheim [37,143,172]. The produced neutrino flux reflects the physical conditions in the AGN jet. Because of the low photon density protons can achieve quite high energy at acceleration ($E_p^{max} \sim 3 \times 10^{10}$ GeV in the frame moving with the bulk flow of gas in the jet (jet frame)).

In addition both the acceleration and proton interactions proceed in the jet frame, so the neutrinos are boosted to high energy (blueshifted) with a Doppler factor of order 10. In the case of 3C273 the flux is shown by a dotted line in Fig. 7.

This model [173] of the proton acceleration and interactions envisions a bulk flow of magnetized plasma, streaming from the base of the jet towards its end (the hot spot). The acceleration occurs in a sheets of radial dimension R and thickness D moving out with the jet. In order to explain the variability of 3C279 on timescale of a day the radiating sheet thickness should be $D \sim 10^{15}$ cm, much smaller than its radius ($\sim 10^{18}$ cm). The acceleration

of protons (and possibly nuclei) proceeds *via* first order Fermi acceleration in the frame of the flowing plasma. As usual, the acceleration rate is given by (compare Eq. 50)

$$\frac{1}{E} \frac{dE}{dt} \propto \frac{e B c}{E}. \quad (58)$$

In this model, protons collide with the synchrotron photons generated by the accelerated electrons, and the photon spectrum is approximated as a power law with integral index $\gamma \approx -1$. The threshold photon energy for production of the Δ resonance obeys $E_\gamma(\text{threshold}) \propto E_p^{-1}$, so the density of photons at the resonance is proportional to the proton energy. Since equipartition is assumed between the energy in electrons and the magnetic field, the normalization of the photon field is proportional to B^2 . Thus the loss rate for protons depends on magnetic field and proton energy as

$$(t_p)^{-1} \propto E_p B^2. \quad (59)$$

Combining Eqs. 58 and 59 using the numerical values of Ref. [143], leads to an estimate of the maximum proton energy in the jet frame of

$$E_p^{max,*} \leq 2 \times 10^{10} B^{-1/2} \text{ GeV}, \quad (60)$$

where B is the magnetic field strength in Gauss.

The fact that the dominant energy loss process for high energy protons in the hadronic model of AGN jets is photoproduction at threshold in collisions on a power law spectrum of photons (rather than a thermal spectrum) has an interesting consequence also for the shape of the produced spectrum of secondary pions. If, as expected in first order shock acceleration, the differential proton spectrum is E^{-2} , then the differential pion production spectrum will be harder by one power of energy, i.e. E^{-1} . Occasionally energetic protons also collide with thermal gas in the jet, which leads to an E^{-2} spectrum of pions. Thus the characteristic shape of the production spectrum of pions is E^{-2} at low energy, flattening to E^{-1} at high energy up to some characteristic maximum energy.

The spectrum of neutrinos from decay of π^+ and μ^+ follows the pion production spectrum, shifted down in energy by appropriate kinematic factors. All energies are boosted by the bulk Lorentz factor Γ relative to an external observer. The observed (boosted) maximum neutrino energy is estimated by Mannheim [173] as $E_\nu^{\text{max}} \sim 10^9 \text{ GeV}$. The boosted energy at which the observed neutrino spectrum flattens from E^{-2} to E^{-1} is in the range 10^5 for 3C273 [176] to 10^7 GeV for Mkn 421 and 3C279 [173]. Photons are even more complicated than neutrinos because their spectra at production (from $\pi^0 \rightarrow \gamma\gamma$ and from radiation by electrons) are reprocessed by pair cascading in the ambient photon and magnetic fields. The total photon luminosity eventually emerges from the source at lower energy (but boosted by the bulk Lorentz factor). Approximately equal amounts of energy are carried by the four leptons that result from the decay chain

$$\pi^+ \rightarrow \nu_\mu \mu^+ \rightarrow e^+ \nu_e \bar{\nu}_\mu.$$

In addition,

$$p\gamma \rightarrow p\pi^0 \approx 2 \times p\gamma \rightarrow n\pi^+$$

at the Δ resonance. Thus 3/4 of the energy lost to photoproduction ends up in the electromagnetic cascade and 1/4 goes to neutrinos. In addition, some of the energy of the accelerated protons is lost to direct pair production ($p + \gamma \rightarrow e^+ e^- p$). Thus

$$L_\nu \leq \frac{1}{4} L_\gamma \quad (61)$$

Equation (61) can be used to relate an observed photon spectrum to a predicted neutrino flux in the model. The relation is further complicated by attenuation of high energy (\gtrsim TeV) photons during propagation from the source [116,174].

The spectra of both γ -rays and neutrinos are generated in $p\gamma$ and, to a lesser extent, pp interactions. For photoproduction the energy carried by neutrinos is directly related through kinematics to the γ -ray luminosity as

$$L_\nu = \frac{3}{4} L_{\pi^+} = \frac{3}{13} L_\gamma, \quad (62)$$

where L_γ includes a contribution from e^+e^- pairs. The predicted flux for 3C273 [176] is shown in Fig. 7. It would give a rate of upward muons with $E_\mu > 1$ TeV of ~ 0.1 per year in a 10^5 m² detector.

The simultaneous observation of the BLLac source Mkn 421 by EGRET [178] and the Whipple observatory [115] is especially valuable for the understanding of the physics of AGN jets because of the large range of energy for detected photons. The two observations define an energy spectrum with $\gamma = 2.06 \pm 0.04$ over more than four decades in energy [179]. Mkn 421 is the closest source observed by EGRET at a redshift of 0.031. This is significant because of the absorption on propagation. The exact energy dependence of the absorption feature is uncertain because the magnitude and the energy spectra of the IR and optical background(s) are not well known. Within a factor of 2, however, 3 TeV γ -rays emitted at the distance of Mkn 421 will already start being absorbed and will show an apparent steepening of the spectrum independently of the production spectrum.

One should appreciate that weakly interacting neutrinos will make their way to our detectors unattenuated by ambient matter in the source or by IR light. So, while high energy photons are absorbed on intergalactic IR photons for AGNs much further than Mkn 421, neutrinos are not and sources should be detected with no counterpart in high energy photons. Halzen and Vasquez [180] scale the Mkn 421 γ -ray flux to neutrino flux, making a range of assumptions for the γ -ray absorption at source, expressed in terms of the magnetic field value B of the jet. The VHE γ -ray flux from Mkn 421 is [179]

$$\int_{1/2 \text{ TeV}} dE \left[\frac{E dN_\gamma}{dE} \right] = 1.5 \times 10^{-11} \text{ cm}^{-2} \text{ s}^{-1}. \quad (63)$$

It is assumed [179] that the production spectrum (before attenuation) is given by a power law with integral spectral index γ . The corresponding neutrino flux that would be expected if the observed photon spectrum is to be understood in the hadronic model is quite uncertain. This is because the amount of absorption in the source is not well determined. What is needed is the optical depth of the source, *i.e.* the jet. Biermann [181] gives the following

(admittedly model dependent) estimate:

$$\tau_{\text{optical}} = 2 \left[\frac{B}{1 \text{ Gauss}} \right]^{1/2} \left[\frac{E_\gamma}{1 \text{ TeV}} \right]. \quad (64)$$

The photon flux will be attenuated for energies above which $\tau_{\text{optical}} = 1$. According to (64) the optical depth of the source is unity for the 0.5 TeV photons observed by Whipple for a 1 G field. The true value of the B -field in the jet is a guess which ranges from 10^{-4} to 10^4 G. The gamma ray flux can be computed inside the source by correcting the observed flux (63) for absorption in the jet. The answer depends critically on the magnitude of the B -field. Once the unattenuated photon spectrum is established, the neutrino flux is estimated simply by assuming one neutrino per gamma ray, as appropriate for pion decay.

Table 4 [179] shows the results for a range of assumptions for B and the spectral index γ . We conclude that in this scenario Mkn 421 should produce a handful of upcoming muon events per year in a generic 10^5 m^2 detector. Within the framework of the model the magnetic field would be limited to $B \lesssim 1 \text{ Gauss}$ because the observed γ -ray spectrum extends above 1 TeV. The situation could be different in other potential sources.

Table 4: Number of upcoming muons (N) per 10^5 m^2 per y for the different scenarios. \mathcal{L}_γ is in 10^{43} erg/s .

$B(\text{Gauss})$	γ	E_p^{max}	E_γ for $\tau_{\text{opt}} = 1$	\mathcal{L}_γ	N
10^{-4}	1	$2 \times 10^{22} \text{ eV}$	50 TeV	30	2
	0.8			500	11
	0.4			10^6	450
1	1	$2 \times 10^{20} \text{ eV}$	500 GeV	200	13

Stecker *et al.* [182] use the γ -ray absorption on propagation to normalize the expectations from other GRO sources. They find a flux of neutrinos from the 3C273 jet sufficient to generate ~ 0.1 muons above 1 TeV in 10^5 m^2 per year. The corresponding flux from the 3C273 core is 40% smaller. The quiescent state of 3C279 would generate 5 muons, while the highest observed γ -ray flux from 3C279 would correspond to 25 such muons. The 3C279 core contribution is only 0.1 event. These are the bracketing values for the expectations of neutrino fluxes from active galactic nuclei, if the γ -rays are indeed generated in hadronic interactions by accelerated nuclei.

Analogously to the background from generic, radio-quiet AGN, one can integrate the emission of all AGN jets to obtain an isotropic ultra high energy neutrino background. Two estimates of this background, due to Stecker[183] and Mannheim[173], are shown in Fig. 8. Although the overall normalization of the isotropic neutrino background from AGN jets is lower than that of generic AGN, it extends to higher energy, and crosses it over at some very high energy. The cross-over is explicit in the flux of Mannheim, while Stecker *et al.* give only the slope ($\gamma = 2$) and the normalization. In any case, the normalization is somewhat uncertain because of the variability of the blazars. The normalization of Mannheim's diffuse

flux in Fig. 8 corresponds to an assumption of a 15% duty factor for blazars to be in a high state [184].

7.4 AGN Neutrinos: Discussion and conclusions

Although the spherical accretion model is very useful for estimating the neutrino fluxes that might be expected from cores of AGN, it is subject to criticism from various points of view. The model is only applicable to accretion disks with thickness comparable to or exceeding the dimension of the shock radius. It has to be constructed in such a way that there is no leakage of the generated γ -rays before their energy is downscattered to X-ray and longer wavelengths. Any significant leakage would exceed the experimental limits on diffuse extragalactic γ -rays. At the same time, the radiation density cannot be so high as to prevent the acceleration processes from occurring. Some authors [185] estimate the source efficiency Q to be lower than $1/3$ and ask if the conditions in the AGN nucleus are suitable for shock formation at all. Others [186] show the danger of overproducing background radiation through pair production and synchrotron radiation, which could lead to shock instability and drastically decrease E_p^{max} . Some of these problems might be avoided by placing the shocks in the bases of the AGN jets [157].

The calculations of the neutrino production in AGN jets are no less difficult. To model correctly all the jet physics one has to follow in some detail all the processes involved in the frame of the relativistic plasma flow, including particle acceleration and reacceleration at multiple shocks, γ -ray production, multiplication and absorption in electromagnetic cascades in a non stationary fashion. This is very complicated problem that involves many free parameters. The simple scaling of the neutrino fluxes with the γ -ray luminosity for individual sources may not be exact, since the conditions at the source are poorly known. The ratio of the magnetic to radiation energy density, for example, which is essential for the γ -ray absorption at the source, can vary within at least one order of magnitude. The sources are also highly variable, and many might have been observed during the peak of their activity.

The big question is the fraction of the AGN luminosity that goes through the nucleonic channel. Although it has been pointed out [35,143,144] that hadrons have suitable interaction cross sections and are a natural vehicle for the energy transport throughout the AGN disk, nucleons are not strictly necessary for the solution of this problem. Since the models of the non-nucleonic origin of the Mkn 421 γ -rays are already struggling to extend the theory to γ -rays above 1 TeV, a possible observation of, say, 10 TeV γ -rays would be a confirmation of their π^0 origin.

This is hardly possible, however, because of the absorption on the IR/optical background, even if the production spectrum reaches much higher energy. There is only a slight chance that [174], for very low values of the extragalactic magnetic field, the cascading on this background will flatten considerably the spectrum observed in the GeV/TeV region. Such flattening would reveal the extension of the production spectrum to much higher energy and correspondingly confirm the π^0 origin of the γ -ray flux.

The criticism above does not imply that the current predictions are not reliable. They are results of the first generation of research, which will become more exact in the near future. The differences between various estimates reflects the uncertainties of the calculations. Conclusions are that the expected fluxes of source neutrinos are well below the sensitivity

of the currently active deep underground detectors with effective area less than 1000 m². They are, however, tantalizingly close to being detectable by the new generation of detectors especially designed for neutrino astronomy.

8 Cosmological Neutrinos

Another possible source of extremely energetic diffuse neutrinos could be the interactions of ultra high energy cosmic rays on the microwave background. The importance of such interactions was noted by Greisen [187] and independently by Zatsepin and Kuzmin [188] soon after the discovery of the background radiation. These early papers stated the existence of an universal cut-off of the cosmic ray spectrum due to photopion production. The question of the production of neutrinos and γ -rays was developed later in works by Wdowczyk *et al* [189], Stecker [190], Hill & Scramm [191], Berezhinsky and Grigorieva [192], Halzen *et al* [193] and others, and in a recent paper of Yoshida & Teshima [194], who perform a detailed Monte Carlo calculation of the proton propagation in the microwave background and the generation of neutrinos.

The major source of energy loss is photoproduction, as described in §7.1. Here the target is the microwave background, with a density of ~ 400 photons/cm³ and an average energy $\epsilon \simeq 7 \times 10^{-4}$ eV, corresponding to the temperature of the background radiation. For cosmic rays exceeding

$$E_p \approx \frac{\Delta^2 - m_p^2}{2(1 - \cos \theta)\epsilon} \approx \frac{5 \times 10^{20}}{(1 - \cos \theta)} \text{ eV} , \quad (65)$$

where θ is the angle between the proton and photon directions, the photopion cross-section grows very rapidly to reach a maximum of 540 μb at the Δ^+ resonance ($s = 1.52 \text{ GeV}^2$). The Δ^+ decays to $p\pi^0$ with probability of 2/3, and to $n\pi^+$ with probability 1/3. Neutral pions give rise to ultra-high-energy γ -ray fluxes, and charged pions—to neutrino fluxes through the decay channels of Eq. (12). Decay kinematics is such that all three neutrinos take approximately 1/4 of the parent pion energy. In addition the neutrons also decay and produce a small flux of $\bar{\nu}_e$ at much lower energy.

Because of the width of the thermal photon distribution, and the isotropic nature of the microwave background, there is some phase space for photopion production at proton energies as low as 10^{19} eV. These are only possible in head to head interactions on the high energy tail of the microwave background spectrum (or on the infrared/optical background). Most of the proton energy loss in this energy range, however, is on direct pair production ($p\gamma \rightarrow pe^+e^-$), which has a lower threshold but does not contribute to the neutrino fluxes. Photopion production starts dominating at energy above $3 \times 10^{19} \text{ eV}$ and the cross-section reaches maximum at $\sim 5 \times 10^{20} \text{ eV}$, where the proton mean free path $\lambda_p = (\sigma_{p\gamma} n_\gamma)^{-1}$ is $\simeq 5 \times 10^{24} \text{ cm}$ ($\sim 2 \text{ Mpc}$). Since protons lose on the average 1/5 of their energy per interaction the proton attenuation length Λ_p comes to $\sim 10 \text{ Mpc}$, a number that the exact calculation of Ref. [194] shows is reached for proton energies above 10^{21} eV.

The magnitude and intensity of the cosmological neutrino fluxes is than determined by the maximum injection energy of the ultra-high-energy cosmic rays and by the distribution of the sources. If the sources are relatively close by, at distances measured in tens of Mpc, and the maximum injection energy is not much greater than the highest observed cosmic ray

energy (few $\times 10^{20} \text{ eV}$), the generated neutrino fluxes are negligible. If, however, the highest energy cosmic rays are generated at many sources at large redshift, then a large fraction of their injection energy would be presently contained in γ -ray and neutrino fluxes. The most important reason is that the energy density of the microwave radiation, and the proton photopion production cross-section, scales with $(1+z)^4$. The effect is even stronger if the source luminosity were increasing with z , i.e. cosmic ray sources were more active at large redshifts—‘bright phase’ models.

The neutrino flux is given by an integral identical to Eq. (54), where $g(z)$ and $f(z)$ now correspond to number density and the luminosity function of the cosmic ray sources. In general, the cosmic ray sources are defined by their injection spectra, luminosity and cosmological evolution. The normalization comes from the requirement that the ultra-high-energy cosmic rays after propagation in the microwave background match the observed spectra. The loss resulting in γ -ray fluxes, downscattered on the microwave background, should not violate the experimental limits on isotropic extragalactic γ -rays [195]. Yoshida & Teshima [194] give the muon and electron neutrinos separately for different injection models characterized by the z_{max} value, maximum injection energy E_{max} and different source evolution functions of the form $\eta(z) = \eta_0(1+z)^m$. Fig. 15 below shows these fluxes for $E_{max} = 10^{22} \text{ eV}$ and two extreme sets of evolution parameters: $m = 0$, $z_{max} = 2$ (low) and $m = 4$, $z_{max} = 4$ (high). It is important to remember that such drastically different source evolution models can fit equally well the observed cosmic ray spectrum.

There are specific models that identify the sources of the extragalactic cosmic rays. Rachen & Biermann [196] propose that hot spots of Fanaroff-Riley class II radio galaxies, being the largest and most powerful shock waves in the Universe, are the dominant sources of cosmic rays of energy above 10^{18} eV . In this case $g(z)$ and $f(z)$ are the number and luminosity density functions of FR-II galaxies, derived from radio observations at particular radio frequencies. They do not calculate the neutrino fluxes generated in cosmic ray interactions of the microwave background, but since their models match the observed cosmic ray flux at energies around 10^{18} eV , such a calculation should be close to the results of Ref. [194] for similar source evolution functions, i.e. to be bracketed by the extreme fluxes shown on Fig. 15.

Independently of the specific model of the sources of the highest energy cosmic rays, the associated neutrino fluxes can only dominate the highest energy region, above $E_\nu = 10^{17}\text{--}10^{18} \text{ eV}$. This would only happen in the case that cosmic rays of energy above 10^{18} eV are indeed accelerated at numerous high redshift astrophysical sources. At lower energy the neutrino background is dominated by the neutrinos generated in interactions at active galactic nuclei

An intriguing possibility is (see Refs. [197,198]) that the highest energy cosmic rays are produced by energy loss of superconducting cosmic strings. The strings lose energy in the form of massive fermions ($M_F \propto 10^{15} \text{ GeV}$) that decay into baryons and fermions. The spectrum is modified by interactions on the 3K background but extends up to the Planck mass. This, plus the contribution from strings at large red-shift, increases the cosmic ray energy loss in the $> 10^{19} \text{ eV}$ range. A neutrino flux a factor of 30 higher than the proton flux is created. Only nucleons (not nuclei) can be generated through this channel.

More recently the neutrino emission from cosmic strings has been discussed in the context of ‘cusp annihilation’ [199,200,201]. The total energy of the string in the region of the cusp

is released in the form of massive scalar and gauge particles that decay rapidly into particle jets. Equal numbers of particles and antiparticles are generated by conservation of quantum numbers. Neutrinos come mostly from the ordinary pion decay channels. The shape of the jet fragmentation function is crucial for the number of generated neutrinos and their energy spectrum. The assumptions used require an extrapolation of the observed jet fragmentation function up to the Planck scale. Another crucial parameter is μ , the string mass per unit length, which defines the total luminosity of the string. For $G\mu/c^2 \simeq 10^{-6}$, consistent with large-scale structure formation and the observed anisotropy of the microwave background, the generated neutrino fluxes are smaller than the predictions from ultra-high-energy proton propagation. Maximum neutrino fluxes are obtained for $G\mu/c^2 \simeq 10^{-15}$. In this case, however, the cosmic strings would not have other cosmological implications.

9 Search for Dark Matter

It is believed that most of our Universe is made of cold dark matter particles. In the context of big bang cosmology, these particles have interactions of order the weak scale and masses of order M_W , i.e. they are WIMPs [202]. From rotation curve measurements we also know their density and average velocity in the galactic halo. This information is the basis for estimating the annihilation rate of WIMPs into high energy neutrinos.

Galactic WIMPs, scattering off protons in the sun, lose energy. They may fall below escape velocity and be gravitationally trapped. Trapped dark matter particles eventually come to equilibrium temperature, and therefore to rest at the center of the sun. While the WIMP density builds up, their annihilation rate into lighter particles increases until equilibrium is achieved where the annihilation rate equals half of the capture rate. The sun has thus become a reservoir of WIMPs which annihilate into any open fermion, gauge boson or Higgs channels. The leptonic decays from annihilation channels such as $b\bar{b}$ heavy quark pairs and W^+W^- turn the sun into a source of high energy neutrinos. Their energies are in the GeV to TeV range, rather than in the keV to MeV range familiar from its nuclear burning. These neutrinos can be detected in deep underground experiments.

We will illustrate the power of neutrino telescopes as dark matter detectors using as an example the search for a 500 GeV WIMP with a mass outside the reach of present accelerator and future LHC experiments. A quantitative estimate of the rate of high energy muons of WIMP origin triggering a detector can be made in 5 easy steps. An exact quantitative calculation requires a complex code [203].

Step 1: The halo neutralino flux ϕ_χ . It is given by their number density and average velocity. The cold dark matter density implied by the observed galactic rotation curves is $\rho_\chi = 0.4 \text{ GeV/cm}^3$. The galactic halo is believed to be an isothermal sphere of WIMPs with average velocity $v_\chi = 300 \text{ km/sec}$. The number density is then

$$n_\chi = 8 \times 10^{-4} \left[\frac{500 \text{ GeV}}{m_\chi} \right] \text{ cm}^{-3} \quad (66)$$

and therefore

$$\phi_\chi = n_\chi v_\chi = 2 \times 10^4 \left[\frac{500 \text{ GeV}}{m_\chi} \right] \text{ cm}^{-2} \text{ s}^{-1}. \quad (67)$$

Step 2: Cross section σ_{sun} for the capture of neutralinos by the sun. The probability that a WIMP is captured is proportional to the number of target hydrogen nuclei in the sun (i.e. the solar mass divided by the nucleon mass) and the WIMP-nucleon scattering cross section. From dimensional analysis $\sigma(\chi N) \sim (G_F m_N^2)^2 / m_Z^2$ which we can envisage as the exchange of a neutral weak boson between the WIMP and a quark in the nucleon. The main point is that the WIMP is known to be weakly interacting. We obtain for the solar capture cross section

$$\Sigma_{\text{sun}} = n\sigma = \frac{M_{\text{sun}}}{m_N} \sigma(\chi N) = [1.2 \times 10^{57}] [10^{-41} \text{ cm}^2] . \quad (68)$$

Step 3: Capture rate N_{cap} of neutralinos by the sun. N_{cap} is determined by the WIMP flux (67) and the sun's capture cross section (68) obtained in the first 2 steps:

$$N_{\text{cap}} = \phi_{\chi} \Sigma_{\text{sun}} = 3 \times 10^{20} \text{ s}^{-1} \text{ for } m_{\chi} = 500 \text{ GeV}. \quad (69)$$

Step 4: Number of solar neutrinos of dark matter origin One can check that the sun comes to a steady state where capture and annihilation of WIMPs are in equilibrium. For a 500 GeV WIMP the dominant annihilation rate is into weak bosons; each produces muon-neutrinos with a leptonic branching ratio which is roughly 10%:

$$\chi \bar{\chi} \rightarrow WW \rightarrow \mu \nu_{\mu} . \quad (70)$$

Therefore, as we get 2 W 's for each capture, the number of neutrinos generated in the sun is

$$N_{\nu} = \frac{1}{5} N_{\text{cap}} \quad (71)$$

and the corresponding neutrino flux at Earth is given by

$$\phi_{\nu} = \frac{N_{\nu}}{4\pi d^2} = 2 \times 10^{-8} \text{ cm}^{-2} \text{ s}^{-1} , \quad (72)$$

where the distance d is 1 astronomical unit.

Step 5: Event rate in a high energy neutrino telescope. For (70) the W -energy is approximately m_{χ} and the neutrino energy half that by 2-body kinematics. The energy of the detected muon is given by

$$E_{\mu} \simeq \frac{1}{2} E_{\nu} \simeq \frac{1}{4} m_{\chi} . \quad (73)$$

where we used the fact that, in this energy range, roughly half of the neutrino energy is transferred to the muon. For the neutrino flux given by (72) we obtain

$$\# \text{ events/year} = 10^5 \times \phi_{\nu} \times \rho_{\text{H}_2\text{O}} \times \sigma_{\nu \rightarrow \mu} \times R_{\mu} \simeq 100 \quad (74)$$

for a 10^5 m^2 water cherenkov detector, where R_{μ} is the muon range and $\phi_{\nu} \times \rho_{\text{H}_2\text{O}} \times \sigma_{\nu \rightarrow \mu}$ is the simple analog of Eq. (19).

This exercise illustrates that present high energy neutrino telescopes (of area $\sim 10^4 \text{ m}^2$) are powerful devices in the search for dark matter and supersymmetry. They are complementary to present and future accelerator searches in the sense that they are naturally sensitive

to heavier WIMP's because the underground high energy neutrino detectors have been optimized to be sensitive in the energy region where the neutrino interaction cross section and the range of the muon are large. Also, for high energy neutrinos the muon and neutrino are nicely aligned along a direction pointing back to the sun with good angular resolution. In addition, in the estimate given above we neglected some other decay channels that contribute neutrinos, and we did not include the signal from annihilation of WIMP's trapped in the center of the Earth [205]. Direct searches for dark matter are clearly highly desirable. To achieve comparable sensitivity to these indirect searches requires a sensitivity at the level of 0.05 events/kg day [204].

An elegant way to extend the Standard Model is to make it supersymmetric [207]. If supersymmetry is indeed Nature's extension of the Standard Model it must produce new phenomena at or below the TeV scale. An attractive feature of supersymmetry is that it provides cosmology with a natural dark matter candidate in form of a stable, lightest supersymmetric particle [202]. There are a priori six candidates: the (s)neutrino, axi(o)n(o), gravitino and neutralino. These are, in fact, the only candidates because supersymmetry completes the Standard Model all the way to the GUT scale where its forces apparently unify. Because supersymmetry logically completes the Standard Model with no other new physics threshold up to the GUT-scale, it must supply the dark matter. Here we will focus on the neutralino, which, along with the axion, is for various reasons the most attractive WIMP candidate [206].

The supersymmetric partners of the photon, neutral weak boson and the two Higgs particles form four neutral states, the lightest of which is the stable neutralino

$$\chi = z_{11}\tilde{W}_3 + z_{12}\tilde{B} + z_{13}\tilde{H}_1 + z_{14}\tilde{H}_2. \quad (75)$$

In the minimal supersymmetric model (MSSM) [207] down- and up-quarks acquire mass by coupling to different Higgs particles, usually denoted by H_1 and H_2 , the lightest of which is required to have a mass of order the Z -mass. Although the MSSM provides us with a definite calculational framework, its parameters are many. For the present discussion we only have to focus on the following terms in the MSSM lagrangian

$$L = \cdots \mu \tilde{H}_1 \tilde{H}_2 - \frac{1}{2} M_1 \tilde{B} \tilde{B} - \frac{1}{2} M_2 \tilde{W}_3 \tilde{W}_3 - \frac{1}{\sqrt{2}} g v_1 \tilde{H}_1 \tilde{W}_3 - \frac{1}{\sqrt{2}} g v_2 \tilde{H}_2 \tilde{W}_3 + \cdots, \quad (76)$$

which introduce the (unphysical) masses M_1 , M_2 and μ associated with the neutral gauge bosons and Higgs particles, respectively. M_1 and M_2 are related by the Weinberg angle. The lagrangian introduces two Higgs vacuum expectation values $v_{1,2}$; the coupling g is the known Standard Model SU(2) coupling. Although the parameter space of the MSSM is more complex, a first discussion of dark matter uses just 3 parameters:

$$\mu, M_2, \text{ and } \tan \beta = v_2/v_1. \quad (77)$$

Further parameters which can also be varied include the masses of top, Higgs, squarks, etc.

Neutralino masses less than a few tens of GeV have been excluded by unsuccessful collider searches. For supersymmetry to resolve the hierarchy problem of the Standard Model the masses of supersymmetric particles must be of order the weak scale and therefore, in practice, at the TeV scale or below. Also, if neutralinos have masses of order a few TeV and above,

they overclose the Universe. Despite its rich parameter space supersymmetry has therefore been framed inside a well defined GeV–TeV mass window.

Assuming supersymmetry we can fill in some factors in the “back-of-the-envelope” estimates in the previous section. In supersymmetry, heavy WIMPs annihilate preferentially into weak bosons. Other important annihilation channels include [208]

$$\chi + \bar{\chi} \rightarrow b + \bar{b}. \quad (78)$$

Heavy quark decays dominate neutralino annihilation below the WW -threshold. Also the dimensional estimate of the neutralino-nucleon interaction cross section $\sigma(\chi N)$ can be replaced by an explicit calculation. It supports the dimensional estimate in the previous section. $\sigma(\chi N)$ receives contributions from 2 classes of diagrams: the exchange of Higgses and weak bosons, and the exchange of squarks. The result is often dominated by the large coherent cross section associated with the exchange of the lightest Higgs particle H_2 and is of the form

$$\sigma = \alpha_H (G_F m_N^2)^2 \frac{m_\chi^2}{(m_N + m_\chi)^2} \frac{m_Z^2}{m_H^4} \quad (79)$$

or, for large m_χ

$$\sigma = \alpha_H \left(G_F m_N^2 \right)^2 \frac{m_Z^2}{m_H^4}. \quad (80)$$

The proportionality parameter α_H is of order unity, but can become as small as 10^{-2} in some regions of the MSSM parameter space. This is illustrated in Fig. 12 where the MSSM parameter space is parametrized in terms of the unphysical masses $M(\mu)$ of the unmixed wino(Higgsino). (The ratio of the vacuum expectation values associated with the two Higgs particles $v_2/v_1 (= 2)$ is here fixed to some arbitrary value.) The relation of these parameters to the neutralino mass is shown in the figure. The full lines show fixed values of the neutralino mass m_χ . The lines labelled by squares trace fixed values of the “coupling” α_H . The dashed area indicates M, μ values which are excluded by cosmological considerations. In standard big bang cosmology neutralinos with the corresponding parameters will overclose the Universe.

Note that for a given χ mass there are two possible states with the same α_H value. One of them will preferentially annihilate into weak bosons, the other into fermions. Therefore, their neutrino signature is provided by W, Z decay and semi-leptonic heavy quark decays, respectively. Fig. 12 illustrates that, for heavy neutralinos, which can only be searched for by the indirect methods discussed here and are therefore of prime interest, any detector which can study dark matter with α_H as small as 0.1 can exclude the bulk of the phase space currently available to MSSM dark matter candidates.

Our main conclusions are summarized in Fig. 13 which exhibits, as a function of the neutralino mass, the detector area required to observe one event per year. The detailed calculation confirms our previous estimate of 100 events per 10^5 m^2 per year for a 500 GeV neutralino. The two branches in this and the following figures correspond to the two solutions for a fixed neutralino mass; see also Fig. 12. Various annihilation thresholds are clearly visible, most noticeable is the threshold associated with the W, Z mass near 100 GeV. The graphs confirm that large detectors are required to study the full neutralino mass range. It is clear from Fig. 13, however, that even detectors of more modest size significantly extend

the range explored by accelerators [209,210]. Neutralinos of 1 TeV mass are observable in a detector of area a few times 10^3 m^2 . The energy of the produced neutrinos is typically “a fraction” of the neutralino mass, e.g. 1/2 for neutralino annihilation into a W followed by a leptonic $e\nu$ decay. For lower masses the event rates are small because the detection efficiency for low energy neutrinos is reduced. This mass range has, however, already been excluded by accelerator experiments. For very high masses the number density of neutralinos, and therefore the event rate, becomes small. This is not a problem as problematically large masses are excluded by theoretical arguments as previously discussed. The same results are shown in Fig. 14(a) as contours in the M, μ plane which denote the neutrino detection area required for observation of 1 event per year. Clearly the 10^5 m^2 contour covers the parameter space. The problematic large μ, M_2 -region does not really represent a problem as its parameters lead to values of the matter density Ω exceeding unity as shown in the accompanying Fig. 14(b).

A realistic evaluation of the reach of an underground detector requires more than counting events per year. Realistic simulations of statistics and systematics must be done. Also a more complete mapping of the MSSM parameter space is required. For those interested we refer to Ref. [203].

10 Event Rates in a Generic 0.1 km^2 Detector: Synthesis

In the preceding sections we have attempted to summarize the new limits that will be set and the most likely observations that may be made by the next generation of high energy neutrino telescopes. If past history is a guide, however, the most important discoveries that occur when a new window is opened may be completely unanticipated.

We summarize some of the estimated event rates in Table 5. The corresponding neutrino fluxes are presented on Figs. 15 and 16. We remind the reader that a 0.1 km^2 detector is 2500 times larger than IMB, 100 times MACRO or LVD, but only “a factor” larger than many of the detectors under consideration or construction [211], e.g. AMANDA, BAIKAL, DUMAND and NESTOR. A list of operating and proposed underground detectors having the capability to detect high energy neutrinos is given in Table 6.

Table 5 gives the rates of upward going neutrino induced muons of atmospheric and extraterrestrial origin. The absorption in the Earth becomes important for the flatter extraterrestrial neutrino fluxes and the event rates are given both with and without absorption. The event rates expected from astrophysical neutrino sources are estimated with an account for absorption.

Some of the event rates in Table 5 predicted for the same type of source differ from each other by two orders of magnitude. This reflects the degree of uncertainty of our knowledge about the conditions and the role of different physical processes for the energetics of the source. The low event rates from the diffuse AGN background come from the revised calculations of Stecker *et al.* [36], while the high rates reflect the highest neutrino background of Protheroe and Szabo [38]. These highest rates are, however, in contradiction with limits set by the Frejus experiment [160,161,162]. The highest rate of diffuse TeV muons allowed by the Frejus limit is ~ 200 per 10^5 m^2 per year.

The estimated event rates from galactic sources come from the considerations presented

Table 5:

EVENTS PER YEAR IN 0.1 KM ²			
• ATMOSPHERIC (angle averaged, per steradian)			
	<u>muon energy</u>	[72]	[75]
	> 1 GeV	7800	8300
	> 1 TeV	129	104
• ATMOSPHERIC in 1° circle, Ref. [75]			
	<u>muon energy</u>	<u>cos θ = 0.05</u>	<u>cos θ = 0.95</u>
	> 1 GeV	12.6	5.6
	> 1 TeV	0.21	0.05
• EXTRATERRESTRIAL FLUXES (angle averaged)			
$\phi_\nu = 2.7 \times 10^{-5} (E_\nu/\text{GeV})^{-1.7} \text{ cm}^{-2}\text{s}^{-1}$			
	<u>muon energy</u>	<u>no abs.</u>	<u>with abs.</u>
	> 1 GeV	32.7	32.0
	> 1 TeV	4.3	3.8
$\phi_\nu = 4.0 \times 10^{-8} (E_\nu/\text{GeV})^{-1} \text{ cm}^{-2}\text{s}^{-1}$			
	<u>muon energy</u>	<u>no abs.</u>	<u>with abs.</u>
	> 1 GeV	8.8	6.6
	> 1 TeV	5.0	3.3
• ASTROPHYSICAL DIFFUSE FLUXES (per steradian)			
	<u>muon energy</u>	<u>plane of galaxy</u>	<u>AGN</u>
	> 1 GeV	12–20	80–1600
	> 1 TeV	1.5–3.0	40–800
also $\nu_e (6.3 \text{ PeV}) + e \rightarrow W^-$			0.3 per 1000 kton
• ASTROPHYSICAL POINT SOURCES ($E_\mu > 1 \text{ TeV}$)			
Galactic source (Eq. 35)/100			2.6
Extragalactic source (3C273)			0.1–25
• 500 GeV WIMPS from \odot			100

in §6. The event rate generated by the flux of Eq. (35) is an extreme upper limit, which would be difficult to reconcile with the observational limits from VHE/UHE γ -ray observations. As a conservative estimate we quote a rate corresponding to a neutrino flux smaller by two orders of magnitude. The least certain rate is the one expected for single AGN, given in Table 5 for the source 3C273. The smaller rate (0.1/yr) comes from the estimates for emission from the jets by Mannheim [176] and Stecker *et al* [182]. The highest event rate (25/yr) actually comes to the neutrino flux corresponding to the ‘high state’ γ -ray flux of 3C279 [182]. It is not likely that such a high luminosity could be maintained at the source for periods as long as a whole year. The atmospheric neutrino background relevant for source searches is given in two directions: close to the zenith and close to the horizon.

Even the smallest predicted event rates for the diffuse AGN background are easily detectable by a 10^5 m^2 neutrino telescope. The expected ratio of signal to background for TeV muons is from 0.3 to more than 2. The background, atmospheric neutrino rate, is large and allows calibration and continuous monitoring of the detector. The observations of the diffuse neutrino flux from the plane of the galaxy are much more difficult, although the likely

Table 6:
OPERATING DETECTORS WITH HIGH ENERGY NEUTRINO
DETECTION CAPABILITY

<u>Detector</u>	<u>Location</u>	<u>Area (m²) *</u>	<u>Technique</u>
NUSEX	Mont Blanc	10	streamer tubes/Fe
KGF	India	20	streamer tubes, very deep
SOUDAN II	USA	100	drift tubes/concrete
KAMIOKANDE	Japan	120	water Cherenkov
BAKSAN	Caucasus	250	liquid scintillator tanks
IMB	USA	400	water Cherenkov
LVD	Gran Sasso	300 [†]	liquid scintillator, streamer tubes
MACRO	Gran Sasso	850	liquid scintillator, streamer tubes
FUTURE INITIATIVES (partial list)			
<u>Detector</u>	<u>Location</u>	<u>Area (m²)</u>	<u>Technique</u>
SNO	Canada	600	D ₂ O
SUPERKAMIOKANDE	Japan	740	water Cherenkov
BAIKAL	Baikal	2000	water Cherenkov
GRANDE type	USA, Italy, Japan	~30000	water Cherenkov
DUMAND	Hawaii	20000+	water Cherenkov
AMANDA	South Pole	20000+	Cherenkov in deep ice
RAMAND	Antarctica	10 ⁶ m ² ?	microwave detection

concentration of the excess events in the direction of the galactic plane should be of some help.

The atmospheric background in point source searches is generally small. For energies of a TeV or more the neutrino direction can be reconstructed to 1 degree or better. We therefore expect less than one event per year in a 1° bin from the combined atmospheric and diffuse AGN backgrounds. It is then quite likely that one or more sources will be discovered by a 10⁵ m² detector, *provided* that hadronic processes play an important role in the energetics of powerful astrophysical objects.

With an even larger 1 km² detector we could then begin to study neutrino sources in some detail. It may be possible not only to count sources, but also to observe a multiplicity of sources with enough statistics to begin extracting information from energy spectra and temporal behaviour, particularly in comparison with photon observations. Comparisons of the neutrino and γ -ray spectra contain information about the photon absorption at source

[†]The total detector area for vertical upward going neutrinos is given for all existing detectors. The effective area for source searches depends on the detector and source location and on the detector efficiency for different zenith angles.

²In operation

and during propagation to Earth, i.e. about important physical properties of the sources and the intergalactic medium. We should be able to observe episodic flux increases and maybe even the periodicity of the neutrino emission from binary sources. It is unlikely that such detailed observations can be carried out with detectors smaller than 1 km^2 .

Finally, we mention the possibility that such a neutrino telescope can carry out Earth tomography [212], employing the attenuation of ultra high energy neutrinos, and making a direct density profile of the Earth (seismic measurements only yield velocity profiles, and moreover give little information on the Earth's core).

Halzen & Learned [213] have presented arguments such as these for doing neutrino astronomy on the scale of 1 kilometer. In order to achieve large area it is unfortunately necessary to abandon the low MeV thresholds of detectors such as IMB and Kamiokande. One focuses on high energies where: i) neutrino cross sections are large, ii) the muon range is increased, iii) the angle between the muon and parent neutrino is less than 1 degree and, iv) the atmospheric neutrino background is small. The accelerator physicist's method for building a neutrino detector uses absorber, 3 chambers with x, y wires with associated electronics with a price of 10^4 US dollars per m^2 . Such a 1 km^2 detector would cost 10 billion dollars. It is therefore a high priority to find methods which are more cost-effective to be able eventually to commission neutrino telescopes with effective area of order 1 km^2 . Obviously the proven technique developed by IMB, Kamiokande and others cannot be extrapolated to the 1 km scale. All present proposals do however exploit the Cherenkov technique well-proven by these experiments. The direction of the neutrino is inferred from the muon direction which is reconstructed by mapping the Cherenkov cone of the muon travelling through the detector. The arrival times and amplitudes of the Cherenkov photons, recorded by a grid of detectors, are used to reconstruct the track of the radiating muon.

Detectors presently under construction have a nominal effective area of 10^4 m^2 . Baikal is presently operating 36 optical modules and the South Pole AMANDA experiment started operating 4 strings with 20 optical modules each in January 94. The first generation telescopes [214] will consist of roughly 200 optical modules (OM). The experimental advantages and challenges are different for each experiment and, in this sense, they nicely complement one another. Briefly,

- AMANDA is operating in deep clear ice with an attenuation length in excess of 60 m, which is similar to that of the clearest water used in the Kamiokande and IMB detectors. Although residual bubbles are found at depth as large as 1 km, their density decreases rapidly with depth. Ice at the South Pole should be bubble-free below 1100-1300 m as it is in other polar regions [215]. The ice provides a convenient mechanical support for the detector. The immediate advantage is that all electronics can be positioned at the surface. Only the optical modules are deployed into the deep ice. Polar ice is a sterile medium with a concentration of radioactive elements reduced by more than 10^{-4} compared to sea or lake water. The low background results in an improved sensitivity which allows for the detection of high energy muons with very simple trigger schemes which are implemented by off-the-shelf electronics. Being positioned under only 1 km of ice it is operating in a high cosmic ray muon background. The challenge is to reject the down-going muon background relative to the up-coming neutrino-induced muons by a factor larger than 10^6 . The group claims to be able to meet this challenge

with an up/down rejection which is at present similar to that of the deeper detectors. The task is, of course, facilitated by the low background noise. The polar environment is difficult as well, with restricted access and one-shot deployment of photomultiplier strings. The technology has, however, been satisfactorily demonstrated with the deployment of the first 4 strings. It is now clear that the hot water drilling technique can be used to deploy OM's larger than the 8 inch photomultiplier tubes now used to any depth in the 2.8 km deep ice cover.

- BAIKAL shares the shallow depth with AMANDA, and has half its optical modules pointing up, half down. The depth of the lake is 1.4 km, so the experiment cannot expand downwards and will have to grow horizontally. Optical backgrounds similar in magnitude to ocean water have been discovered in Lake Baikal. The Baikal group has been operating for one year an array with 18 down-looking Quasar photomultiplier (a Russian-made 15 inch tube) units in April 1993, and may well count the first neutrinos in a natural water Cherenkov detector.
- DUMAND will be positioned under 4.5 km of ocean water, below most biological activity and well shielded from cosmic ray muon backgrounds, which are a factor of 100 lower than for the shallower detectors. One nuisance of the ocean is the background light resulting from radioactive decays, mostly K^{40} , plus some bioluminescence, yielding a noise rate of 60 kHz in a single OM. Deep ocean water is, on the other hand very clear, with an attenuation length of order 40 m in the blue. The deep ocean is a difficult location for access and service. Detection equipment must be built to high reliability standards, and the data must be transmitted to the shore station for processing. It has required years to develop the necessary technology and learn to work in an environment foreign to high-energy physics experimentation. The DUMAND group has successfully analysed data on cosmic ray muons from the deployment of a test string [19]. The power and signal cables from the detector location to shore (length 25 km) and the junction box are already installed. The group will proceed with the deployment of three strings in 1995.
- NESTOR is similar to DUMAND, being placed in the deep ocean (the Mediterranean), except for two critical differences. Half of its optical modules will point up as in BAIKAL. The angular response of the detector is being tuned to be much more isotropic than either AMANDA or DUMAND, which will give it advantages in, for instance, the study of neutrino oscillations. Secondly, NESTOR will have a higher density of photocathode (in some substantial volume) than the other detectors, and will be able to make local coincidences on lower energy events, even perhaps down to the supernova energy range (tens of MeV).

Other detectors have been proposed for near surface lakes or ponds (e.g. GRANDE, LENA, NET, PAN and the Blue Lake Project), but at this time none is in construction [214]. These detectors all would have the great advantage of accessibility and ability for dual use as extensive air shower detectors, but suffer from the 10^{10} – 10^{11} down-to-up ratio of muons, and face great civil engineering costs (for water systems and light-tight

containers). Even if any of these are built it would seem that the costs may be too large to contemplate a full, kilometer-scale detector.

In summary, there are four major experiments proceeding with construction, each of which has different strengths and faces different challenges. For the construction of a 1 km scale detector one can imagine any of the above detectors being the basic building block for the ultimate 1 km³ telescope. The redesigned AMANDA detector (with spacings optimized to the attenuation length in excess of 60 m), for example, consists of 5 strings on a circle with 60 meter radius around a string at the center (referred to as a 1 + 5 configuration). Each string contains 13 OM's separated by 15-20 m. Its effective volume is just below 10⁷ m³. Imagine AMANDA “supermodules” which are obtained by extending the basic string length (and module count per string) by a factor close to 4. Supermodules would then consist of 1 + 5 strings with 51 OM's separated by 20 meters on each string, for a total length of 1 km. A 1 km scale detector then might consist of a 1 + 7 + 7 configuration of supermodules, with the 7 supermodules distributed on a circle of radius 250 m and 7 more on a circle of 500 m. The full detector then contains 4590 phototubes, which is less than the 7000 used in the SNO detector. Such a detector (see Fig. 17) can be operated in a dual mode:

- it obviously consists of roughly 4×15 the presently designed AMANDA array, leading to an effective volume of $\sim 6 \times 10^8$ m³. Importantly, the characteristics of the detector, including threshold in the GeV-energy range, are the same as those of the AMANDA array module.
- the 1 + 7 + 7 supermodule configuration, looked at as a whole, instruments a 1 km³ cylinder with diameter and height of 1000 m with optical modules. High-energy muons will be superbly reconstructed as they can produce triggers in 2 or more of the supermodules spaced by large distance. Reaching more than one supermodule (range of 250 m) requires energy of 50 GeV. We note that this is the energy for which a neutrino telescope has optimal sensitivity to a typical E^{-2} source (background falls with threshold energy, and until about 1 TeV little signal is lost).

Alternate methods to reach the 1 km scale have been discussed by Learned and Roberts [216].

How realistic are the construction costs for such a detector? AMANDA's strings (with 10 OM's) cost \$150,000 including deployment. By naive scaling the final cost of the postulated 1 + 7 + 7 array of supermodules is of order \$75 million, comparable to that of Superkamiokande [217] (with $11,200 \times 20$ inch photomultiplier tubes in a 40 m diameter by 40 m high stainless steel tank in a deep mine). It is clear that the naive estimate makes several approximations over- and underestimating the actual cost.

In the next and final section of this paper we will briefly review alternate ideas for making a kilometer-scale neutrino detector in a cost-effective manner.

11 Alternative Methods for Neutrino Detection

11.1 Radio Detection

Over 30 years ago the suggestion was first made that radio antennas might be able to detect microwave emission from neutrino-induced cascades [218]. This method can in principle lead

to the construction of relatively inexpensive neutrino telescopes. Until recently only rough estimates have been made of the power emitted [219,220]. They indicated that the detection threshold is quite high, so high that the technique is probably insensitive to the atmospheric neutrinos.

That the radio signals emitted by neutrino-induced electromagnetic cascades are even close to observability is the result of interesting physics. According to the Frank-Tamm formula the power radiated by a particle with charge ze travelling a pathlength l in a medium of refractive index n is given by [221]

$$\frac{dW}{d\nu} = \left[\frac{4\pi^2\hbar}{c} \alpha \right] z^2 \nu \left[1 - \frac{1}{\beta^2 n^2} \right] l, \quad (81)$$

where ν is the frequency and $\alpha = (137)^{-1}$. Naively one might expect the power generated in a shower of N charged particles to be proportional to $N\langle l \rangle$. This is not correct. If the emitted wavelength is large compared to the physical dimensions of the shower, or equivalently, the electric pulse generated by the shower is short compared to the period of the waves observed, then the emission by the shower particles is coherent and the power is of order $(\Delta q \cdot N)^2 \langle l \rangle$ [218,222]. Here Δq is the excess negative charge in the shower

$$\Delta q = \frac{N(e^-) - N(e^+)}{N(e^-) + N(e^+)}, \quad (82)$$

which enters in the coherent case because the electric fields from opposite charges cancel for the same $\langle l \rangle$. Δq is positive mainly because Compton scattering of shower photons on atomic electrons creates an excess of negative charges in the shower. Coherence thus implies an enhancement $(\Delta q)^2 N$ which can compensate the loss in power associated with the ν dependence of Eq. (81). Roughly, from visible light to GHz radiowaves the suppression associated with the factor ν in the Frank-Tamm relation is a factor 10^6 which can be compensated by coherence because N is of order 10^6 for PeV showers.

The technique has been successfully tested in experiments measuring radio emission by air showers observed in coincidence with particle arrays [223]. Whereas atmospheric fluctuations make the systematics of the radioemission difficult to handle, this is not a problem in denser material, like ice. The physical dimension of the shower is reduced because the radiation length is only 39 cm. The coherence is retained to higher frequencies, where more energy is available. Determination of the precise threshold for observation in a medium like ice depends on the details of the cascade and one has to perform a real time numerical simulation of electromagnetic cascades in ice. The calculations [224] show that to a very good precision the enhancement factor from coherence $(\Delta q)^2 N$ is proportional to the primary energy, and therefore the power of the radioemission is proportional to the square of the cascade energy.

The critical parameter is the energy threshold for detection which not only depends on the power generated but also on the absorption in the ice and the background noise from the apparatus and its environment. Absorption at 1 GHz depends critically on temperature and therefore on the location of the experiment. Determination of *in situ* background noise is a complex problem. Experiments indicate that thermal noise of temperature 300K represents an adequate guess of the background [225]. For this assumption the amplitude of the noise spectrum rises linearly with frequency, i.e. it exhibits the same dependence as the signal below

~ 1 GHz [223]. In a detector of bandwidth $\Delta\nu$ the noise varies as $\Delta\nu^{1/2}$, and therefore the bandwidth enhances the signal to noise ratio by the square root of the bandwidth. Neglecting absorption and assuming $\Delta\nu = 1$ GHz, a signal to noise ratio of unity is achieved for a detection threshold linearly proportional to the distance r from the shower,

$$E_{\text{th}} (\text{PeV}) \simeq 5 \times 10^3 r (\text{m}) . \quad (83)$$

E.g. only neutrinos of 5 PeV and above can be sampled in 1 km of ice. This is a very high threshold. Existing experiments already set limits on high neutrino fluxes which imply extremely low event rates above 5 PeV. This threshold estimate is based on a signal to noise argument. The power in the signal is about an order of magnitude smaller than the result quoted by Zeleznykh and collaborators [219].

11.2 Acoustic Detection

High detection threshold may also be the main shortcoming of the idea of acoustic detection of neutrinos, originally suggested by Bowen [226]. Acoustic waves are produced by the heating of the medium by the ionization loss of the cascade particles. Shower direction can also be determined by the timing and amplitude of the signal in different detectors [227]. The beam pattern is coherent and reinforcing in a plane perpendicular to the cascade direction. One can envisage a detector consisting of pressure transducers placed in an array. The optimal depth is not as yet clear, but it would have to be deep enough to avoid the problem of acoustic wave scattering, and perhaps also to escape high frequency surface noise. The acoustic losses set the size scale of the detector.

Laboratory data [228] indicate that pure ice has a sound velocity (of compressional waves) of $v = 3200$ m/s and a Q of perhaps 1000 at low temperatures. South Pole ice near the surface is below -50° C. With an attenuation length of about 100 m, one can imagine detectors in a lattice of roughly 100 m spacing. Using Bowen's [226] figure of merit, we estimate a signal-to-noise ratio of unity in a single detector at 100 m distance from a 6 PeV cascade, with the signal-to-noise ratio scaling as the square of energy/distance. The frequency maximum is about 20k Hz. Despite the dauntingly high detection threshold in comparison to the optical technique, acoustic detection remains interesting enough for further investigation for several reasons. First, acoustic sensors are compact, pressure tolerant, inexpensive (piezoelectric sensors are cheap compared to photomultipliers), and could be installed relatively easily. It does not seem outrageous to imagine a 30×30 lattice of strings extending downwards for several kilometers thus covering a volume of the order of 30 billion tons.

11.3 Horizontal Air Showers Revisited

We already discussed in section 3.3 the implications of horizontal air shower measurements for atmospheric muons and neutrinos, especially the high energy component of charm origin. We discuss here the use of horizontal air showers to search for cosmic neutrinos. Given a flux $\phi_\nu(E_\nu)$, the expected event rate for neutrino-induced horizontal showers is calculated as described in §3.4, Eqs. (24) and (27).

The atmospheric muon spectrum falls rapidly with energy ($\gamma \sim 3.7$ for π , K decay muons; ~ 2.7 for muons from charm decay), while neutrino cross sections rise with energy.

For large enough fluxes of astrophysical neutrinos, neutrino-induced showers can dominate at sufficiently high energies. In addition to charge current $\nu_\mu(\bar{\nu}_\mu)$ interactions, there will be a contribution from $\nu_e(\bar{\nu}_e)$. For flat spectra and ν_μ and ν_e fluxes of a similar order of magnitude, the resonant W^- production dominates the rate of ν -induced horizontal air showers for shower sizes in the narrow range $[2 \times 10^6 \text{ to } 4 \times 10^6]$.

Horizontal shower measurements [90] have been compared to expectations from diffuse AGN fluxes in Ref. [89], where the potential of air shower arrays for detection of diffuse neutrino fluxes was demonstrated. Similar limits have been obtained recently by the EASTOP Collaboration [92]. Muon-poor showers are selected in the Tokyo data [90], so that the limit is stronger for $\nu_e(\bar{\nu}_e)$ fluxes, which actually dominate the neutrino-induced horizontal air shower signal.

Figure 18 shows the rate of (muon-poor) horizontal showers associated with the neutrino emission by active galaxies. Also shown is the background from atmospheric muons. The signal-to-background increases with shower size and exceeds unity for shower sizes exceeding 10^6 for the prediction of reference [38]. The figure illustrates the kind of sensitivity air shower arrays can reach in the detection of cosmic neutrinos. An improved detection method would be to select all, not only muon-poor, showers that are very close to the horizon. This would avoid any contamination from cosmic rays without rejecting hadron-like neutrino induced showers. Unless prompt muon production by charm turns out to be unexpectedly large, the larger of the range of AGN isotropic backgrounds of Szabo and Protheroe [38] should be detectable by a horizontal shower measurement with enough exposure to detect showers with $N_e > 10^6$. A flux peaked at energies exceeding 1 PeV, will be strongly attenuated in the earth and only detectable in upward going muons close to horizontal angles. Under these circumstances, neutrino detection via horizontal air showers may be a useful alternative detection method.

Acknowledgements. We are grateful for helpful discussions with many colleagues, including Karl Mannheim, Ray Protheroe, David Seckel, Floyd Stecker and Enrique Zas. This research is supported in part by DOE Grants DE-FG-91ER40626 (TKG & TS) and DE-AC02-76ER00881(FH). The work of FH is also supported by the University of Wisconsin Research Committee with funds granted by The Wisconsin Alumni Research Foundation.

References

- [1] Y. Totsuka, *Rep. Prog. Phys.* **55** (1982) 377.
- [2] J.N. Bahcall & M.H. Pinsonneault, *Revs. Mod. Phys.* **64** (1992) 885.
- [3] J.N. Bahcall, *Neutrino Astrophysics* (Cambridge University Press, 1989).
- [4] S. Turck Chieze *et al.*, *Ap. J.* **355** (1988) 415.
- [5] K. Greisen, *Ann. Rev. Nucl. Sci* **10**, (1960) 63.
- [6] M.A. Markov & I.M. Zheleznykh, *Nucl. Phys.* **27** (1961) 385. See also M.A. Markov in *Proc. 1960 Annual International Conference on High Energy Physics at Rochester* (ed. E.C.G. Sudarshan, J.H. Tinlot & A.C. Melissinos) (1960).

- [7] C.V. Achar *et al.*, *Phys. Letters* **18**, 196 and **19** (1965) 78.
- [8] M.G.K. Menon *et al.* *Proc. Roy. Soc.* **A301**, (1967) 137.
- [9] F. Reines *et al.*, *Phys. Rev. Letters* **15**, (1965) 429.
- [10] F. Reines, *Proc. Roy Soc.* **A301**, (1967) 125.
- [11] K.S. Hirata *et al.*, (Kam-II Collaboration), *Phys. Letters*, **B280** (1992) 146.
- [12] R. Becker-Szendy *et al.*, (IMB Collaboration), *Phys. Rev.* **D46** (1992) 3720. See also D. Casper *et al.* *Phys. Rev. Letters*, **66** (1991) 2561.
- [13] M.R. Krishnaswami *et al.*, *Nuovo Cimento*, **C9** (1986) 167; *Phys. Letters*, **106B**, 339 (1981) and **115B** (1982) 349; *Proc. 6th Workshop on Grand Unification* (World Scientific, Singapore, 1986) eds. S. Rudaz and T. Walsh, p. 97.
- [14] Ch. Berger *et al.*, *Physics Letters* **B245** (1990) 305 and **227** (1989) 489.
- [15] M. Aglietta *et al.*, *Europhysics Letters* **8** (1989) 611; *Physics Letters*, **B280** (1992) 146.
- [16] M.C. Goodman (Soudan 2 Collaboration), in *Proc. DPF '92 Meeting*, eds. C. H. Albright *et al.*, (World Scientific, Singapore, 1993) p. 1300.
- [17] BAIKAL Collaboration, I. Sokalski and C. Spiering, "The BAIKAL Neutrino Telescope NT-200," BAIKAL 92-03 (1992).
- [18] I.A. Belolaptikov *et al.*, *Nucl. Phys. B (Proc. Suppl.)* **35** (1994) 290.
- [19] J. Babson *et al.* (DUMAND Collaboration), *Phys. Rev.* **D42** (1990) 3613.
- [20] S. Barwick, *et al.*, *J. Phys. G: Nucl. Part. Phys.* **18** (1992) 225.
- [21] D. Lowder *et al.*, *Nature* **353** (1991) 331; T. Miller *et al.*, *Proceedings of the 23rd International Cosmic Ray Conference*, Calgary, Canada (1993); S. Tilav *et al.*, *Proceedings of the 23rd International Cosmic Ray Conference*, Calgary, Canada (1993).
- [22] *Proceedings of the NESTOR Workshop at Pylos, Greece*, ed. L. K. Resvanis, October 1992, U. Athens (1993).
- [23] J.J. Engelmann *et al.*, *Astronomy & Astrophys.* **233** (1990) 96.
- [24] T.K. Gaisser, *Cosmic Rays and Particle Physics*, Cambridge University Press (1990).
- [25] Paolo Lipari, *Astroparticle Physics* **1** (1993) 195.
- [26] H. Bloemen, *Ann. Revs. Astron. Astrophys.* **27** (1989) 469.
- [27] V.S. Berezinsky, T.K. Gaisser, F. Halzen & Todor Stanev, *Astroparticle Physics* **1** (1993) 281. See also T.K. Gaisser, T. Stanev and F. Halzen, in *Proc. 22nd Int. Cosmic Ray Conf.* (Dublin Inst. Adv. Studies, 1991) Vol. 1, p. 564.

- [28] P.O. Lagage and C.J. Cesarsky, *Astron. Astrophys.* **125** (1983) 249.
- [29] B. Peters, *Nuovo Cimento* **22** (1961) 800.
- [30] W. I. Axford, in *Proceedings of 1990 Kofu Symposium on "Astrophysical Aspects of the Most Energetic Cosmic Rays"* (eds. M. Nagano and F. Takahara, World Scientific) p. 406 (1991).
- [31] H.J. Völk and P.L. Biermann, *Ap. J. Lett.* **333** (1988) L65.
- [32] J. R. Jokipii, *Astro. Journal* **313**(1987) 842.
- [33] R.J. Protheroe & D. Kazanas, *Ap. J.* **265** (1983) 620.
- [34] D. Kazanas & D. Ellison, *Ap. J.* **304** (1986) 178.
- [35] M. Sikora *et al.*, *Ap. J. Lett.* **320** (1987) L81.
- [36] F.W. Stecker, C. Done, M.H. Salamon and P. Sommers, *Phys. Rev. Lett.* **66** (1991) 2697 and **69** 2738(E) (1992).
- [37] K. Mannheim and P.L. Biermann, *Astron. Astrophys.* **253** (1992) L21.
- [38] A.P. Szabo & R.J. Protheroe, in *Proc. High Energy Neutrino Astrophysics Workshop* (Univ. of Hawaii, March 1992, ed. V.J. Stenger, J.G. Learned, S. Pakvasa & X. Tata, World Scientific, Singapore) and *Astroparticle Physics* (to be published).
- [39] G. Barr, T.K. Gaisser & Todor Stanev, *Phys. Rev.* **D39** (1989) 3532.
- [40] H. Lee & Y.S. Koh, *Nuovo Cimento B* **105** (1990) 883.
- [41] M. Honda, K. Kasahara, K. Hidaka & S. Midorikawa, *Physics Letters B* **248** (1990) 193.
- [42] E.V. Bugaev & V.A. Naumov, *Physics Letters B* **232** (1989) 391. The published fluxes do not account for muon polarization. The results of a new calculation including the effect are available now (V.A. Naumov, private communication).
- [43] T.K. Gaisser *Phil. Trans. R. Soc. Lond.* **A346** (1994) 75.
- [44] T. Kajita, in *Frontiers of Neutrino Astrophysics* (Takayama, ed. Y. Suzuki & K. Nakamura, Universal Academy Press, Tokyo, (1992) p. 293.
- [45] E.W. Beier *et al.*, *Physics Letters B* **283** (1992) 446.
- [46] D. Casper *et al.*, *Phys. Rev. Letters* **66** (1991) 2561.
- [47] T.K. Gaisser & J.S. O'Connell, *Phys. Rev.* **D34** (1986) 822.
- [48] E. Beier & E. Frank, *Phil. Trans. R. Soc. Lond.* **A346** (1994) 63.
- [49] M. Takita, Ph.D. Thesis, Univ. of Tokyo, February 1989, ICR-Report-186-89-3.

- [50] David W. Casper, Ph.D. Thesis, Univ. of Michigan, 1990.
- [51] J. Engel, E. Kolbe, K. Langanke & P. Vogel, *Phys. Rev.* **D48** (1993) 3048.
- [52] R. Merenyi *et al.*, *Phys. Rev.* **D45** (1992) 743.
- [53] D.D. Koetke *et al.*, *Phys. Rev.* **C46** (1992) 2554.
- [54] M. Honda, K. Kasahara & S. Midorikawa in *Frontiers of Neutrino Astrophysics* (Takayama, ed. Y. Suzuki & K. Nakamura, Universal Academy Press, Tokyo, 1992) p. 309.
- [55] G.L. Fogli, E. Lisi & D. Montanino, *Phys. Rev.* **D49** (1994) 3628.
- [56] W.A. Mann, T. Kafka & W. Leeson, *Physics Letters* **B291** (1992) 200.
- [57] T.K. Gaisser, *Nucl. Phys. B (Proc. Suppl.)* **35** (1994) 209.
- [58] M. Conversi, *Phys. Rev.* **79** (1950) 749.
- [59] E.A. Bogomolov *et al.* as quoted by E.V. Bugaev, G.V. Domogatsky & V.A. Naumov in Proc. Japan-U.S. Seminar on Cosmic Ray Muon and Neutrino Physics/Astrophysics (ed. Y. Ohashi & V.Z. Peterson, 1986) p. 232.
- [60] L.T. Baradzei *et al.*, *Zh. Eksp. Teor. Fiz.* **36** (1959) 1617.
- [61] M. Circella *et al.*, *Proc. 23rd Int. Cosmic Ray Conf.* (Calgary) **4** (1993) 503.
- [62] W. Lohmann, R. Kopp & R. Voss, CERN Yellow Report No. EP/85-03 (unpublished).
- [63] Paolo Lipari & Todor Stanev, *Phys. Rev.* **D44** (1991) 3543.
- [64] T.K. Gaisser & A.F. Grillo, *Phys. Rev.* **D36** (1987) 2752. See also T.K. Gaisser & Todor Stanev, *Phys. Rev.* **D31** (1985) 2770.
- [65] C. Quigg, M.H. Reno and T.P. Walker, *Phys. Rev. Lett.* **57** (1986) 774; also see M.H. Reno and C. Quigg, *Phys. Rev.* **D37** (1988) 657.
- [66] R. Becker-Szendy *et al.* (IMB Collaboration) *Phys. Rev. Lett.* **69** (1992) 1010.
- [67] R. Becker-Szendy *et al.*, in *Proceedings of the XXVth International Conference on High Energy Physics*, Singapore, 1990, edited by K.K. Phua and Y. Yamaguchi (World Scientific, Singapore, 1991) p. 662.
- [68] M.M. Boliev *et al.*, in *Proc. 3rd Int. Workshop on Neutrino Telescopes* (ed. M. Baldo Ceolin) (1991) 235.
- [69] M. Mori *et al.*, *Phys. Letters* **B210** (1991) 89.
- [70] W. Frati, T.K. Gaisser, A.K. Mann & T. Stanev, *Phys. Rev.* **D48** (1993) 1140.

- [71] KAMIOKANDE Collaboration (Y. Fukuda *et al.*, ICRR-Report-321-94-16, submitted to *Physics Letters B*.
- [72] L.V. Volkova, *Yad. Fiz.* **31** (1980) 784 (*Sov. J. Nucl. Phys.* **31** (1980) 1510).
- [73] K. Mitsui, Y. Minorikawa & H. Komori, *Nuovo Cimento* **9C** (1986) 995.
- [74] A.V. Butkevich, L.G. Dedenko & I.M. Zheleznykh, *Yad. Fiz.* **50** (1989) 142 (*Sov. J. NuclPhysics* **50** (1989) 90).
- [75] V. Agrawal, T.K. Gaisser, Paolo Lipari & T. Stanev, in preparation.
- [76] E. Eichten, I. Hinchcliffe, K.Lane & C. Quigg, *Revs. Mod. Phys.* **56** (1984) 578 (Erratum **58**, 1065 (1986)).
- [77] J.F. Owens, *Physics Letters* **B266** (1991) 126.
- [78] MACRO Collaboration, talk presented by D. Michael, Snowmass, July 1994.
- [79] H. Adarkav *et al.*, *Proc. of the 21st Int. Cosmic Ray Conference*, ed. R. Protheroe, Adelaide (1990), Vol. 9, p. 310.
- [80] Yu M. Andreyev *et al.*, *Proc. of the 21st Int. Cosmic Ray Conference*, ed. R. Protheroe, Adelaide (1990), Vol. 9, p. 301.
- [81] R.P. Kokoulin and A.A Petrukhin, *Proc. of the 22nd Int. Cosmic Ray Conference*, ed. M. Cawley *et al.*, Dublin (1991) Vol. 4, p. 537.
- [82] F. Halzen, R. Vázquez and E. Zas, *Astroparticle Physics* **1** (1993) 297.
- [83] J.P. Guillet, P. Nason and H. Plothow-Besch, *Proc. of the Large Hadron Collider Workshop*, Aachen 1990, Vol. II, p. 116.
- [84] J.C. Collins and R.K. Ellis, *Nucl. Phys.* **B380** (1991) 3.
- [85] See Review of Particles Properties, J.J. Hernández *et al.* *Phys. Lett.* **B239** (1990) 1.
- [86] R. Ammar *et al.*, *Phys. Lett.* **B183** (1987) 110.
- [87] P. Nason, S. Dawson and R.K. Ellis, *Nucl. Phys.* **B303** (1988) 607.
- [88] T.N. Afanasieva *et al.*, *Proc. of the 20th Int. Cosmic Ray Conference*, (Moscow) Vol. 9, p. 161 (1987).
- [89] F. Halzen and E. Zas, *Phys. Lett.* **B289** (1992) 184.
- [90] M. Nagano *et al.*, *J. Phys. Soc. Japan* **30** (1971) 33.
- [91] S. Mikamo *et al.*, *Lett. al Nuovo Cimento* **34** (1982) 273.
- [92] M. Aglietta *et al.* (EASTOP Collaboration) LNGS preprint 94/96, May 1994.

- [93] M. Nagano *et al.*, *J. Phys. G: Nucl. Phys.* **12** (1986) 69.
- [94] T.K. Gaisser, T. Stanev, F. Halzen, W.F. Long and E. Zas, *Phys. Rev.* **D43** (1991) 314.
- [95] E. Zas, F. Halzen and R.A. Vázquez, *Proc. of the International Symposium on Multiparticle Dynamics*, Santiago de Compostela 1992, ed. C. Pajares, World Scientific, Singapore (1992).
- [96] C. Gonzales-Garcia, F. Halzen, R. Vázquez and E. Zas, *Phys. Rev.* **D49** (1994) 2310.
- [97] D. Eichler, *Nature* **275** (1978) 725. See also W.Y. Vestrand & D. Eichler, *Ap. J.* **261** (1982) 251.
- [98] V.S. Berezinsky, *Proc. 1979 DUMAND Workshop* (ed. J. Learned) (1980) 674.
- [99] T.K. Gaisser & Todor Stanev, *Phys. Rev. Letters* **54** (1985) 2265.
- [100] A.K. Harding & T.K. Gaisser, *Ap. J.* **358** (1990) 561.
- [101] V.S. Berezinsky, C. Castagnoli & P. Galeotti, *Nuovo Cimento* **8C** (1985) 185.
- [102] V.S. Berezinsky and O.F. Prilutsky, *Astron. Astrophys.* **66** (1978) 325.
- [103] H. Sato, *Prog. Theor. Phys.* **58** (1977) 549.
- [104] M.M. Shapiro & R. Silberberg, in *Relativity, Quanta and Cosmology*, (ed. DeFinis, New York: Johnson Reprint) Vol. 2, p. 745 (1979).
- [105] T.K. Gaisser & Todor Stanev, *Phys. Rev. Letters*, **58** (1987) 1695. See also T.K. Gaisser, Alice K. Harding & Todor Stanev, *Ap. J.* **345** (1989) 423.
- [106] S. Biller *et al.* *Ap. J.* **423** (1994). See also D.E. Alexandreas *et al.* *Ap. J.* **383** (1991) L53.
- [107] T.A. McKay *et al.*, *Ap. J.* **417** (1993) 742.
- [108] J. van Stekelenborg *et al.*, *Phys. Rev.* **D48** (1993) 4504.
- [109] W.H. Allen *et al.*, *Phys. Rev.* **D48** (1993) 466. See also W.H. Allen *et al.*, *Astroparticle Physics* **1** (1993) 269.
- [110] M. Amenomori *et al.*, *Phys. Rev. Letters* **69** (1992) 2468.
- [111] J.W. Cronin, K.G. Gibbs and T.C. Weekes, *Ann. Revs. Nucl. Part. Phys.* **43** (1993) 883.
- [112] A. Borione *et al.* *Proc. 23rd Int. Cosmic Ray Conf.* (Calgary) Vol. 1 p. 385 (1993).
- [113] V.S. Berezinsky & John G. Learned, in *Proc. High Energy Neutrino Astrophysics Workshop* (Univ. of Hawaii, 1992, ed. V.J. Stenger, J.G. Learned, S. Pakvasa & X. Tata, World Scientific, Singapore).

- [114] T.K. Gaisser, Proc. 2nd Int. Workshop on Neutrino Telescopes (ed. Milla Baldo-Ceolin) (1990) p. 397.
- [115] M. Punch *et al.*, *Nature* **358** (1992) 477.
- [116] F.W. Stecker, O.C. De Jager and M.H. Salamon, *Ap. J.* **390** (1992) L49.
- [117] Talks by P. L. Biermann, K. Mannheim, R. J. Protheroe and F. W. Stecker in *High Energy Neutrino Astronomy*, V. Stenger, J. Learned, S. Pakvasa and X. Tata, Editors, 1992 (World Scientific, Singapore).
- [118] P. Biermann, in *Proceedings of 1990 Kofu Symposium on "Astrophysical Aspects of the Most Energetic Cosmic Rays"* (eds. M. Nagano and F. Takahara, World Scientific) p. 301 (1991).
- [119] C.D. Dermer, R. Schlickeiser and A. Mastichiadis, *Astron. Astrophys.* **256** (1992) L27.
- [120] A.A. Zdziarski & J.H. Krolik, *Ap. J.* **409** (1993) L33.
- [121] M. Sikora, M.C. Begelman and M.J. Rees, *Ap. J.* **421** (1994) 153.
- [122] F. W. Stecker, *Astro. Journal* **228** (1979) 919.
- [123] T.K. Gaisser & R.S. Schaefer, *Ap. J.* **394** (1992) 174.
- [124] V. S. Berezinsky, T. K. Gaisser, F. Halzen and T. Stanev, *Astropart. Phys.* **1** (1993) 281. See also V. S. Berezinsky and V. A. Kudryavtsev, *Sov. Astron. Lett.* **14** (1988) 873.
- [125] J. Matthews *et al.* *Ap. J.* **375** (1991) 202.
- [126] H. Bloemen *et al.*, COMPTEL Preprint No. 10 (1993).
- [127] H. Bloemen *et al.*, *Astron. Astrophys.* **139** (1984) 37.
- [128] D. Seckel, Todor Stanev & T.K. Gaisser, *Ap. J.* **382** (1991) 652.
- [129] T.K. Gaisser, in *Proceedings of 1990 Kofu Symposium on "Astrophysical Aspects of the Most Energetic Cosmic Rays"* (eds. M. Nagano and F. Takahara, World Scientific) p. 146 (1991).
- [130] A.M. Hillas, *Nature* **312** (1984) 50.
- [131] R. Cowsik & T.K. Gaisser, *Proc. 17th Int. Cosmic Ray Conf.* (Paris) **2** (1981) 218.
- [132] R.J. Protheroe and T. Stanev, *Ap. J.* **322** (1987) 838.
- [133] V. S. Berezinsky, *Proc. of the Third International Symposium on Neutrino Telescopes*, Venice (1991), ed. by M. Baldo-Ceolin, p. 125.
- [134] M. Samorski and W. Stamm, *Ap. J. Lett.* **268** (1983) L17; J. Lloyd-Evans *et al.* *Nature* **305** (1983) 784.

- [135] T.K. Gaisser and T. Stanev, *Phys. Rev. Lett.* **54** (1985) 2265; E.W. Kolb, M.S. Turner and T.P. Walker, *Phys. Rev* **D32** (1985) 1145; V.S. Berezinsky, C. Castagnoli and P. Galeotti, *Il Nuovo Cim.* **8C** (1985) 185.
- [136] P.M. Chadwick *et al.*, *Nature* **318** (1985) 642.
- [137] V.S. Berezinsky and O.F. Prilutsky *Astron. Astrophys.* **66** (1978) 325.
- [138] H. Sato *Prog. Theor. Phys.* **58** (1978) 549x.
- [139] T.K. Gaisser, Alice K. Harding & Todor Stanev, *Ap. J.* **345** (1989) 423.
- [140] Y. Yamada, T. Nakamura, K. Kasahara & H. Sato, *Prog. Theor. Phys.* **79** (1987) 426.
- [141] V. S. Berezinsky and V.S. Ptuskin, *Astron. Astrophys.* **215** (1989) 399.
- [142] V. S. Berezinsky, in *Proc. Neutrino 77* (Nauka, Moscow, 1977) **1**, p. 177; D. Eichler, *Ap. J.* **232** (1979) 106; R. Silberberg and M.M. Shapiro, in *Proc. 16th Int. Cosmic Ray Conf.* Vol. 10 (1979) p. 357; V.S. Berezinsky and V.L. Ginzburg, *Mon. Not. Royal Astr. Soc.* **194** (1981) 3.
- [143] P.L. Biermann and P.A. Strittmatter, *Ap. J.* **322** (1987) 643.
- [144] M. C. Begelman, B. Rudak and M. Sikora, *Ap. J.* **362** (1990) 38.
- [145] M.J. Rees, *Ann. Rev. Astron. Astrophys.* **22** (1984) 471.
- [146] J.H. Krolik *et al.*, *Ap. J.* **371** (1991) 541.
- [147] J. Clavel *et al.*, *Ap. J.* **393** (1992) 113.
- [148] R.F. Mushotzky, C. Done and K.A. Pounds, *Ann. Rev. Astron. Astrophys.* **31** (1993) 717.
- [149] D.B. Sanders *et al.*, *Ap. J.* **347** (1989) 29.
- [150] K.I. Kellerman *et al.*, *Astron. J.* **98** (1989) 1195.
- [151] R.D. Blandford in *Active Galactic Nuclei* (Springer-Verlag, Berlin, ed. R.D. Blandford, H. Netzer & L. Woltjer) pp. 161-275.
- [152] M. Sikora and M.C. Begelman, in *High Energy Neutrino Astronomy*, eds. V.J. Stenger *et al.* (World Scientific, Singapore, 1992), p. 114.
- [153] F.W. Stecker, *Phys. Rev. Lett.* **21** (1968) 1016.
- [154] M. Sikora, M.C. Begelman & B. Rudak, *Ap. J. Lett.* **341** (1968) L33.
- [155] D. Kazanas & P.M. Giovanoni in *Proc. Workshop on High Energy Neutrino Astronomy*, (ed. V.J. Stenger, J.G. Learned, S. Pakvasa & X. Tata, World Scientific, 1992) p. 94.

- [156] R.J. Protheroe and T. Stanev, in *High Energy Neutrino Astronomy*, eds. V.J. Stenger *et al.* (World Scientific, Singapore, 1992), p. 40.
- [157] L. Nellen, K. Mannheim and P.L. Biermann, *Phys. Rev.* **D47** (1993) 5270.
- [158] T. Maccacaro *et al.* *Ap. J.* **374** (1991) 117.
- [159] K. Morisawa *et al.* *Astron. Astrophys.* **236** (1990) 299.
- [160] T.K. Gaisser, *Nucl. Phys. B (Proc. Suppl.)* **31** (1993) 399.
- [161] H. Meyer, in *4th Int. Workshop on Neutrino Telescopes*, ed. M. Baldo-Ceolin, p. 213.
- [162] W. Rhode, preprint (University of Wuppertal, 1994).
- [163] T.K. Gaisser, in *Proc. 1994 Venice Workshop on Neutrino Telescopes* (in press).
- [164] R.M. Baltrusaitis *et al.* *Phys. Rev.* **D31** (1985) 2192.
- [165] S.L. Glashow *Phys. Rev.* **118B** (1960) 316.
- [166] Francis Halzen & Alan D. Martin, *Quarks & Leptons*, John Wiley & Sons, New York (1984) pp. 269 and 374.
- [167] J.G. Learned and T. Stanev, in *Proc. 3rd Int. Workshop on Neutrino Telescopes*, ed. M. Baldo-Ceolin, p. 473.
- [168] D.A. Morris and A. Ringwald, in *Proc. 23rd ICRC*, eds. D.A. Leahy *et al.* **4**, p. 407.
- [169] R.C. Hartman *et al.* *Ap. J. Lett.* **385** (1992) L1.
- [170] C.E. Fichtel *et al.* Preliminary EGRET Source Catalog, in *Proc. Compton Symposium*, in print.
- [171] J. Frank, A.R. King & D.J. Raine, *Accretion Power in Astrophysics*, Cambridge University Press (1985) p. 193.
- [172] K. Mannheim and P.L. Biermann, *Astron. Astrophys.* **22** (1989) 211.
- [173] K. Mannheim, *Astron. Astrophys.* **269** (1993) 67.
- [174] R.J. Protheroe and T. Stanev, *Mon. Not. Royal A. Soc.* **264** (1993) 191.
- [175] K. Mannheim, in *High Energy Neutrino Astronomy*, eds. V.J. Stenger *et al.* (World Scientific, Singapore, 1992), p. 105.
- [176] K. Mannheim, *Phys. Rev.* **D48** (1993) 2408.
- [177] G.G. Lichti *et al.*, to appear in *Proc. 2nd Compton Symposium, College Park, 1993*.
- [178] Y.C. Lin *et al.* *Ap. J. Lett.* **401** (1992) L61.

- [179] G. Mohanty *et al.* in *Proc. 23rd ICRC*, eds. D.A. Leahy *et al.* **1**, p. 440.
- [180] F. Halzen and R. A. Vazquez, in *Proc. 23rd ICRC*, eds. D.A. Leahy *et al.* **1**, p. 447.
- [181] P.L. Biermann, in *Cosmic Gamma Rays, Neutrinos and Related Astrophysics*, eds. M.M. Shapiro and J.P. Wefel (Kluwer, Dordrecht, 1988) p. 21.
- [182] F.W. Stecker *et al.* in *High Energy Neutrino Astronomy*, eds. V.J. Stenger *et al.* (World Scientific, Singapore, 1992), p. 105.
- [183] F.W. Stecker, in *Proceedings of the Fifth International Workshop on Neutrino Telescopes*, Venice, 1993, ed. M. Baldo-Ceolin, p. 443.
- [184] K. Mannheim, private communication.
- [185] V.S. Berezinsky and J.G. Learned, in *High Energy Neutrino Astronomy*, eds. V.J. Stenger *et al.* (World Scientific, Singapore, 1992), p. 43.
- [186] A. Mastichiadis and J.G. Kirk, in *High Energy Neutrino Astronomy*, eds. V.J. Stenger *et al.* (World Scientific, Singapore, 1992), p. 63.
- [187] K. Greisen, *Phys. Rev. Lett* **16** (1966) 748.
- [188] G.T. Zatsepin and V.A. Kuzmin, *Pis'ma Zh. Eksp. Teor. Fiz.* **4** (1966) 53 (*JETP Lett.* **4** (1966) 78).
- [189] J. Wdowczyk, W. Tkaczyk and A.W. Wolfendale, *J. Phys.* **A 5** (1972) 1419.
- [190] F.W. Stecker, *Astrophys. Space Sci.* **20** (1973) 47.
- [191] C.T. Hill and D.N. Schramm, *Phys. Rev.* **D31** (1985) 564.
- [192] V.S. Berezinsky and S.I. Grigor'eva, *Astron. Astrophys.* **199** (1988) 1.
- [193] F. Halzen, R.J. Protheroe, T. Stanev and H.P. Vankov, *Phys. Rev.* **D41** (1990) 342.
- [194] S. Yoshida and M. Teshima, *Progr. Theor. Phys.* **89** (1993) 833.
- [195] J. Wdowczyk and A.W. Wolfendale, *Ann. Rev. Nucl. Part. Sci.* (1989).
- [196] J. P. Rachen and P. L. Biermann, *Astron. Astrophys.* **272** (1993) 161.
- [197] J. Ostriker, G. Thompson and E. Witten, *Phys. Lett.* **B180** (1986) 231.
- [198] C.T. Hill, D.N. Schramm and T.P. Walker, *Phys. Rev.* **D36** (1987) 1007.
- [199] P. Bhattacharjee, *Phys. Rev.* **D40** (1989) 3968.
- [200] J. MacGibbon and R. Brandenberger, *Nucl. Phys.* **B331** (1990) 153.
- [201] P. Bhattacharjee and N. Rana, *Phys. Lett.* **246B** (1990) 365.

- [202] J. R. Primack, B. Sadoulet, and D. Seckel, *Ann. Rev. Nucl. Part. Sci.* **B38** (1988) 751.
- [203] F. Halzen, M. Kamionkowski, and T. Stelzer, *Phys. Rev.* **D45** (1992) 4439.
- [204] A. Bottino *et al.* *Mod. Phys. Lett.* **A7** (1992) 733.
- [205] A. Gould, *Ap. J.* **321** (1987) 571; *Ap. J.* **368** (1991) 610.
- [206] V. S. Berezinsky, in *Proc. of the Fourth International Symposium on Neutrino Telescopes*, Venice (1992), ed. M. Baldo-Ceolin.
- [207] H. E. Haber and G. L. Kane, *Phys. Rep.* **117** (1985) 75.
- [208] M. Drees and M. M. Nojiri, *Phys. Rev.* **D47** (1993) 376.
- [209] M. Mori *et al.*, KEK Preprint 91-62; N. Sato *et al.*, *Phys. Rev.* **D44** (1991) 2220.
- [210] J. M. LoSecco *et al.* (IMB Collaboration), *Phys. Lett.* **B188** (1987) 388; R. Svoboda *et al.*, *Ap. J.* **315** (1987) 420.
- [211] J. G. Learned, *Proceedings of the Venice Workshop on Neutrino Telescopes*, (ed. M. Baldo-Ceolin, February 1990) p. 103.
- [212] A. DeRujula, S.L. Glashow, R.R. Wilson and G. Charpak, *Phys. Reports*, **99** (1983) 341.
- [213] F. Halzen and J.G. Learned, *Proc. of the Fifth International Symposium on Neutrino Telescopes*, Venice (1993), ed. M. Baldo-Ceolin, p. 483.
- [214] See recent reports on these experiments in the following reference, and a critical summary of the various projects in J. G. Learned, *Proceedings of the European Cosmic Ray Symposium*, Geneva, Switzerland, July 1992, ed. by P. Grieder and B. Pattison, *Nucl. Phys. B* (1993); see also presentations in *Proceedings of the High Energy Neutrino Astrophysics Workshop*, ed. by V. J. Stenger, J. G. Learned, S. Pakvasa, and X. Tata, World Scientific, Singapore (1992).
- [215] AMANDA-collaboration, submitted to *Nature*.
- [216] J. G. Learned and A. Roberts, *Proceedings of the 23rd International Cosmic Ray Conference*, Calgary, Canada (1993), Vol. 4, p. 579.
- [217] Y. Suzuki, *Proceedings of the 3rd International Workshop on Neutrino Telescopes*, Venice, March 1992, ed. M. Baldo-Ceolin, Venice (1992) p. 237.
- [218] G. A. Askar'yan, *Soviet Physics JETP* **14** (1962) 441–443; **48**, (1965) 988–990.
- [219] M. A. Markov and I. M. Zeleznykh, *Nucl. Inst. Methods* **A 248** (1986) 242–251.
- [220] I. M. Zeleznykh, *Proc. XXIst International Cosmic Ray Conference* (Adelaide, 1989), Vol. 6, p. 528–533; J. P. Ralston and D. M. McKay, *Astrophysics in Antarctica*, American Institute for Physics Conference Proceedings **198** (1990) 24.

- [221] I. Frank and I. Tamm, *Proc. Acad. Sc. USSR* **14** (1937) 109.
- [222] M. Fujii and J. Nishimura, *Proc. XIth International Cosmic Ray Conference*, (Budapest 1969), pp. 709–715.
- [223] For a review see, H. R. Allan, *Progress in Elementary Particles and Cosmic Ray Physics* **10** (1971) 171 (North Holland Publ. Co.).
- [224] F. Halzen, T. Stanev, and E. Zas, *Phys. Lett.* **257B** (1991) 432 and *Phys. Rev.* **D45** (1992) 362.
- [225] I. N. Boldyrev, G. A. Gusev, M. A. Markov, A. L. Provorov and I. M. Zeleznykh, *Proc. XXth International Cosmic Ray Conference*, (Moscow, 1987) Vol. 6, p. 472.
- [226] T. Bowen, *Proceedings of the 16th International Cosmic Ray Conference*, (Kyoto, 1979), Vol. 11, p. 184, T6-1.
- [227] J. G. Learned, *Phys. Rev.* **D19** (1979) 3293.
- [228] H. Spetzler and D. L. Anderson, *J. Geophys. Res.* **73** (1968) 6051.

Figure Captions

Fig.1. A schematic presentation of neutrino fluxes of different origin. (1) atmospheric neutrinos; (2) neutrinos from cosmic ray interactions on galactic matter; (3) source neutrinos.

Fig. 2. P_ν for two values of muon threshold energy, 1 GeV and 1 TeV. The solid lines are for ν and the dashed lines for $\bar{\nu}$. The dotted lines show the power law approximations.

Fig. 3. Neutrino energies giving rise to contained events, stopping and throughgoing muons.

Fig. 4. Upward going muon fluxes detected by IMB [66,67](squares), Baksan [68](stars) and Kamiokande [69](circles), converted to a common muon threshold energy of 3 GeV.

Fig. 5. Prompt neutrino (or muon) fluxes corresponding to five parametrizations of the high energy behavior of the charm production cross section. The vertical and horizontal fluxes of muons from the decay of pions and kaons are shown with dash lines. See text and Ref. [82] for details.

Fig. 6. Rates of horizontal showers, initiated by the muon fluxes shown in Fig. 5. See text. The data points are from Ref. [90] and the dotted line shows the shower rate expected from muons from π and K decay.

Fig. 7. Neutrino fluxes from 3C273 predicted in different AGN models. Thick solid line shows the flux of Stecker *et al* [36]; thin solid lines show several models due to Szabo and Protheroe [38]; and the dash line is from Ref. [152] (see text). These three models are for neutrinos from the AGN nucleus. The dotted line shows the calculation of Mannheim for the neutrino emission from the AGN jet [176].

Fig. 8. The isotropic neutrino background from AGN. The thick line is the prediction of Stecker *et al* [36] for generic AGN, and the thin lines represent models of Szabo and Protheroe [38]. The backgrounds from AGN jets are calculated by Mannheim [173] (dotted line) and Stecker *et al* [183] (dash-dot line). The shaded area shows the angle averaged flux of atmospheric neutrinos.

Fig. 9. Horizontal ($-0.3 < \cos\theta < 0.3$) muon fluxes generated by the isotropic neutrino background as in the bracketing high and low models of Szabo & Protheroe [38] (thin solid lines) and by Stecker *et al.* [36] (thick solid line). The 90% C.L. upper limit of the Frejus experiment [161] is shown for muon threshold energy of 2 TeV.

Fig. 10. Differential interaction rate of $\nu_e + \bar{\nu}_e$ as a function of E_ν . Dotted line: atmospheric; thin solid line: Ref. [38]; thick solid line: Ref. [36]. The numbers by the curves are number of interactions per 1000 kT per year, calculated for $E_\nu > 1$ TeV.

Fig. 11. Comparison of quasi-simultaneous observations of 3C273 in the optical, X-ray and γ -ray bands [177] with the predictions of a synchrotron-self-Compton model [119] (solid line) and a hadronic model [176]. See Ref. [177] for references to all experimental data.

Fig. 12. Contours in the M, μ plane of constant $\alpha_H = 1.0, 0.1, 0.01$ (boxes) and constant neutralino mass $M_\chi = 30, 100, 500$ and 1000 GeV (solid). The shaded region is excluded by cosmological considerations.

Fig. 13. As a function of the neutralino mass we show the telescope size required to be sensitive at the one event per year level. We fix $\tan\beta = 2$, $\alpha_H = 0.1$. The two branches correspond to the two solutions for fixed α_H .

Fig. 14. In the M_2, μ plane for $M_{\tilde{q}} = \infty$, (a) contours of constant detection rate (events $\text{m}^{-2} \text{yr}^{-1}$) and (b) regions of $\Omega_\chi h^2 > 1$ and $\Omega_\chi h^2 < 0.02$ which are ruled out by cosmological considerations.

Fig. 15. Summary of isotropic neutrino fluxes of energy above 1 GeV. (1) atmospheric neutrinos; (2) diffuse galactic neutrinos; (3) diffuse extragalactic neutrinos—maximum and minimum predictions of Ref. [38]; (4) cosmological neutrinos—maximum and minimum predictions of Ref. [194].

Fig. 16. Summary of source neutrino fluxes of energy above 1 GeV. (1) neutrinos generated by cosmic rays in the Sun [128]; (2) a galactic neutrino source; (3) extragalactic neutrino source (3C273) [38]; (4) AGN jet emission (3C279 high state) [37]. The atmospheric neutrino background within 1° is shown with a dash line.

Fig. 17. A possible configuration of a 1 km neutrino detector, based on AMANDA-design supermodules.

Fig. 18. Rate of (muon-poor) horizontal showers associated with the neutrino emission by active galaxies (thin lines are the upper and lower bound of Ref. [38], the thick line shows the background of Ref. [36]) compared to the background from atmospheric muons (dotted line) and the experimental results of Ref. [90].

This figure "fig1-1.png" is available in "png" format from:

<http://arXiv.org/ps/hep-ph/9410384v1>

This figure "fig1-2.png" is available in "png" format from:

<http://arXiv.org/ps/hep-ph/9410384v1>

This figure "fig1-3.png" is available in "png" format from:

<http://arXiv.org/ps/hep-ph/9410384v1>

This figure "fig1-4.png" is available in "png" format from:

<http://arXiv.org/ps/hep-ph/9410384v1>

This figure "fig1-5.png" is available in "png" format from:

<http://arXiv.org/ps/hep-ph/9410384v1>

This figure "fig1-6.png" is available in "png" format from:

<http://arXiv.org/ps/hep-ph/9410384v1>

This figure "fig1-7.png" is available in "png" format from:

<http://arXiv.org/ps/hep-ph/9410384v1>

This figure "fig1-8.png" is available in "png" format from:

<http://arXiv.org/ps/hep-ph/9410384v1>

This figure "fig1-9.png" is available in "png" format from:

<http://arXiv.org/ps/hep-ph/9410384v1>

This figure "fig1-10.png" is available in "png" format from:

<http://arXiv.org/ps/hep-ph/9410384v1>

This figure "fig1-11.png" is available in "png" format from:

<http://arXiv.org/ps/hep-ph/9410384v1>

This figure "fig1-12.png" is available in "png" format from:

<http://arXiv.org/ps/hep-ph/9410384v1>

This figure "fig1-13.png" is available in "png" format from:

<http://arXiv.org/ps/hep-ph/9410384v1>

This figure "fig1-14.png" is available in "png" format from:

<http://arXiv.org/ps/hep-ph/9410384v1>

This figure "fig1-15.png" is available in "png" format from:

<http://arXiv.org/ps/hep-ph/9410384v1>

This figure "fig1-16.png" is available in "png" format from:

<http://arXiv.org/ps/hep-ph/9410384v1>

This figure "fig1-17.png" is available in "png" format from:

<http://arXiv.org/ps/hep-ph/9410384v1>

This figure "fig1-18.png" is available in "png" format from:

<http://arXiv.org/ps/hep-ph/9410384v1>

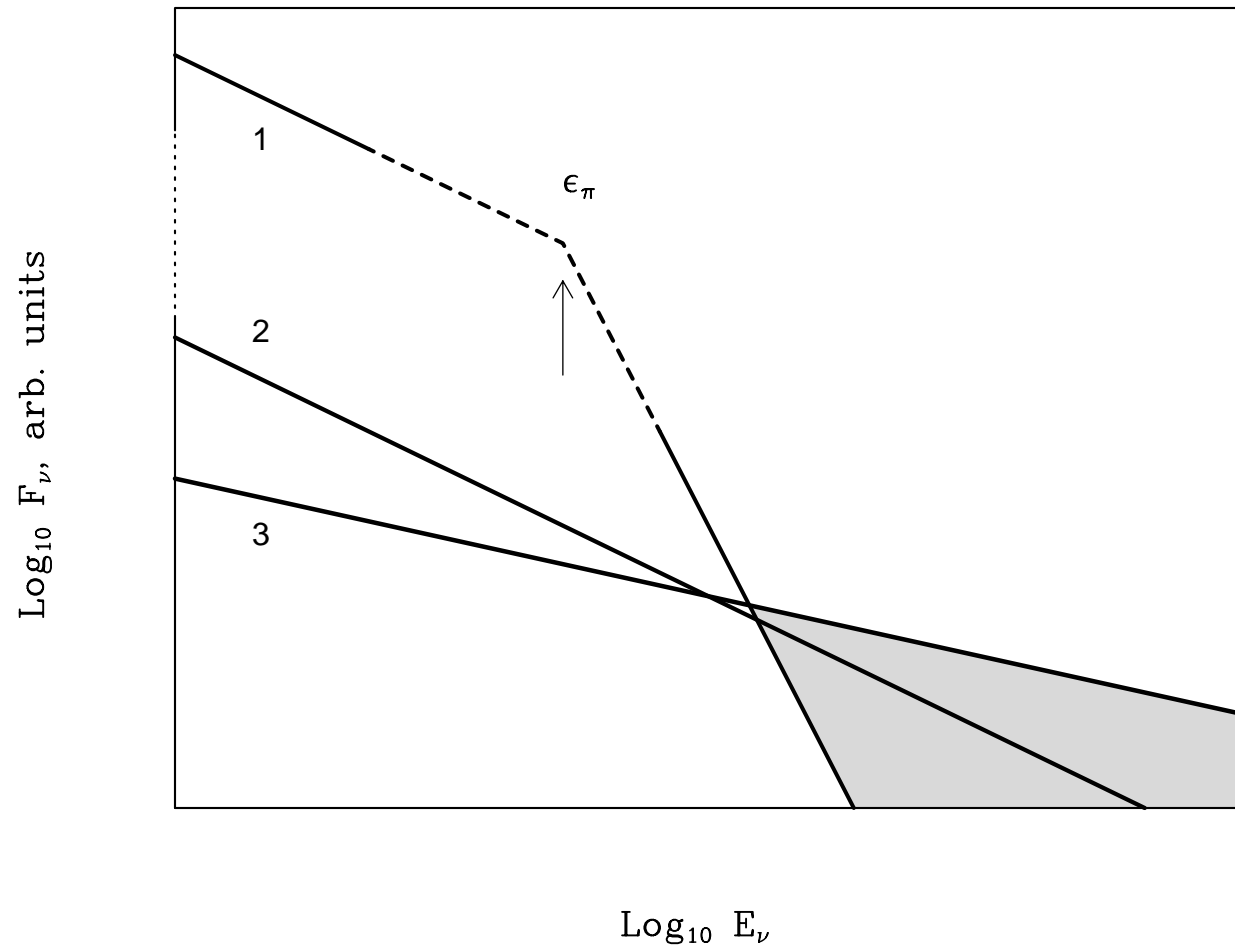


Fig. 1

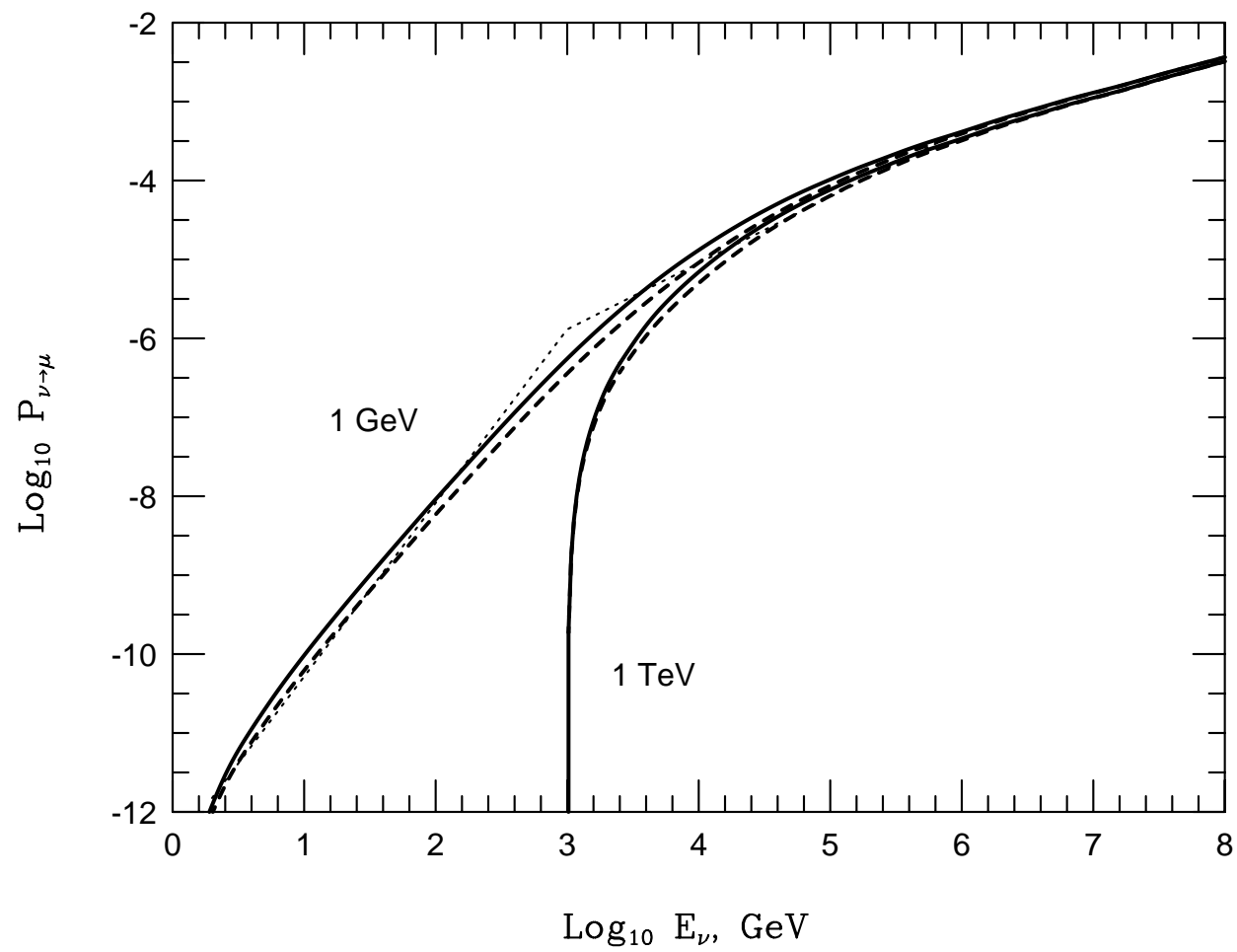


Fig. 2

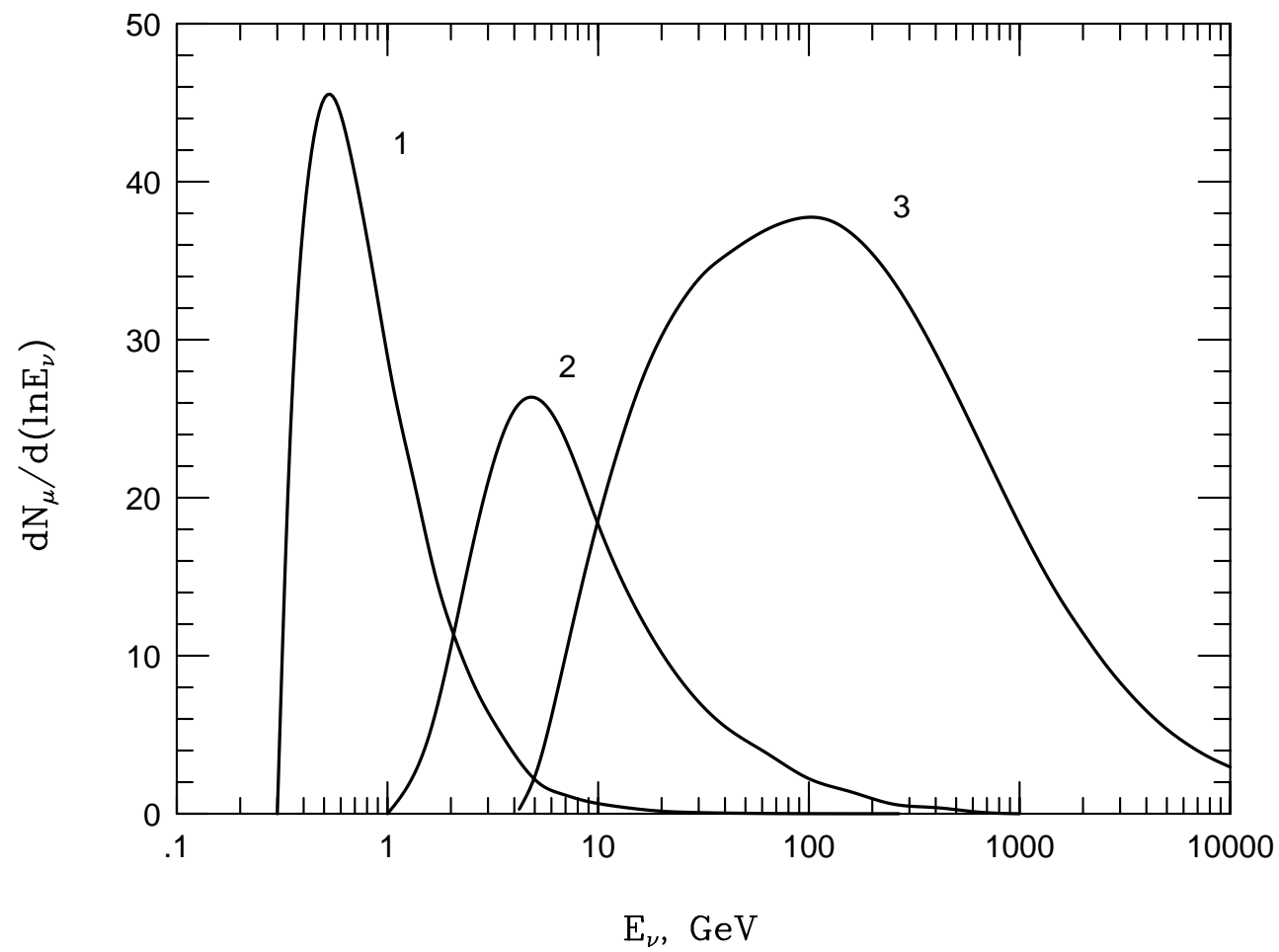


Fig. 3

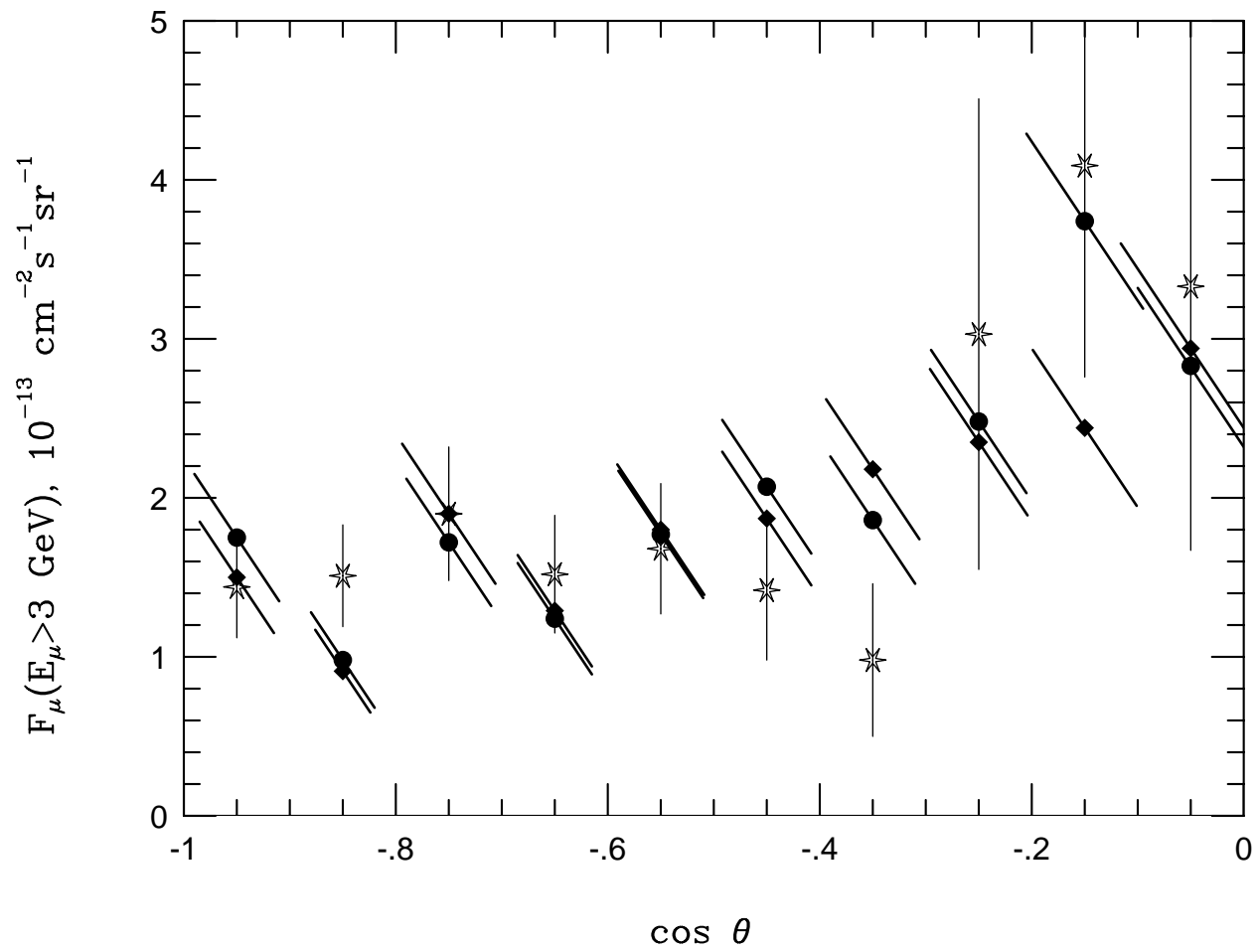


Fig. 4

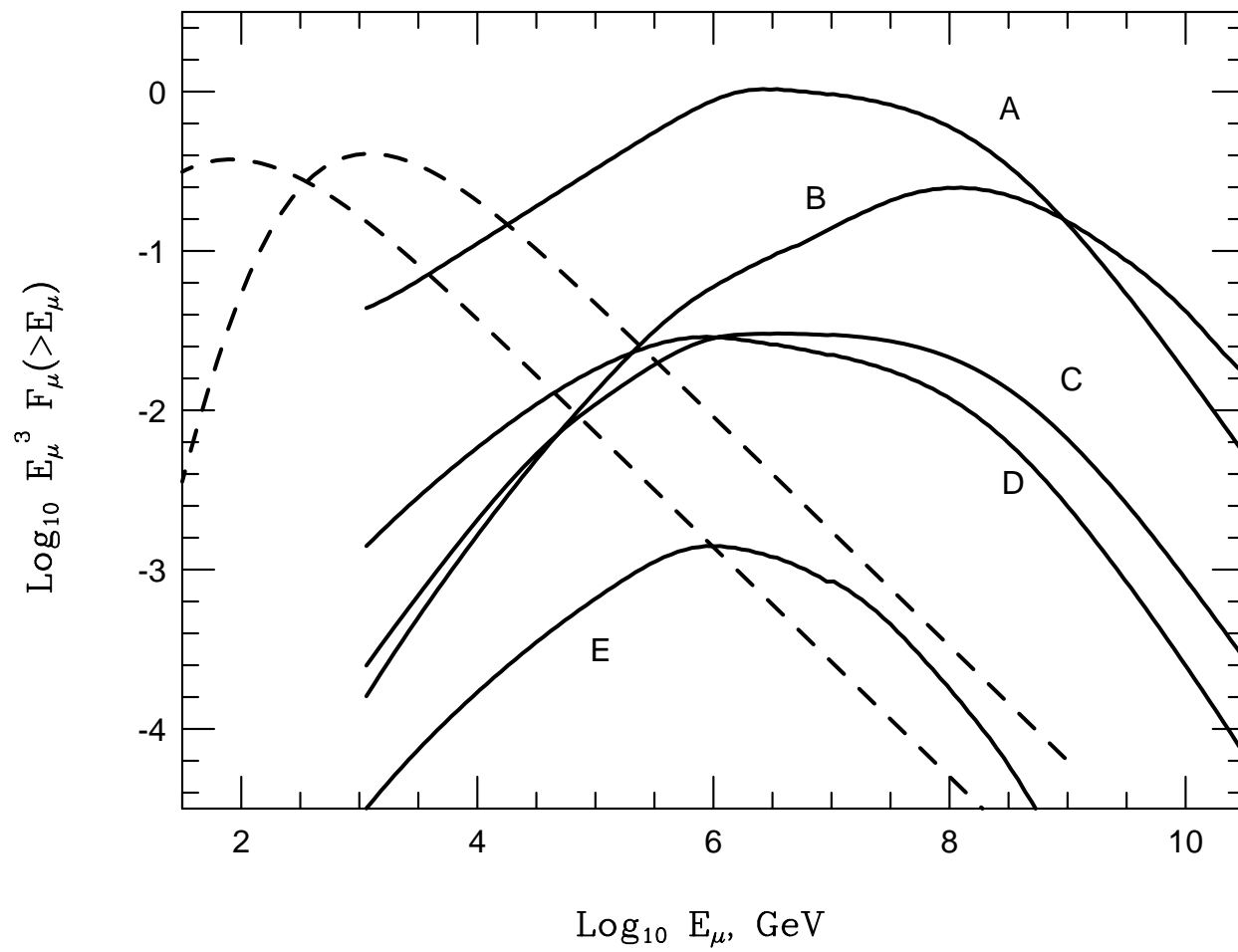


Fig. 5

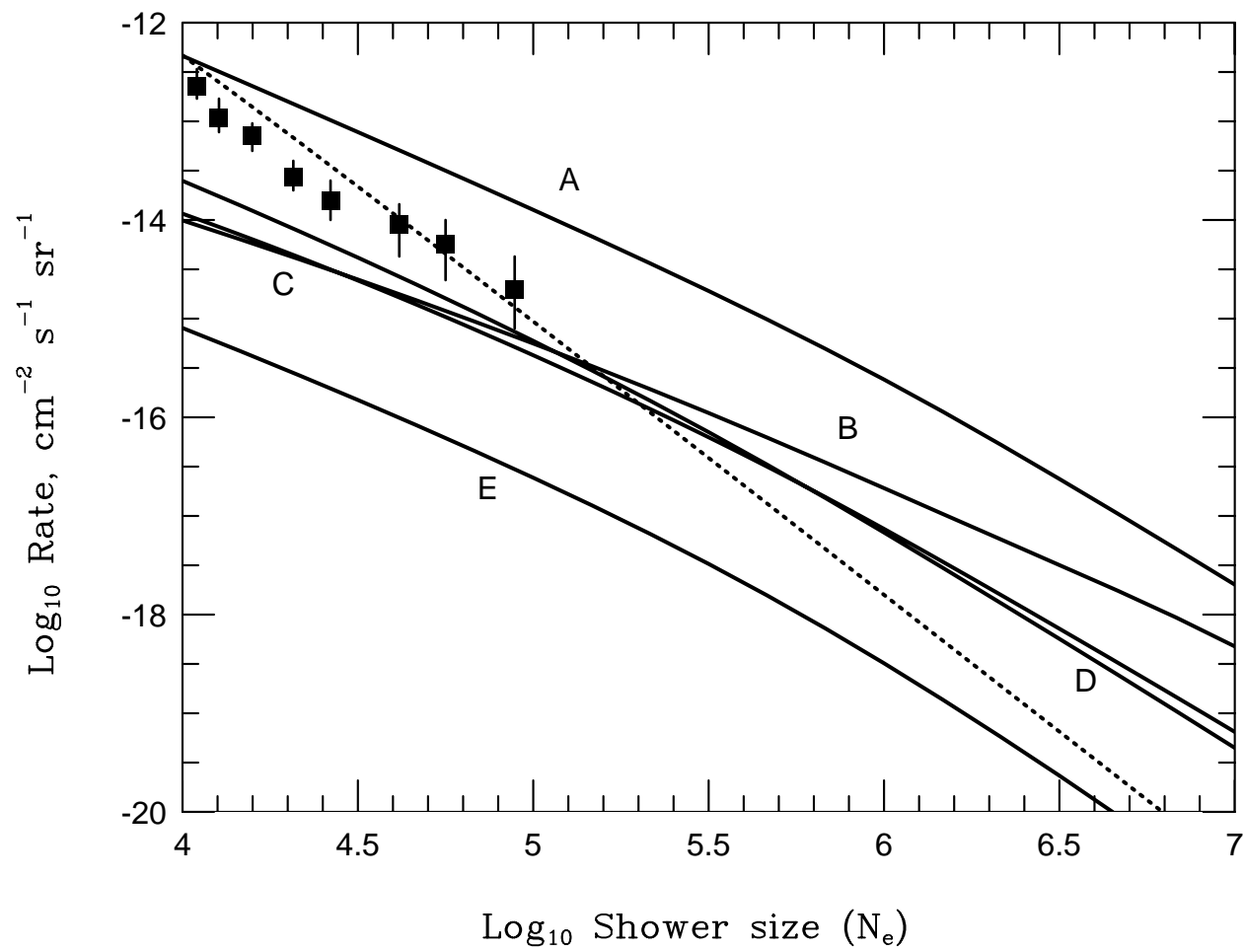


Fig. 6

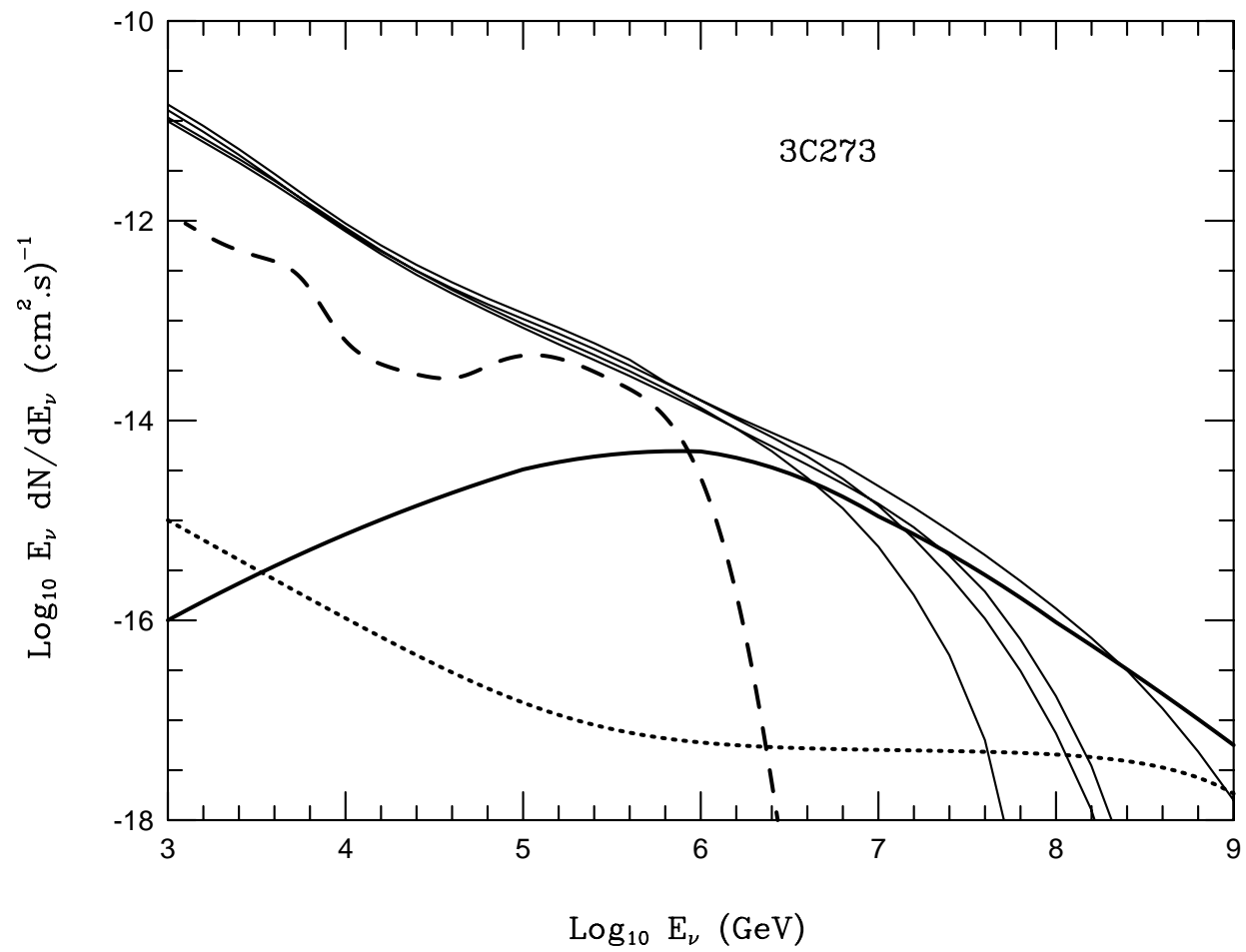


Fig. 7

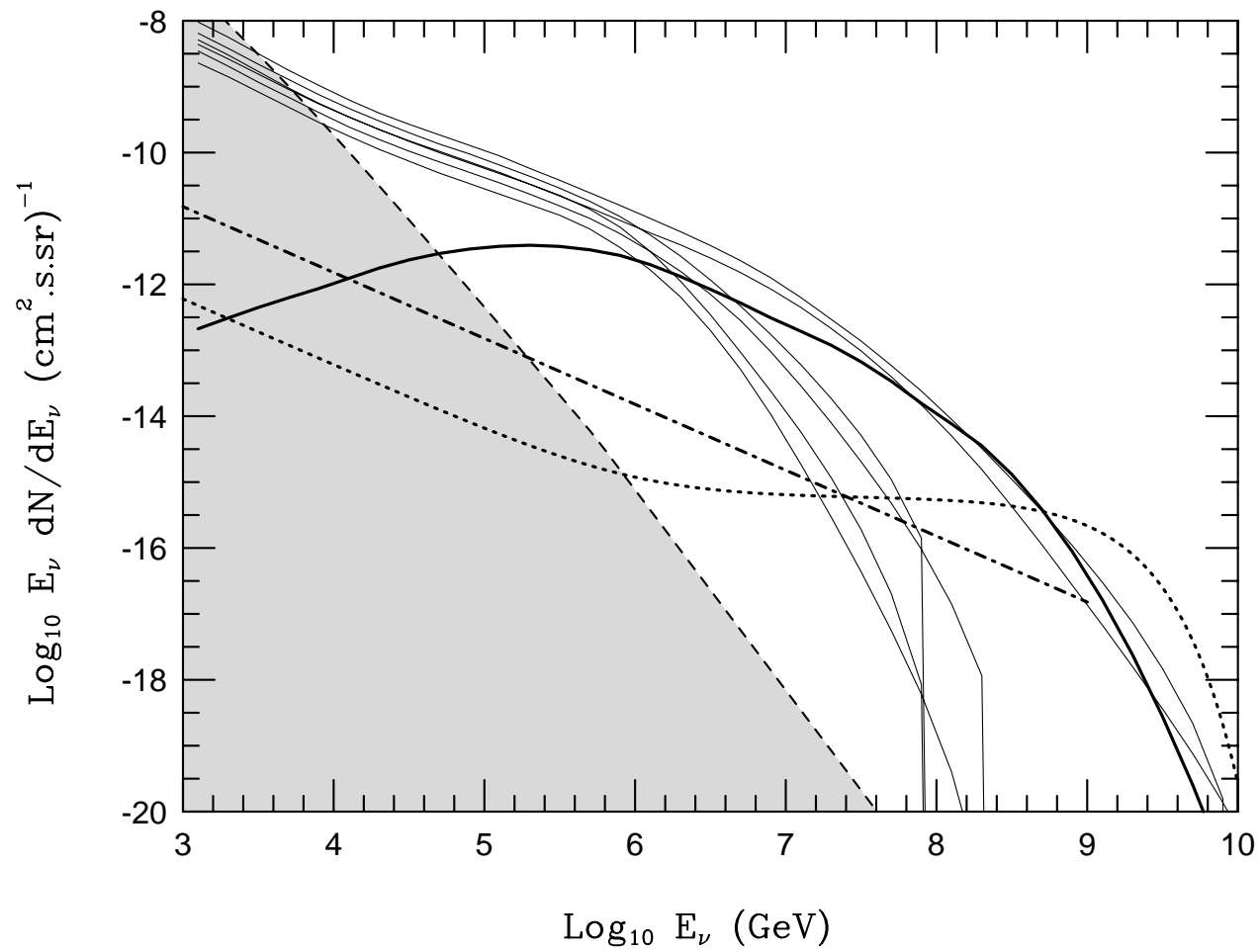


Fig. 8

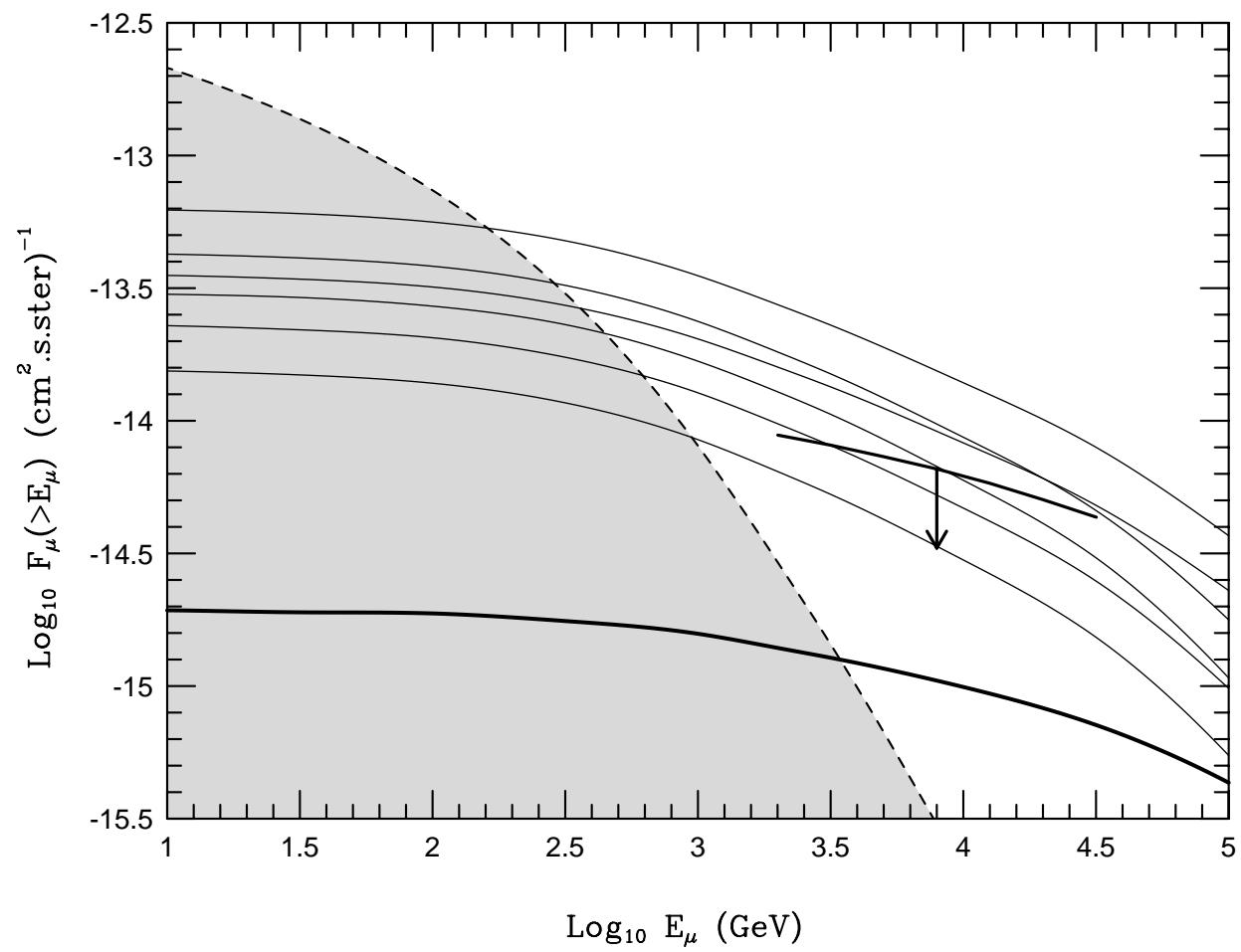


Fig. 9

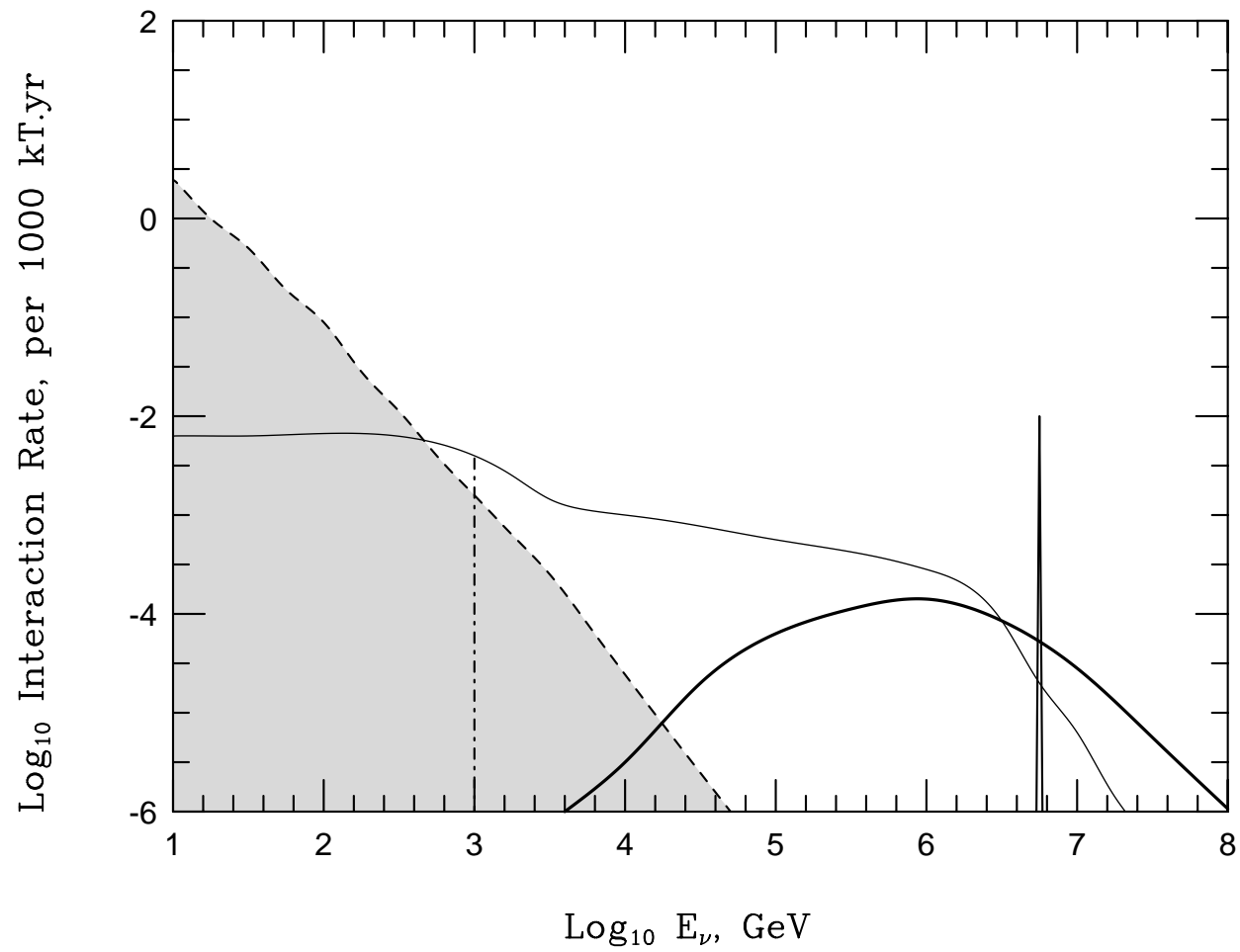


Fig. 10

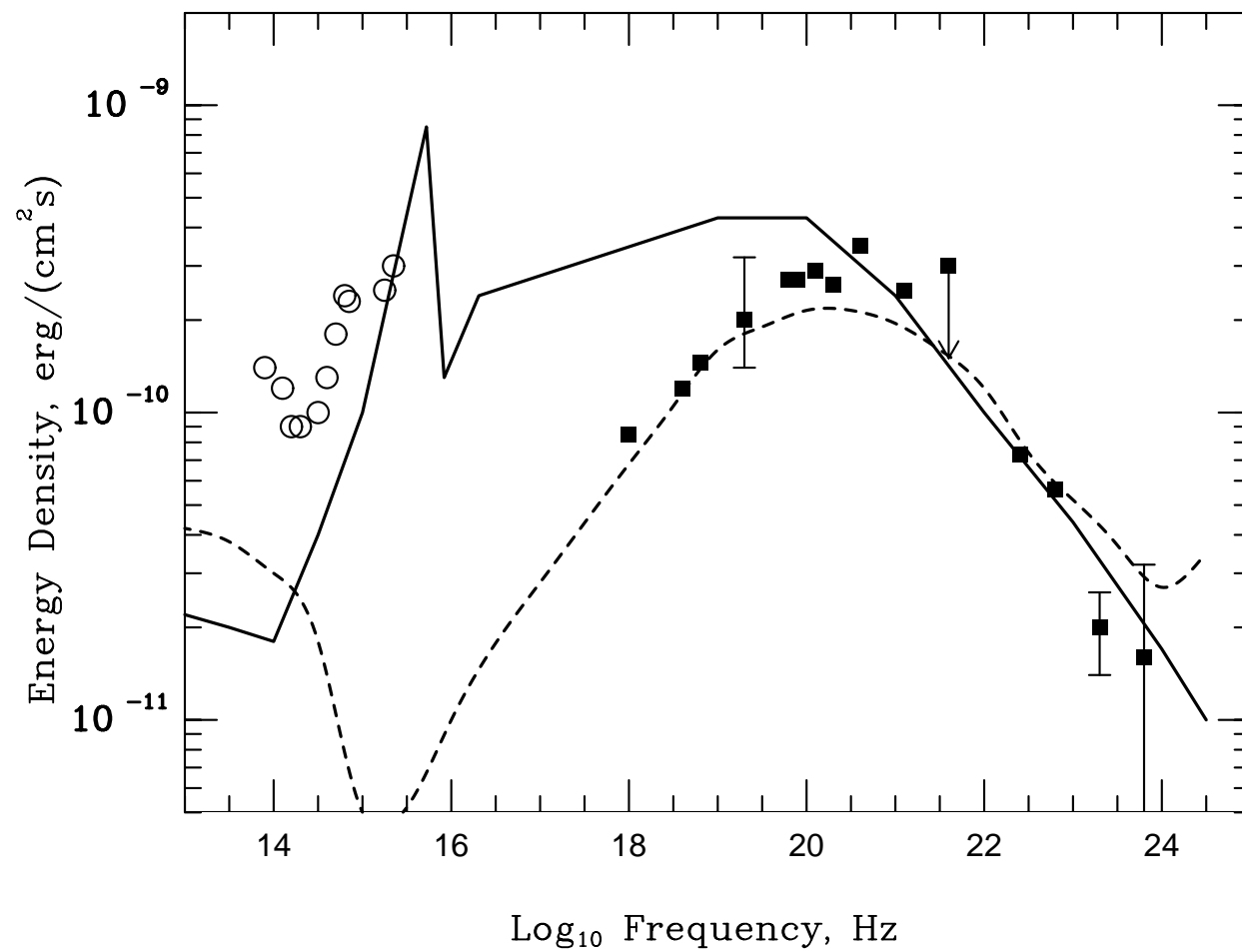


Fig. 11

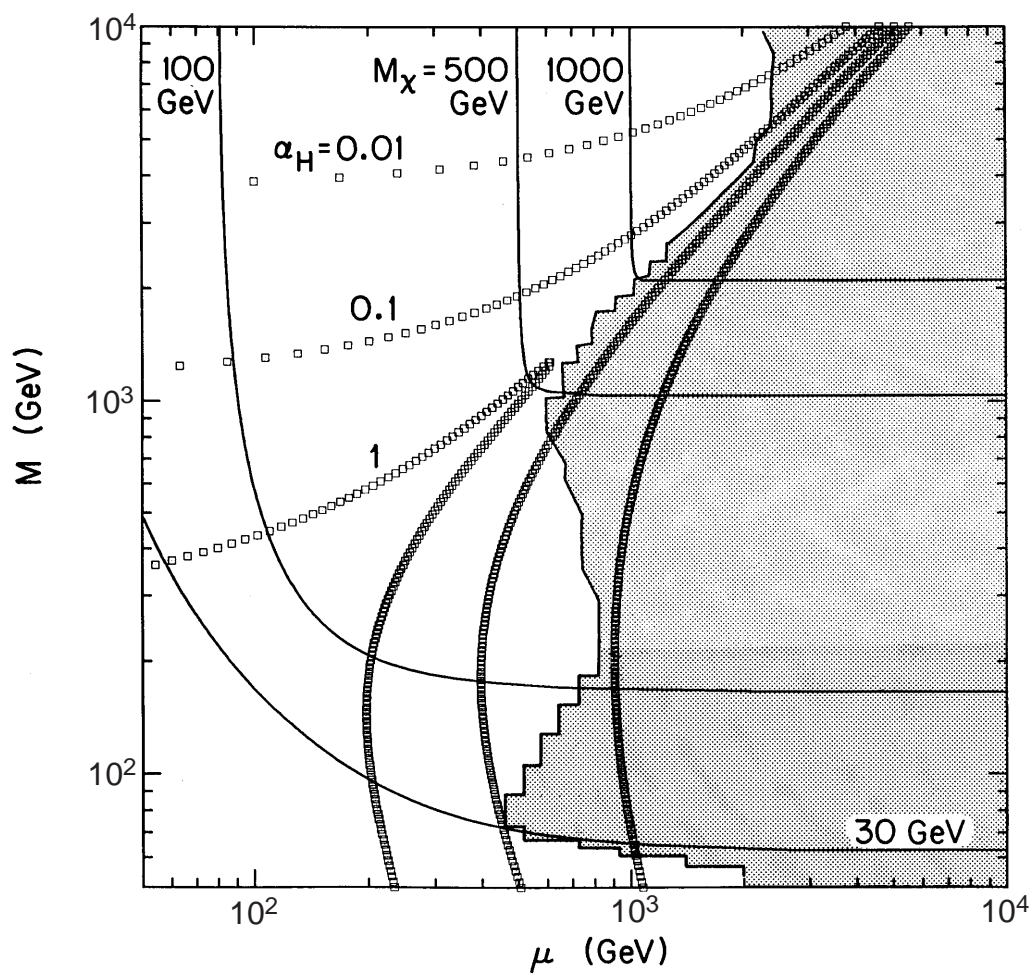


Fig. 12

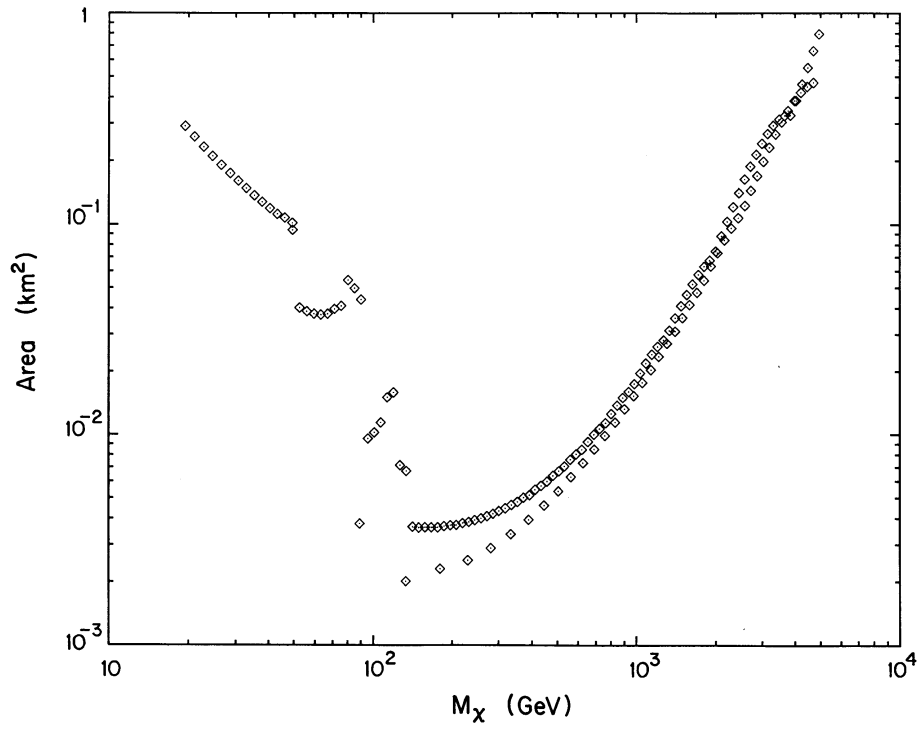


Fig. 13

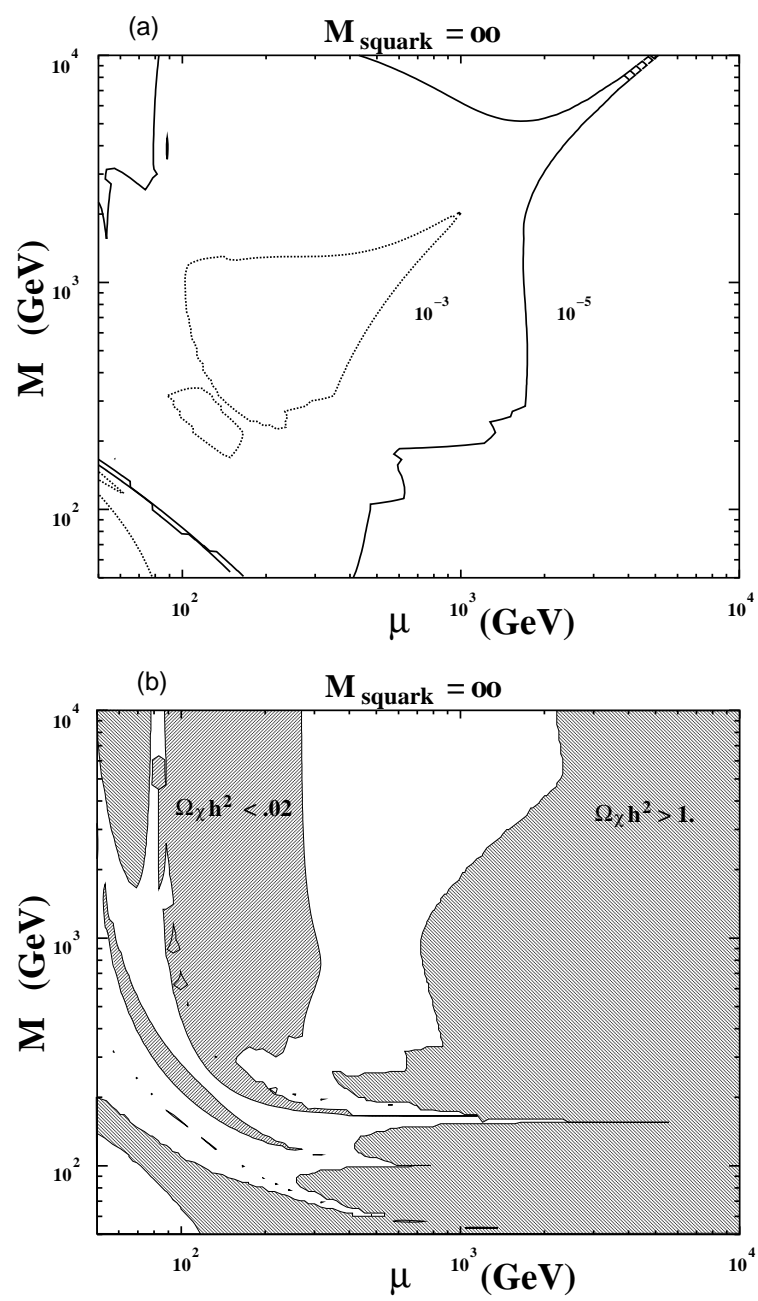


Fig. 14

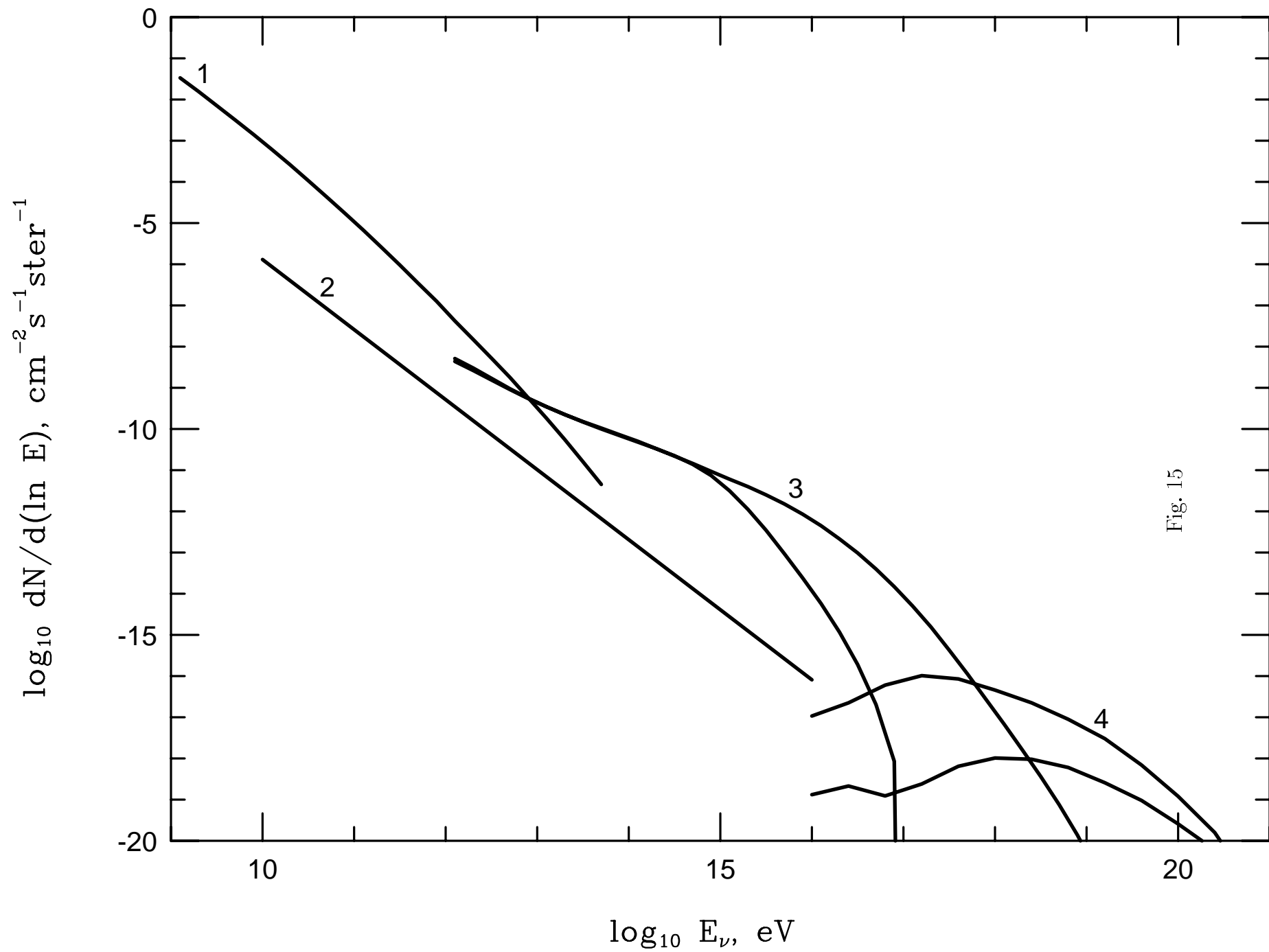


Fig. 15

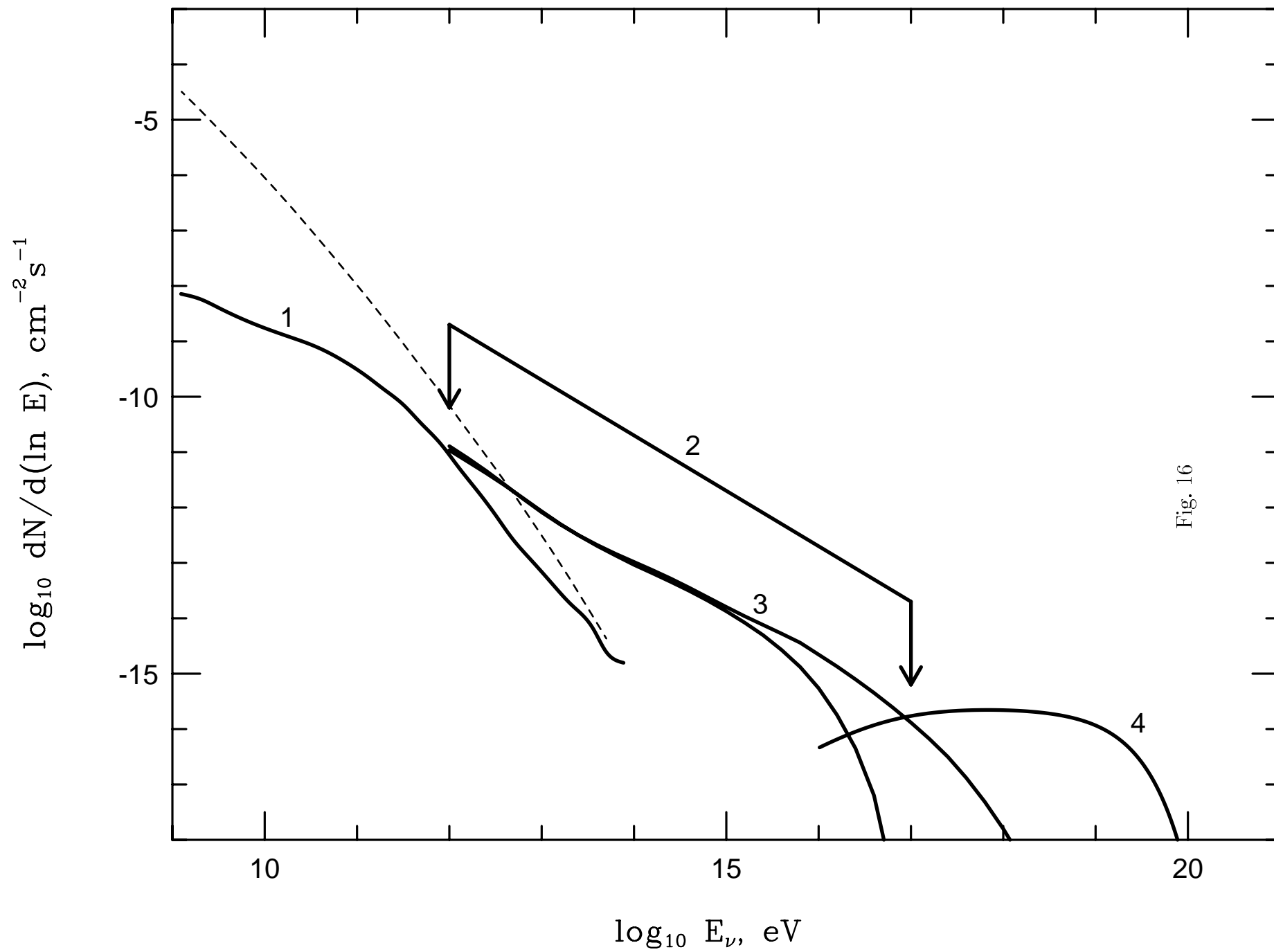


Fig. 16

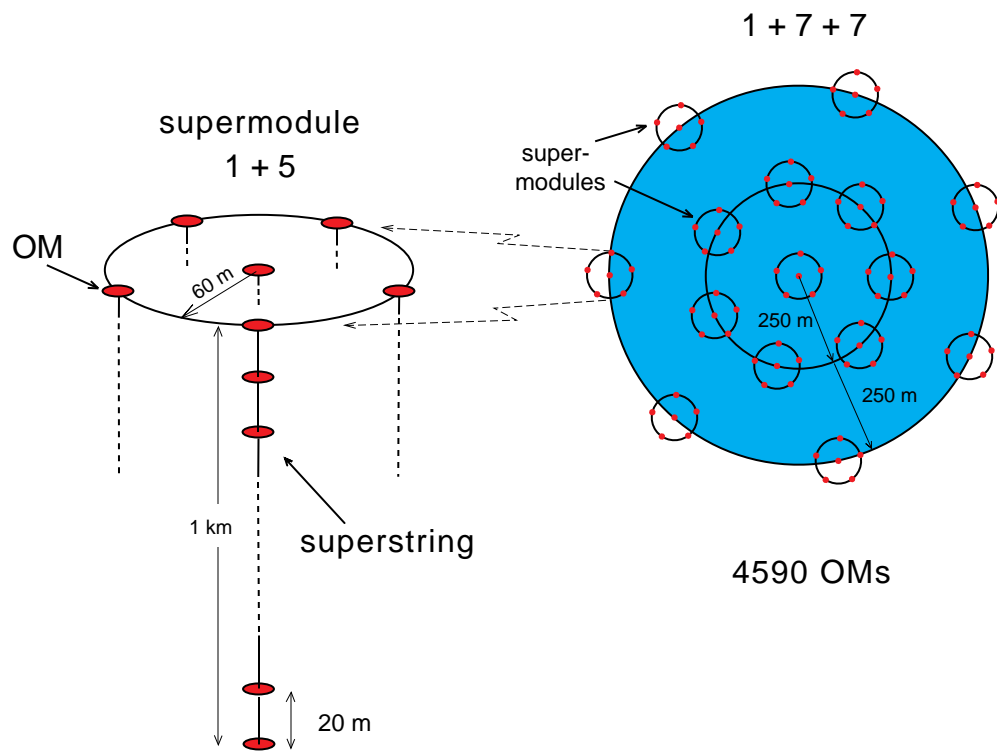


Fig. 17

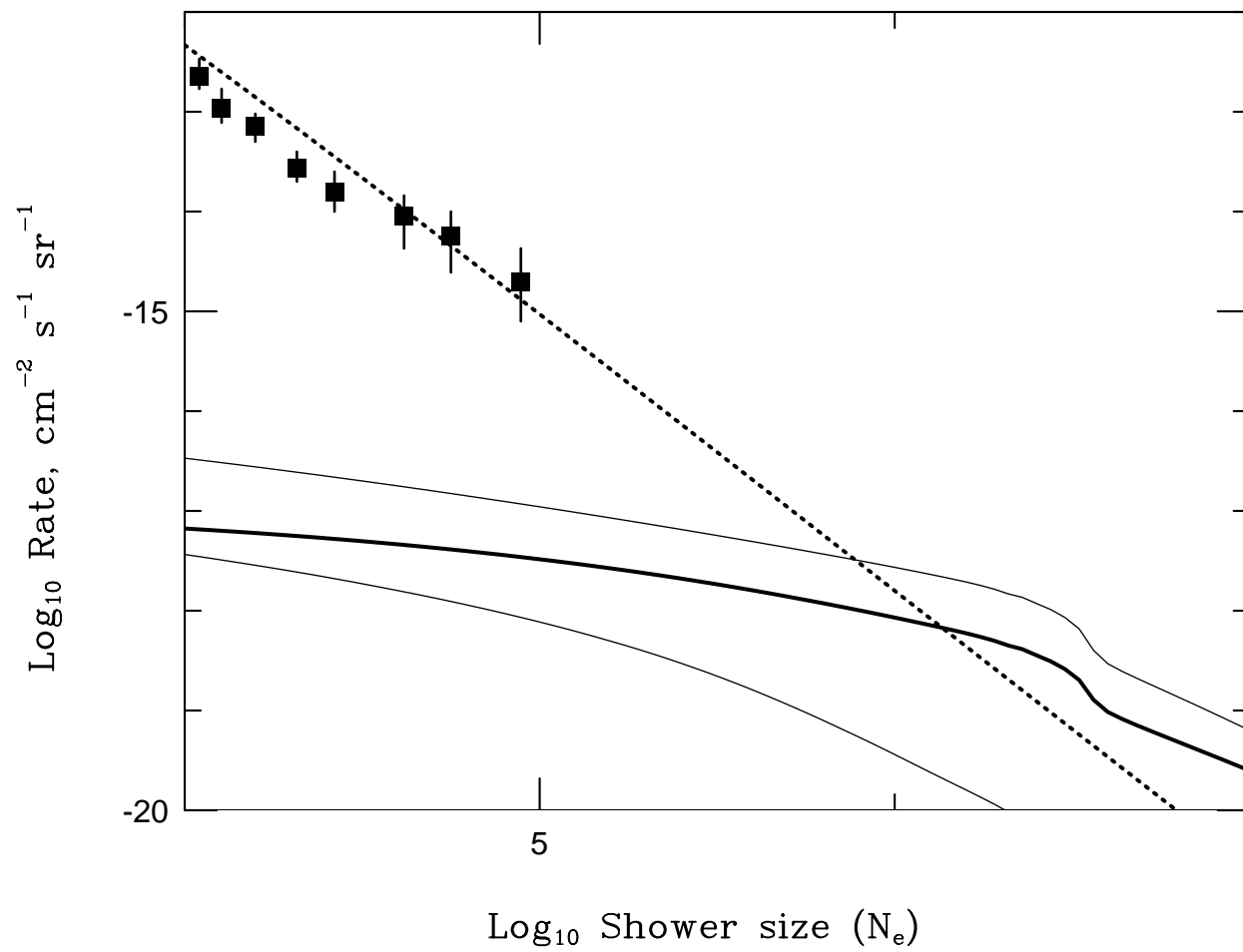


Fig. 18